EISCAT Svalbard Radar studies of meso-scale plasma flow channels in the polar cusp ionosphere

by

Yvonne Rinne

Thesis submitted to the Department of Physics, University of Oslo, June 2010

Series of dissertations submitted to the
Faculty of Mathematics and Natural Sciences, University of Oslo
No. 1008

ISSN 1501-7710

Cover: Inger Sandved Anfinsen.
Printed in Norway: AiT e-dit AS.

Produced in co-operation with Unipub.
The thesis is produced by Unipub merely in connection with the
thesis defence. Kindly direct all inquiries regarding the thesis to the copyright
holder or the unit which grants the doctorate.

To Basti

Thanks for all the good times I got to share with you; endless hours of taking apart, building, fixing and creatively modifying all sorts of technical and non- technical devices, and philosophizing about the meaning of life. Your urge to explore our World and the Universe has inspired and motivated me. Nothing was ever impossible, nothing ever too complicated. Our limit was our own imagination. Without you I would not be here.

Vonni

Acknowledgements

This thesis has been supported by a four year grant from the Department of Physics at University of Oslo. In addition, the following grants were provided: The Kristine Bonnevie travel scholarship from the Faculty of mathematics and natural science, University of Oslo was used for a research stay at the Solar Terrestrial Environment Laboratory at the University of Nagoya, Japan. The Amelia Earhart fellowship from Zonta International was used for research stay at the University Centre in Svalbard. Two Arctic Scholarships from the Norwegian Polar Institute were used for radar campaigns at the EISCAT Svalbard radar in Longyearbyen.

The list of people who have inspired and helped me throughout these four years is long, and I would like to apologize for everyone I may have forgotten to include. First of all I would like to thank my main supervisor Jøran Moen, who has given me incredibly many opportunities during these four years. I would also like to thank my co-supervisor Per Even Sandholt, as well as Herb Carlson and Tony van Eyken who have been great sources of inspiration, and my co-authors Herb Carlson, Kjellmar Oksavik, Marc Hairston and Jo Baker for collaborating with me on the papers presented in this thesis.

Also, I am very thankful to Ryo Fujii and the students and employees at STELAB in Nagoya as well as Dag Lorentzen and Fred Sigernes and the students and staff at UNIS for making me feel welcome and at home both in Japan and at UNIS. A big thanks to the EISCAT Svalbard Radar staff for all their support and many good hours at the radar site, and to Espen Trondsen for all technical support and for always being there for me as a friend. I was fortunate enough to get the opportunity to lecture and be course responsible during my PhD and would like to thank the two great groups of students taking FYS3610 in autumn 2006 and 2007, as well as the students and employees at the Space Physics group in Oslo for all the good times we shared.

Thanks to all my colleagues who have made travelling around the world to conferences like coming home, and to my friends who have motivated me, and shared great times. In particular I would like to mention Lisa Baddeley, Vigdis Lonar Barth, Rico Behlke, Karoline Bælum, Ian McCrea, Kenneth Dåbakk, Silje Eriksen Holmen, Jeff Holmes, Karolina Karas, Ellen and Vegard Rekaa, Lucie Strub-Klein, Johanne Sundby, Monika Trümper, everyone I forgot. A big thanks also to my sister, Sandra Rinne Dahl, and her Husband, Trond Dahl, for always being there for me, and my family, especially my parents, for their support and understanding of my somewhat unconventional science-gypsy life for the past four years.

Las but certainly not least I would like to thank my biathlon athletes for many wonderful ours of training and competition, and my 4-legged friends Okinawa, Jonas and Isikajia, a number of dogs in Longyearbyen Hundeklubb and all of Johanne Sundby's dogs for giving me the greatest joy and mind-clearing experiences on our many dog-sledding trips, and for being faithful companions at all times ☺

Oslo, June 2010 Yvonne Rinne

Contents

Paper 1 *Reproduced by permission of American Geophysical Union*

Y. Rinne, J. Moen, K. Oksavik, and H. C. Carlson, Reversed flow events in the winter cusp ionosphere observed by the European Incoherent Scatter (EISCAT) Svalbard radar, *J. Geophys. Res.*, 112, A10313, doi:10.1029/2007JA012366, 2007

Paper 2 *Reproduced by permission of American Geophysical Union*

J. Moen, **Y. Rinne**, H. C. Carlson, K. Oksavik, R. Fujii, and H. Opgenoorth, On the relationship between thin Birkeland current arcs and reversed flow channels in the winter cusp/cleft ionosphere, *J. Geophys. Res.*, 113, A09220, doi:10.1029/2008JA013061, 2008

Paper 3 *Reproduced by permission of American Geophysical Union*

Y. Rinne, J. Moen, H.C. Carlson, M. R. Hairston, Stratification of east-west plasma flow channels observed in the ionospheric cusp in response to IMF B_Y polarity changes, *Geophys. Res. Lett 2010,* 37, L13102, doi:10.1029/2010GL043307, 2010

Paper 4

Y. Rinne, J. Moen, J. Baker, H.C. Carlson, Convection surrounding meso-scale ionospheric flow channels

Submitted to J. Geophys. Res.2010

1. Introduction

The archipelago of Svalbard is at daytime located underneath the polar cusp, the window towards the interplanetary space. The polar cusp region is where the solar-terrestrial coupling by a process referred to as magnetic reconnection is most direct and strongest. Magnetic reconnetion gives rise to a variety of disturbances like ionospheric flow channels, plasma instabilities or turbulence. The EISCAT Svalbard Radar (ESR) located in Longyearbyen, Svalbard provides, combined with optical observations of daytime auroras, a unique opportunity for detailed studies of plasma processes in the polar cap and the active cusp region.

A new azimuth scan mode at the EISCAT Svalbard Radar resulted in high resolution data with good spatial and temporal resolution which proved to be ideal for the study of meso-scale flow channels in the polar cusp ionosphere. The motivation of this thesis was to gain a more thorough understanding of such channels. The emphasis is on two categories of flow channels: Direct reconnection flow channels and the so-called Reversed flow events, opposing the IMF BY associated magnetic tension force. Common for both classes of flow channels is their linkage to magnetic reconnection at the dayside magnetopause.

The thesis is organized as follows: First a brief background on magnetic reconnection and ionospheric flow signatures in the ionosphere is given. Then a summary of the four papers in this thesis is presented, followed by a few words about future prospects for this research activity and a list of references.

2. Background

2.1. Magnetic reconnection

The discovery of the Interplanetary magnetic field (IMF) by Pioneer V [*Coleman et al.*, *1960*] led to one of the most interesting and fundamental topics in space physics; the concept of magnetic reconnection as energy transfer mechanism between the solar wind and the Earth's magnetosphere. Half a decade later, the existence and importance of this fundamental process itself seems to be widely accepted for the Sun-Earth system, although its nature and rate are still debated. In his famous, qualitative model, *Dungey* [*1961*] envisaged reconnection between a southward IMF and the Earth's magnetic field at the dayside magnetopause as a quasi steady process, occurring at the sub solar point of the Earth's magnetosphere. He suggested that the newly opened field lines, which are connected to the IMF at one end, and the geomagnetic field on the other, should be swept across the polar cap due to the motion of the solar wind, and eventually reconnect again in the magneto tail. This process is often referred to as the Dungey cycle (Figure 1). Extending his initial model, Dungey predicted that reconnection would take place at the magnetospheric lobes for northward IMF conditions.

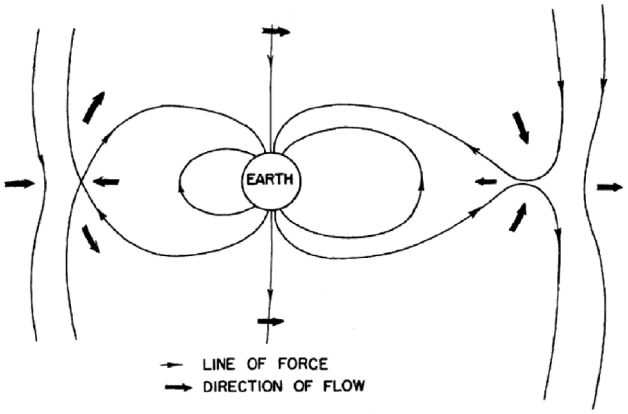

Figure 1: Dungey [*1961*] cycle for IMF B_Z negative. Figure from *Dungey* [*1961*].

Jørgensen et al. [*1972*] extended Dungey's initial idea for meridional components to the equatorial components of the IMF and the geomagnetic field. The east-west component of the IMF causes asymmetries for reconnection between the IMF and the geomagnetic field at the magnetopause, and displaces the reconnection site out to the flanks towards dawn for negative values, and towards dusk for positive values.

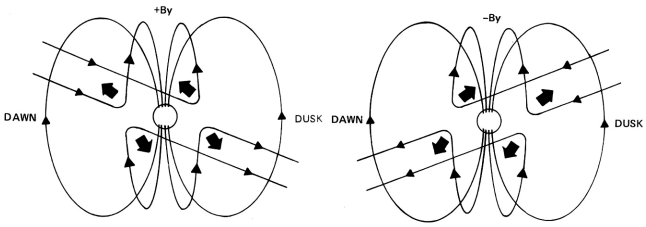

Figure 2: Newly reconnected field lines with a positive B_Y (left side) and negative B_Y (right side) component. The thick black arrows indicate the direction of the magnetic tension force which acts on the curved field lines to stretch them out. Figure from *Gosling et al.* [*1990*]

The magnetic tension force will act to straighten out bent flux tubes, and hence flux tubes will experience an initial westward pull for positive values of the east-west component of the IMF (B_Y), and an initial eastward pull for negative IMF B_Y, as shown in Figure 2.

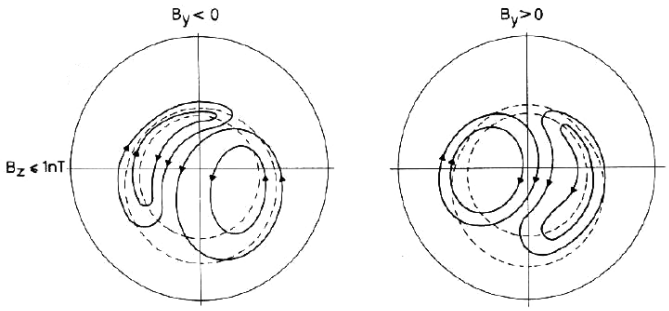

Figure 3: Sketch showing high latitude ionospheric convection in the northern hemisphere for IMF $B_Z < 0$ and IMF $B_Y < 0$ (left panel), IMF $B_Y > 0$ (right panel). Figure from *Cowley and Lockwood* [*1992*].

Electric field measurements made by satellites at high geomagnetic latitudes reveal that the pattern of magnetic field line convection in the Earth's polar cap depends strongly on the sign of IMF B_Y, as shown in Figure 3 [e.g. *Heelis et al.*, *1982; Heppner and Maynard*, *1987*]. This effect, first described by *Svalgaard* [1968; 1972] and independently *Mansurov* [*1969*], is often referred to as the Svalgaard-Mansurov effect. It is a key characteristic of magnetopause reconnection as transient reconnection is communicated to the ionosphere as an Alfvén pulse with an associated field aligned current (FAC) system [*K-H Glassmeier and Stellmacher*, 1996; *D. J. Southwood*, 1985; 1987; *D. J. Southwood and Hughes*, 1982]. The polarity of these FAC sheets is consistent with the IMF B_Y dependent polarity of large scale cusp currents. Hence, when B_Y is positive (negative) there is a strong eastward (westward) magnetic perturbation caused by a pair of FAC sheets having upward (downward) current, as shown in Figure 4 [*Taguchi et al.*, *1993*].

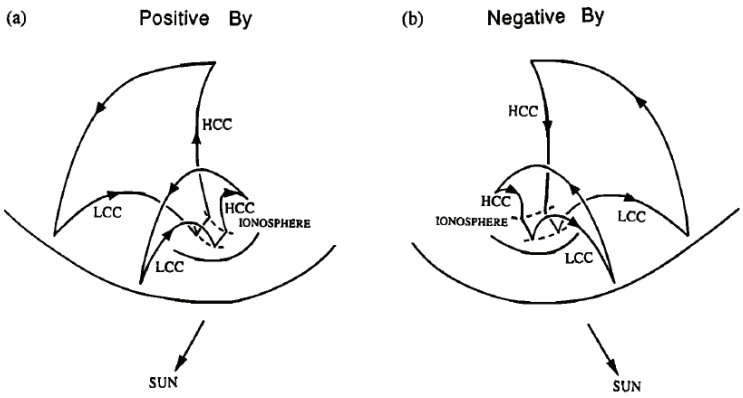

Figure 4: Northern hemisphere current circuits for a) IMF B_Y positive and b) IMF B_Y negative. Figure from Taguchi et al. [*1993*]

2.2 Transient magnetic reconnection

Nearly twenty years later *Haerendel et al.* [*1978*] suggested the transient or intermittent nature of magnetic reconnection by examining HEOS 2 high latitude plasma and magnetic field data. Using ISEE 1 and 2 data from low latitudes, *Russel and Elphic* [*1978; 1979*]

confirmed Haerendels suggestion and presented observations of patchy reconnection at low latitudes. They designated the term Flux Transfer Events (FTEs) to describe a characteristic set of signatures seen in the magnetic field close to the magnetopause. FTEs are identified in boundary normal co-ordinates by a bipolar signature in the B_N component and in increase in the total magnetic field. In boundary normal coordinates, the N component is normal to the local magnetopause boundary, the L component is along the projection of the solar magnetospheric Z component, and the M component completes the right hand orthogonal set.

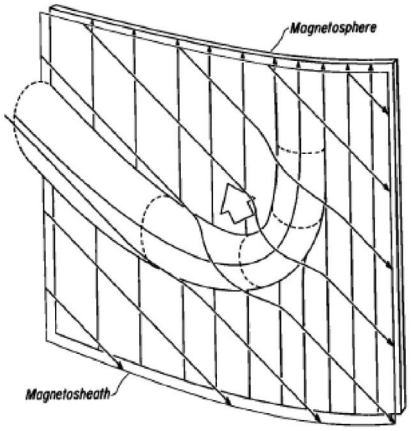

Figure 5: Qualitative sketch of an FTE as envisaged by *Russel and Elphic* [1978]. Magnetosheath field lines, represented as slanted arrows, have reconnected with magnetospheric field lines, shown as vertical arrows. Reconnection is envisaged to have taken place off the lower edge of the figure. Figure from *Russel and Elphic* [1978].

Russel and Elphic [*1978*] interpreted their observations in term of a flux rope model in three dimensions (Figure 5). According to this model, a single magnetic flux tube, resulting from transient reconnection between the IMF and the magnetospheric field, will move under the influence of magnetic tension. The characteristic increase, then decrease through a negative maximum is then what one would expect if the magnetopause bulged out and the bulge subsequently travelled from the nose region and past the spacecraft.

2.3. Ionospheric signatures of transient magnetic reconnection

The search for ionospheric signatures at the magnetically conjugate locations at the high-latitude ionosphere has evolved to one of the popular and controversial topics in ionospheric physics. In particular, ground magnetic [*K H Glassmeier et al.*, 1984 and references therein], optical [*Fasel*, 1995; *Moen et al.*, 1995; *Sandholt et al.*, 1998; *Sandholt et al.*, 1993; *Sandholt et al.*, 1990; *Øieroset et al.*, 1997] and ionospheric radar observations were used [*Greenwald et al.*, 1999; *Lockwood et al.*, 1989; *Lockwood et al.*, 1993; e.g. *Milan et al.*, 2000; *Moen et al.*, 1999; *Moen et al.*, 2001; *Nishitani et al.*, 1999; *Oksavik et al.*, 2004; *Oksavik et al.*, 2005; 1995; *Pinnock et al.*, 1993; *Provan et al.*, 1998]. *Goertz et al.* [*1985*] were the first to relate ionospheric flow bursts observed by the STARE radar to magnetopause reconnection. They interpreted their results in terms of a ground signature of FTEs. However, as pointed out by *Glassmeier and Stellmacher* [*1996*], the interpretation of ionospheric transients in terms of FTEs is ambiguous when no suitable correlated spacecraft observations at the magnetopause are available. The first simultaneous observation of a FTE at the magnetopause and its associated flow enhancement in the ionosphere were made by *Neudegg et al.* [*1999*] using Equator-S spacecraft observations at the magnetopause and SuperDARN HF radar measurements in the ionosphere.

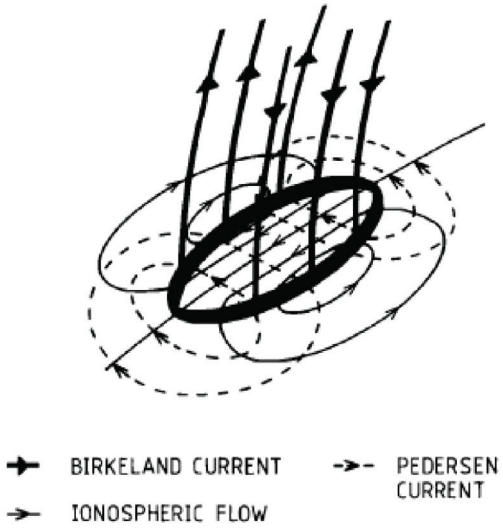

Figure 6: The field flow and current pattern set up by motion of the foot of a connected flux tube through the ionosphere (after *Southwood* [*1985; 1987*]). The pattern is appropriate for the northern hemisphere with a flux tube moving towards the left.

The *Southwood* [*1985; 1987*] model describes the ionospheric flow surrounding a single flux tube. According to his model, the motion of a newly reconnected flux will set up a vortex like plasma motion, with a bipolar associated FAC system (Figure 6). The FAC system along the edges of the flux tube transfers stress, and also drives the return flow outside the flux tube. Modeling the effects of elongated newly opened flux, *Lockwood et al.* [1990] proposed that the vortical nature of FTEs may not be very pronounced and that they appear as flow channels. The flow disturbance should be short lived, of the order of 10 minutes, and confined to a narrow region just polewards of the cleft [*M. Lockwood et al.*, 1990]. Their displacement in the ionosphere should though be by an amount which is not much greater than their own spatial extent. There has been a systematic search for the three key elements of the twin vortex flow in the *Southwood* [*1985; 1987*] model:

(1) The fast moving flux inside the newly opened flux tube [e. g. *Oksavik et al.*, 2005; *Pinnock et al.*, 1995; *Pinnock et al.*, 1993; *Provan et al.*, 1998].

(2) The pair of FAC sheets flowing on the edges of the flux tube to transfer stress [*Marchaudon et al.*, 2004; *Sandholt et al.*, 1990].

(3) The proposed return flow resulting from plasma being pushed aside by the motion of the flux tube [*Oksavik et al.*, 2005; *Pinnock et al.*, 1993; *Thorolfsson et al.*, 2000].

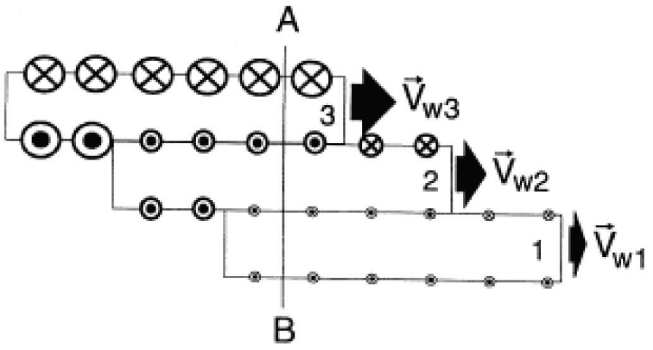

Figure 7: Three idealized square chunks of newly opened flux, produced by very short pulses of very fast reconnection with large IMF $B_Y > 0$ in the northern hemisphere. The northward (poleward) direction is toward the bottom of the figure, and the patches move westward (towards the right). The newest chunk is the most equatorwards, having the largest FACs. The chunks of plasma are appended immediately adjacent to each other. FAC sheets are indicated at the channel boundaries. Figure from *Lockwood et al*. [*2001*]

Lockwood et al. [*2001*] suggested a conceptual model for how a sequence of newly reconnected flux created due to very short reconnection pulses should arrange in the ionosphere (Figure 7). According to their model, channels of newly opened flux would append immediately adjacent to each other. The field aligned current sheets associated with each channel would decrease in strength as the tension force on each set of flux tubes decays with increasing time elapsed since reconnection.

2.4 Excitation of large scale ionopsheric flows in response to transient reconnection

A conceptual model to explain the excitation and decay of large-scale polar cap convection by transient reconnection was introduced by *Lockwood et al.* [1990] and *Cowley and Lockwood* [*1992*] (Figure 8). According to the model, the creation of new, open flux on the dayside impulsively displaces the open closed field line boundary equatorwards (Figure 8b). Flows are excited in order to move the perturbed boundary towards the new equilibrium configuration (Figure 8c). These flows are in accordance with the observed large scale ionospheric two cell convection. The contribution of FTEs to the total voltage across the

polar cap potential is not known. Using the *Russel and Elphic* [*1978; 1979*] circular flux tube model and interpreting magnetopause data yields estimates of 10-20 kV. The models by *Southwood et al.* [*1988*] and *Scholer* [*1988*] multiply this estimate by a factor roughly equal to the ratio of the length of the elongated neutral line to the diameter of the *Russel and Elphic* [*1978; 1979*] flux tube. This yields reconnection voltages of 50-100 kV for a 5-10 R_E long X line. *Lockwood et al.* [1990] have estimated that large FTEs contribute about 30 kV to the total transpolar voltage, which is about 30%. *Milan et al.* [*2000*] suggested based on combined HF radar and optical observations that an individual PMAF can extend azimuthally through 7 hours in MLT (~3500km). They interpreted their data within the context of the predicted ionospheric convection response to transient dayside reconnection as proposed by *Lockwood et al.* [1990] and *Cowley and Lockwood [1992],* and found their data consistent with each transient reconnection event not being an isolated pulse of reconnection, but an ongoing event propagating across large portions of the magnetopause. They also suggested that reconnection can occur at several positions on the magnetopause simultaneously.

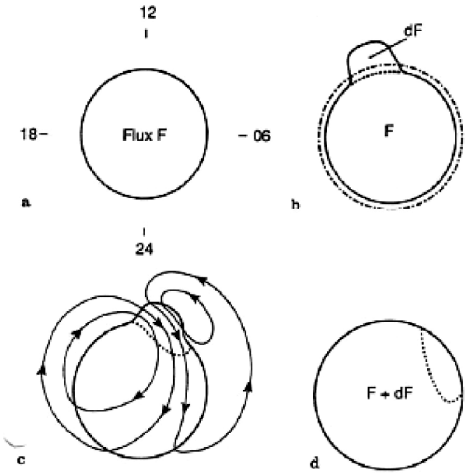

Figure 8: Sketch illustrating the response to an impulse of dayside reconnection, including the effect of IMF B_Y positive (northern hemisphere). a) Initial zero flow equilibrium configuration with open flux F, the solid line indicating the OCB. b) Perturbed OCB following the impulse, new zero flow equilibrium indicated by dashed line. c) Flows excited to take the system to the new equilibrium state. d) New

zero flow equilibrium with flux F+dF, the dotted line indicates the boundary of the open flux created during the impulse. Figure from *Cowley and Lockwood* [*1992*].

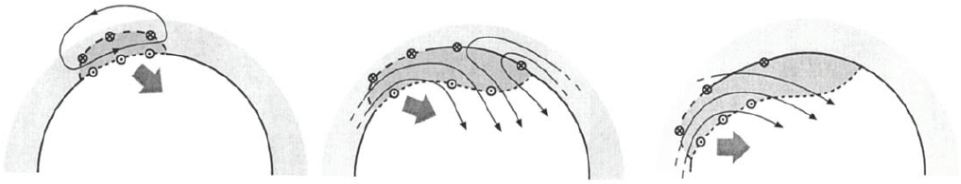

Figure 9: Schematic diagram illustrating a model of the ionospheric flow response to the addition of a region of new open flux to the front and the polar cap by an FTE for IMF Bz < 0, B_Y >0. Light grey shading indicates the location of the main auroral oval on closed field lines and dark grey shading indicates the region of newly opened flux. FACs indicated by circled dots and crosses. Figure by *Milan et al.* [*2000*].

3. Summary of papers:

Y. Rinne, J. Moen, K. Oksavik, and H. C. Carlson, Reversed flow events in the winter cusp ionosphere observed by the European Incoherent Scatter (EISCAT) Svalbard radar, *J. Geophys. Res.*, 112, A10313, doi:10.1029/2007JA012366, 2007

This paper presents a statistical study of the occurrence of meso-scale flow channels in the ion velocity data from the EISCAT Svalbard Radar during 11 days in January and December 2001. The term Reversed Flow Events (RFE) is introduced to describe this new class of flow channels. A Reversed Flow Event is an elongated segment of enhanced ion flow in the opposite direction of the background flow. RFEs seem be regular feature of the cusp ionosphere, occurring at least 16% of the time in the current data set. Their average lifetime is 19 minutes. They occur near the cusp inflow region in the MLT range from 11:45 to 12:45 in association with enhanced plasma flow, and seem to be L-shell aligned. The occurrence of RFEs is independend of IMF B_Z (and B_Y), and 86% of the RFEs were characterized by ion flow opposite to the magnetic tension force, meaning that they cannot be interpreted as FTE centre flux according to the *Southwood* [*1985; 1987*] model. RFEs coexist but never appear simultaneously, and can hence not be attributed the return flow around the same FTE as suggested by Oksavik et al. [*2004*]. In *Rinne et al.* [*2007*] we propose an asymmetric version of the Southwood [*1985; 1987*] model for significant IMF B_Y in which only the poleward cell located on open field lines develops.

J. Moen, **Y. Rinne**, H. C. Carlson, K. Oksavik, R. Fujii, and H. Opgenoorth, On the relationship between thin Birkeland current arcs and reversed flow channels in the winter cusp/cleft ionosphere, *J. Geophys. Res.*, 113, A09220, doi:10.1029/2008JA013061, 2008

Moen et al. [*2008*] present a combined optical and radar data study of RFEs. The occurrence of RFEs seems to be regulated by Birkeland current arcs in the winter cusp ionosphere, and that their onset occurs with the brightening of a discrete auroral arc near the OCB. The arc is found to separate from the background arc and be located at the sharp, clockwise flow reversal, consistent with a converging electric field and an upward field aligned current (FAC). *Moen et al.* [*2008*] find two categories of RFEs; one that propagates into the polar cap together with the poleward moving auroral forms, and one moving with the background arc. Common for both categories is that the RFE phenomenon is associated with a region void of precipitation. *Moen et al.* [*2008*] propose two possible explanations for the phenomenon: (1) the RFE channel may be a region where two MI current loops, forced by independent voltage generators, couple through a poorly conducting winter ionosphere, or (2) the RFE may be the ionospheric footprint of an inverted V-type coupling region.

Y. Rinne, J. Moen, H.C. Carlson, M. R. Hairston, Stratification of east-west plasma flow channels observed in the ionospheric cusp in response to IMF B_Y polarity changes, *Geophys. Res. Lett 2010,* 37, L13102, doi:10.1029/2010GL043307, 2010

This paper presents evidence for how a sequence of reconnection events results in the stratification of flow channels appended immediately adjacent to each other, as suggested conceptually by *Lockwood et al.* [2001]. During a period of predominantly north-westward flow for IMF B_Z negative and IMF B_Y positive, a sequence of three distinct negative excursions of IMF B_Y resulted in a train of three eastward directed flow channels, interleaved by westward flow enhancements consistent with the magnetic tension drag on newly opened field lines, propagating into the polar cap. The IMF B_Y reversals were accompanied by almost simultaneous IMF B_Z polarity reversals, and the IMF alternations likely stimulated two distinct reconnection sites on the magnetopause, one at a time. The observations are consistent with the view that a new region of reconnected flux manifests as development of a distinct flow channel near the polar cap boundary, and that successive events stay separated while

pushing each other into the polar cap. Each flow channel will remain separated from neighboring channels as long as the magnetic tension force with its associated field aligned current systems is maintained.

Y. Rinne, J. Moen, J. Baker, H.C. Carlson, Convection surrounding meso-scale ionospheric flow channels, 2010

Submitted to J. Geophys. Res.2010

In this paper we have attempted to visualize the flow surrounding meso scale ionospheric flow channels presented by *Rinne et al. [2010]* with the SuperDARN convection patterns. Radar data from the EISCAT Svalbard radar and DMSP satellite data were given as input into the SuperDARN convection patterns. The two most prominent eastward flow channels are in strong contrast to the general westward convection as they developed in response to sharp IMF B_Y polarity reversals. The resulting flow streamlines from the convection maps are consistent with the line of sight data from the ESR within a ~10 minute response time. They suggest twin vortex flow to form with the eastward channels being the twin vortices centre flow. We have, however, no vector data to confirm this vortex flow. Having been designed for large scale polar cap convection, the fitting algorithm has been pushed to its very limits in this analysis of meso scale features in terms of the spatial resolution as well as the types of flows it can represent. The flow lines suggest cell closure and plasma flow across the anticipated non-reconnecting OCB as well as FAC sheets. We have attempted a mixture of quantitative analysis and qualitative reasoning by looking to the convection patterns from the model as a guide, and evaluate where flows should be different based on our general knowledge. The two channels analyzed in this study contributed with 24 and 33 kV significantly to the overall polar cap potential. The strong flow shears associated with the flow channels may create plasma instabilities and turbulence with potential severe impact for communication and navigation systems in the Polar Regions [*Carlson et al.*, *2007*]. They also cause significant HF backscatter formation inside the channels.

4. Future Prospects

Common for both types of flow channels studied in this thesis is that more data is needed in order to be able to learn more and better understand the phenomena, their creation mechanisms, and their impact on man made technologies.

Still questions like their seasonal dependence and if and to what degree the two types of channels are related to one another remain unanswered. Also, the effect of the channels on convection needs to be investigated further in order to improve statistical convection patterns like the SuperDARN convection maps presented in the fourth paper. These maps are a great resource for understanding global convection and are much used to monitor the large scale conditions as background during campaigns. However, as shown in the fourth paper, the patterns have limitations when it comes to transient reconnection or multiple-site reconnection involving flow boundaries. More data is needed in order to improve the maps and learn more about how to include meso scale phenomena.

Hence, a larger data base, preferably including several incoherent scatter radars run simultaneously in order to cover larger portions of the polar cap in great detail, as well as other instruments both ground based and onboard spacecrafts providing additional information, is needed. Resolving the fine structure of the ionospheric cusp, is an important step towards opening the black box and understanding solar wind-magnetosphere coupling and its impact on the magnetosphere-ionosphere system and space weather effects.

5. References

Carlson, H. C., T. Pedersen, S. Basu, M. Keskinen, and J. Moen (2007), Case for a new process, not mechanism, for cusp irregularity production, *J. Geophys. Res., 112*(A11304), doi: 10.1029/2007JA012384.

Coleman, P. J., D. Leverett, and C. P. Sonett (1960), Steady component of the interplanetary magnetic field: PIONEER V, *Phys. Rev. Lett.*, *5*(2), 43-48.

Cowley, S. W. H., and M. Lockwood (1992), Excitation and decay of solar wind-driven flows in the magnetosphere-ionosphere system, *Annales Geophysicae*, *10*, 103-115.

Dungey, J. W. (1961), Interplanetary Magnetic Field and the Auroral Zones, *Physical Review Letters*, *6*(2), 47-48.

Fasel, G. J. (1995), Dayside poleward-moving auroral foms: A statistical study, *J. Geophys. Res.*, *100*, 11,891-811,905.

Glassmeier, K.-H., and M. Stellmacher (1996), Mapping Flux Transfer Events to the Ionosphere, *Advances in Space Research*, *18*(8), (8)151-(158)160.

Glassmeier, K. H., M. Lester, W. A. C. Mier-Jedrzejowicz, C. A. Green, G. Rostoker, D. Orr, U. Wedeken, H. Junginger, and E. Amata (1984), Pc5 pulsations and their possible source mechanisms - A case study, *J. Geophys. - Zeitschrift für Geophysik*, *55*, 108-119.

Goertz, C. K., E. Nielsen, A. Korth, K. H. Glassmeier, C. Haldoupis, P. Hoeg, and D. Hayward (1985), Observations of a possible ground signature of flux transfer events, *J. Geophys. Res.*, *90*, 4069-4078.

Gosling, J. T., M. F. Thomsen, S. J. Bame, T. G. Onsager, and C. T. Russell (1990), The electron edge of the low latitude boundary layer during accelerated flow events, *Geophysical Research Letters*, *17*(11), 1833-1836.

Greenwald, R. A., J. M. Ruohoniemi, K. B. Baker, A. Bristow, G. J. Sofko, J.-P. Villain, M. Lester, and J. Slavin (1999), Convection response to a transient increase in dayside reconnection, *J. Geophys. Res.*, *104*(A5), 10,007-010,015.

Haerendel, G., G. Paschmann, N. Sckopke, H. Rosenbauer, and P. C. Hedgecock (1978), The Frontside Boundary Layer of the Magnetosphere and the Problem of Reconnection, *J. Geophys. Res.*, *83*(A7), 3195-3216.

Heelis, R. A., J. K. Lowell, and R. W. Spiro (1982), A Model of the High-Latitude Ionospheric Convection Pattern, *J. Geophys. Res.*, *87*(A8), 6339-6345.

Heppner, J. P., and N. C. Maynard (1987), Empirical High-Latitude Electric Field Models, *J. Geophys. Res.*, *92*(A5), 4467-4489.

Jørgensen, T. S., E. Friis-Christensen, and J. Wilhjelm (1972), Interplanetary Magnetic-Field Direction and High-Latitude Ionospheric Currents, *J. Geophys. Res.*, *77*(10), 1976-1977.

Lockwood, M., S. W. H. Cowley, and M. P. Freeman (1990), The Excitation of Plasma Convection in the High-Latitude Ionosphere, *Journal of Geophysical Research*, *95*(A6), 7961-7972.

Lockwood, M., P. E. Sandholt, S. W. H. Cowley, and T. Oguti (1989), Interplanetary Magnetic Field Control of Dayside Auroral Activity and the Transfer of Momentum Across the Dayside Magnetopause, *Planetary Space Science*, *37*(11), 1347-1365.

Lockwood, M., S. W. H. Cowley, P. E. Sandholt, and R. P. Lepping (1990), The Ionospheric Signatures of Flux Transfer Events and Solar Wind Dynamic Pressure Changes, *J. Geophys. Res.*, *95*(A10), 17,113-117,135.

Lockwood, M., J. Moen, S. W. H. Cowley, A. D. Farmer, U. P. Løvhaug, H. Lühr, and V. N. Davda (1993), Variability of dayside convection and motions of the cusp/cleft aurora, *Geophys. Res. Lett.*, *20*, 1011-1014.

Lockwood, M., S. E. Milan, T. Onsager, C. H. Perry, J. A. Scudder, C. T. Russell, and M. Brittnacher (2001), Cusp ion steps, field-aligned currents and poleward moving auroral forms, *J. Geophys. Res.*, *106*(A12), 29,555-529,569.

Mansurov, S. M. (1969), New evidence of a relationship between magnetic fields in space and on earth, *Geomagn. Aeron.*, *9*, 622-623.

Marchaudon, A., J.-C. Cerisier, R. A. Greenwald, and G. J. Sofko (2004), Electrodynamics of a flux transfer event: Experimental test of the Southwood model, *Geophys. Res. Lett., 31*, doi: 10.1029/2004GL019922.

Milan, S. E., M. Lester, S. W. H. Cowley, and M. Brittnacher (2000), The convection and auroral response to a southward turning of the IMF: POLAR UVI, CUTLASS and IMAGE signatures of transient magnetic flux transfer at the magnetopause, *J. Geophys. Res.*, *105*(15741-15755).

Moen, J., H. C. Carlson, and P. E. Sandholt (1999), Continuous Observation of Cusp Auroral Dynamics in Response to an IMF By Polartity Change, *Geophys. Res. Lett.*, *26*(9), 1243-1246.

Moen, J., A. P. van Eyken, and H. C. Carlson (2001), EISCAT Svalbard Radar observations of ionospheric plasma dynamics in relation to dayside auroral transients, *J. Geophys. Res.*, *106*(21453-21461).

Moen, J., Y. Rinne, H. C. Carlson, K. Oksavik, R. Fujii, and H. Opgenoorth (2008), On the relationship between Birkeland current arcs and reversed flow channels in the winter cusp/cleft ionosphere, *Journal of Geophysical research, 113*, doi: 10.1029/2008JA013061.

Moen, J., P. E. Sandholt, M. Lockwood, W. F. Denig, U. P. Løvhaug, B. Lybekk, A. Egeland, D. Opsvik, and E. Friis-Christensen (1995), Events of Enhanced Convection and Related Dayside Auroral Activity, *J. Geophys. Res.*, *100*(A12), 23,917-923,934.

Neudegg, D. A., T. K. Yeoman, S. W. H. Cowley, G. Provan, G. Haerendel, W. Baumjohann, U. Auster, K.-H. Fornacon, E. Georgescu, and C. J. Owen (1999), A flux transfer event observed at the magnetopause by the Equator-S spacecraft and in the ionosphere by the CUTLASS HF radar, *Annales Geophysicae*, *17*, 707-711.

Nishitani, N., T. Ogawa, M. Pinnock, M. P. Freeman, J. R. Dudeney, J.-P. Villain, K. B. Baker, N. Sato, H. Yamagishi, and H. Matsumoto (1999), A very large scale flow burst observed by the SuperDARN radars, *J. Geophys. Res.*, *104*, 22,469-422,486.

Oksavik, K., J. Moen, and H. C. Carlson (2004), High-resolution observations of the small-scale flow pattern associated with a poleward moving auroral form in the cusp, *Geophys. Res. Lett., 31*, doi: 10.1029/2004GL019838.

Oksavik, K., J. Moen, H. C. Carlson, R. A. Greenwald, S. E. Milan, M. Lester, W. F. Denig, and R. J. Barnes (2005), Multi-instrument mapping of the small-scale flow dynamics related to a cusp auroral transient, *Annales Geophysicae, 23*, 2657-2670.

Pinnock, M., A. S. Rodger, J. R. Dudeney, F. J. Rich, and K. B. Baker (1995), High spatial and temporal resolution observations of the ionospheric cusp, *Annales Geophysicae*, *13*, 919-925.

Pinnock, M., A. S. Rodger, J. R. Dudeney, K. B. Baker, P. T. Newell, R. A. Greenwald, and M. E. Greenspan (1993), Observations of an Enhanced Convection Channel in the Cusp Ionosphere, *J. Geophys. Res.*, *98*(A3), 3767-3776.

Provan, G., T. K. Yeoman, and S. E. Milan (1998), CUTLASS Finland radar observations of the ionospheric signature of flux transfer events and the resulting plasma flow, *Annales Geophysicae*, *16*, 1411-1422.

Rinne, Y., J. Moen, K. Oksavik, and H. C. Carlson (2007), Reversed flow events in the winter cusp ionosphere observed by the European Incoherent Scatter (EISCAT) Svalbard radar, *Journal of Geophysical research, 112*, doi: 10.1029/2007JA012366.

Rinne, Y., J. Moen, H. C. Carlson, and M. R. Hairston (2010), Stratification of east-west plasma flow channels observed in the ionospheric cusp in response to IMF BY polarity changes, *Geophys. Res. Lett., 37*, doi: 10.1029/2010GL043307.

Russell, C. T., and R. C. Elphic (1978), Initial ISEE Magnetometer Results: Magnetopause Observations, *Space Science Reviews*, *22*, 681-715.

Russell, C. T., and R. C. Elphic (1979), ISEE Observations of Flux Transfer Events at the Dayside Magnetopause, *Geophys. Res. Lett.*, *6*(1), 33-36.

Sandholt, P. E., C. J. Farrugia, J. Moen, and S. W. H. Cowley (1998), Dayside auroral configurations: Responses to southward and northward rotations of the interplanetary magnetic field, *J. Geophys. Res.*, *103*, 20,279-220,295.

Sandholt, P. E., J. Moen, A. Rudland, D. Opsvik, W. F. Denig, and T. Hansen (1993), Auroral Event Sequences at the Dayside Polar Cap Boundary for Positive and Negative Interplanetary Magnetic Field By, *Journal of Geophysical Research*, *98*(A5), 7737-7755.

Sandholt, P. E., M. Lockwood, T. Oguti, S. W. H. Cowley, K. S. C. Freeman, B. Lybekk, A. Egeland, and D. M. Willis (1990), Midday Auroral Breakup Events and Related Energy and Momentum Transfer from the Magnetosheath, *J. Geophys. Res.*, *95*(A2), 1039-1060.

Scholer, M. (1988), Magnetic Flux Transfer at the Magnetopause based on single X line bursty reconnection, *Geophys. Res. Lett.*, *15*(4), 291-294.

Southwood, D. J. (1985), Theoretical aspects of ionosphere-magnetosphere-solar wind coupling, *Advances in Space Research*, *5*(4), 7-14.

Southwood, D. J. (1987), The Ionospheric Signature of Flux Transfer Events, *J. Geophys. Res.*, *92*(A4), 3207-3213.

Southwood, D. J., and W. J. Hughes (1982), Theory of hydromagnetic waves in the magnetosphere, *Space Science Rewievs*, *35*, 301-366.

Southwood, D. J., C. J. Farrugia, and M. A. Saunders (1988), What are Flux Transfer Events?, *Planet. Space Sci.*, *36*(5), 503-508.

Svalgaard, L. (1968), Sector structure of the interplanetary magnetic field and the daily variation of the geomagnetic field at high latitudes, *Geophys. Pap. Dan. Met. Inst. Geophys.*, *R-6*(11), p. 11.

Svalgaard, L. (1972), Interplanetary Magnetic-Sector Structure, 1926-1971, *J. Geophys. Res.*, *77*(22).

Taguchi, S., M. Sugirua, J. D. Winningham, and J. A. Slavin (1993), Characterization of the IMF BY_Dependent Field-Aligned Currents in the Cleft Region Based on DE 2 Observations, *J. Geophys. Res.*, *98*, 1393-1407.

Thorolfsson, A., J.-C. Cerisier, M. Lockwood, P. E. Sandholt, C. Senior, and M. Lester (2000), Simultaneous optical and radar signatures of poleward-moving auroral forms, *Annales Geophysicae*, *18*, 1054-1066.

Øieroset, M., P. E. Sandholt, W. F. Denig, and S. W. H. Cowley (1997), Northward interplanetary magnetic field cusp aurora and high-latitude magnetopause reconnection, *Journal of Geophysical Research*, *102*(A6), 11,349-311,362.

I

JOURNAL OF GEOPHYSICAL RESEARCH, VOL. 112, A10313, doi:10.1029/2007JA012366, 2007

Reversed flow events in the winter cusp ionosphere observed by the European Incoherent Scatter (EISCAT) Svalbard radar

Y. Rinne,[1] J. Moen,[1,2] K. Oksavik,[3] and H. C. Carlson[1,4]

Received 27 February 2007; revised 13 June 2007; accepted 20 June 2007; published 31 October 2007.

[1] High-resolution fast azimuth sweeps by the European Incoherent Scatter (EISCAT) Svalbard radar provide an unparalleled opportunity to study small-scale flow disturbances in the cusp ionosphere. Observations from 11 days of the winter cusp ionosphere of high-resolution ion flow data have been analyzed. Transient channels of reversed plasma flow appear to be a regular feature of the cusp, and they were seen in 16% of 767 analyzed EISCAT Svalbard Radar (ESR) scans. We introduce a new descriptive term, reversed flow events (RFEs), for this class of events. RFEs are defined as longitudinally elongated segments of transiently enhanced ion flow in the direction opposite to the background flow. RFEs typically occurred near the cusp inflow region in association with enhancements in the polar cap convection observed by the Super Dual Auroral Radar Network (SuperDARN). Their lifetime was found to be ~19 min on average. Their longitudinal dimension typically exceeded the ESR field of view (>400–600 km), and ranged from ~50 to 250 km in latitude. The occurrence rate of RFEs appears independent of the B_Z and B_Y component polarity of the interplanetary magnetic field (IMF), and RFEs occurred for clock angles between 40° and 240°. RFE ion flow was in 95% of the cases documented to oppose the magnetic tension force, and RFEs cannot be interpreted in terms of newly opened flux. RFEs formed one by one and never simultaneously in pairs. To explain these observations, we propose an asymmetric version of the Southwood (1987) twin cell flux transfer event model to account for significant IMF B_Y, in which only the poleward cell located on open field lines develops.

Citation: Rinne, Y., J. Moen, K. Oksavik, and H. C. Carlson (2007), Reversed flow events in the winter cusp ionosphere observed by the European Incoherent Scatter (EISCAT) Svalbard radar, *J. Geophys. Res.*, *112*, A10313, doi:10.1029/2007JA012366.

1. Introduction

[2] Magnetic reconnection was first described by *Dungey* [1961] as a steady process. Several years later, *Russel and Elphic* [1978, 1979] and *Haerendel et al.* [1978] found evidence for a pulsed nature of the reconnection process. This transient, impulsive reconnection at the dayside magnetopause is called flux transfer events (FTEs). The first radar observations of FTE flow transients were carried out by *van Eyken et al.* [1984] and *Goertz et al.* [1985].

[3] *Southwood* [1987] proposed a model of the plasma flow associated with the ionospheric footprint of an FTE, hereafter referred to as the Southwood model. According to this model, a pair of field-aligned currents (FAC) with opposite polarity flows on the poleward and equatorward edge of the newly reconnected flux tube and transfers stress to the ionosphere. The resulting motion of the foot of the flux tube through the ionosphere sets up a twin vortex flow pattern. This pattern is understood as the newly opened flux moving faster than the surrounding flux, pushing its way through the plasma and thereby creating return flow on either side.

[4] Over the past 2 decades there have been made many attempts to find observational evidence for the Southwood model. *Lockwood et al.* [1989] and *Sandholt et al.* [1990] suggested that discrete cusp auroral events are related to flow shears consistent with the clockwise cell of the Southwood FTE model. However, *Lockwood et al.* [1990] suggested that the return flow in the Southwood model may not be very pronounced, but rather a reduction in the background convection. *Denig et al.* [1993] reported evidence for a Southwood FTE twin-cell moving with the large-scale convection. *Pinnock et al.* [1993] reported the observation of a "longitudinally elongated (>900 km), latitudinally narrow (~100 km) channel of enhanced convection" by combining observations from the PACE high-frequency (HF) radar and the DMSP F9 polar-orbiting satellite. Within the channel, the line-of-sight velocity of the plasma was enhanced compared to the background flow. In the regions bordering the channel, the background flow was diminished, however not reversed. *Pinnock et al.* [1993] interpreted the weakening of the background convection as return flow in the Southwood model as proposed by *Lockwood et al.* [1990].

[1]Department of Physics, University of Oslo, Oslo, Norway.
[2]Arctic Geophysics, University Centre in Svalbard, Longyearbyen, Norway.
[3]Johns Hopkins University Applied Physics Laboratory, Laurel, Maryland, USA.
[4]Center for Atmospheric and Space Sciences, Utah State University, Logan, Utah, USA.

0148-0227/07/2007JA012366$09.00

[5] *Marchaudon et al.* [2004] observed an azimuthally elongated convection enhancement by two Super Dual Auroral Radar Network (SuperDARN) radars in conjunction with FACs observed by the Ørsted satellite. They found that the direction of the FAC pair was in entirely agreement with the Southwood model. Furthermore, the current densities of each FAC and the Pedersen current indicated that the closure current for the pair of FACs was inside the flow burst. The dimensions of the ionospheric convection enhancement were 1000 km in length and 100 km in width, and the flow was larger than 1000 m/s, exceeding the background flow. *Marchaudon et al.* [2004] claimed the validity of the Southwood model based on their observations.

[6] The development of the Special Norwegian Fast Azimuth Scan Mode (SP-NO-FASM) for the European Incoherent Scatter (EISCAT) Svalbard Radar (ESR) by *Carlson et al.* [2002] provided a new tool to map out flow patterns with high spatial and temporal resolution. *Oksavik et al.* [2004, 2005] reported the first high resolution measurements of the flow disturbance around poleward moving auroral forms (PMAFs) by this radar technique. *Oksavik et al.* [2004] concluded that the spatial structure of a small-scale twin-cell system was in accordance with the Southwood prediction. The enhanced convection channel interpreted as the center flux in the Southwood model was only 50–60 km wide, and surrounded by flow running in the opposite direction. The PMAF was situated at the poleward edge of the flow channel thereby being consistent with the signature of an upward Birkeland current filament as predicted by the Southwood model. *Oksavik et al.* [2005] presented a train of narrow flow channels associated with a sequence of PMAFs. They plausibly related reversed flow channels to flux transfer events.

[7] *Neudegg et al.* [2000] showed that reconnection bursts at the magnetopause may take place for a wide range of clock angles from 30° to 330°. Hence if reversed flow channels represent an observable FTE signature, such as stated by *Oksavik et al.* [2005], they should be a frequently occurring phenomenon in the SP-NO-FASM database. In this study, the available SP-NO-FASM database has been analyzed systematically with the aim to characterize the occurrence and lifetime as well as dependency on magnetic local time (MLT) and interplanetary magnetic field (IMF) conditions of transient flow channels with reversed plasma flow with respect to the background convection. We focus on the RFE events as they have not been resolved by other radars and hence represent a new observable feature. Interestingly, we find that RFE events never develop in pairs, which means that they cannot be a symmetric Southwood FTE pattern.

[8] This paper is structured in the following way: Section 2 describes the instrument modes and techniques used in the study; section 3 introduces the data set and the analysis criteria that were used by providing one event as an example. Section 4 presents the results, followed by the discussion in section 5 and a summary in section 6.

2. Instrument Modes and Techniques

[9] This section provides brief descriptions of the ESR scan mode that has been used to gather the data (section 2.1), the SuperDARN global convection maps (section 2.2), and how the time lag between the Advanced Composition Explorer (ACE) satellite and the ionospheric response has been calculated (section 2.3).

2.1. ESR Scan Mode

[10] The primary data source in this paper is ionospheric line-of-sight data from the SP-NO-FASM program at the ESR which is located in Longyearbyen (78.15°N and 16.03°E). This windshield wiper mode was originally designed by *Carlson et al.* [2002] to monitor the formation of polar cap patches near the cusp inflow region with an unprecedented combination of wide area coverage (~600 km in width × 1000 km in length), quick scan time (2 min), and fine spatial resolution (~15 km × 30 km). Magnetic noon at the ESR site corresponds to 0900 universal time (UT).

[11] In the SP-NO-FASM program, the ESR 32 m steerable antenna sweeps azimuthally back and forth at a fixed elevation angle of 30°. The sweeps follow the surface of a cone. The azimuth angle is determined with respect to geographic north (0° and 360°) increasing clockwise. The elevation angle is the angle with the horizon increasing from 0° to 90° at zenith. In the discussion to follow elevation refers to the angle between the radar dish pointing direction and the local horizon; i.e., so that 150° elevation and 0° azimuth will be referred to as 30° elevation and 180° azimuth. The transmission pulse code used for the SP-NO-FASM program is tau0, consisting of two 960 μs alternating codes that are sampled every 16 μs (2.4 km). The first of the two alternating codes, AC1, covers ranges from 212 to 1306 km, whereas the second, AC2, covers the region between 58 and 1153 km. Data is stored every 3.2 s, and each 3.2 s data set has been analyzed separately.

[12] Reconnection signatures can be expected in the dayside boundary layers, the low-latitude boundary layer (LLBL), cusp, and mantle. These boundary layers typically span from 0900 to 1500 MLT [*Newell and Meng*, 1992] but due to IMF B_Y controlled shifts around magnetic noon may start as early as 0600 MLT and end as late as 1800 MLT [*Milan et al.*, 2000; *Moen et al.*, 2001; *Newell et al.*, 2004]. The width of the instantaneous active cusp may be at least 4 hours or more in MLT [*Maynard et al.*, 1997]. Under moderate conditions the daytime auroral precipitation region is located around 75° magnetic latitude (MLAT), but depending on IMF B_Z strength and polarity the precipitation region and reconnection signatures may be located between 70° and 80° MLAT [*Sandholt et al.*, 1998].

[13] In this radar study we have not made any attempt to locate the cusp precipitation region. However, during the campaign the ESR sweeps were directed toward where the active cusp region was assumed to be for the prevailing IMF conditions and MLT. Scanning at a constant elevation of 30° the radar field of view extends over ~1.5 hours in MLT along the line-of-sight if pointed directly east or west, and ~7° in latitude if pointed north or south. The fan-shaped field of view spanned usually 90–120° in azimuth throughout the data set, which means that the ESR can give an instantaneous snapshot of up to half the area of the cusp at one time. If the ESR was situated in the middle of the cusp and was scanning 360° in azimuth, it could in principle see most of the cusp except from a large "doughnut hole"

Table 1. Overview of Available European Incoherent Scatter (EISCAT) Svalbard Radar (ESR) Data and Specification of the Scan Modes Used

Date (2001)	Available ESR Data	Elevation, deg	Azimuth, deg	Azimuth Width, deg	Period, s	Speed, deg/s	Excluded Scans	Number of Scans	Center MLT
16.01.	06:03:10–07:38:34	30	−75 to 15	90	128	0.703	None	45	08:33:10–10:08:34
16.01.	08:34:22–11:01:34	30	−165 to −75	90	128	0.703	9:10, 9:20, 11:01	64	10:24:22–12:51:34
17.01.	06:01:02–07:15:07	30	15 to 105	90	128	0.703	6:01, 6:11, 6:13	32	10:11:02–11:25:07
17.01.	09:16:02–10:50:38	30	−75 to 15	90	128	0.703	9:16,	44	11:46:02–13:20:38
18.01.	06:05:07–07:34:18	30	30 to 90	60	192	0.313	All	0	09:05:07–10:34:18
19.01.	06:02:38–07:57:47	30	15 to 105	90	128	0.703	None	54	10:12:38–12:07:47
19.01.	09:31:42–11:59:46	30	−75 to 15	90	128	0.703	11:58	69	12:01:42–14:29:46
20.01.	06:03:02–07:17:17	30	15 to 105	90	128	0.703	6:19–6:34 (7 scans)	28	10:13:02–11:27:17
20.01.	09:55:22–10:59:54	30	−75 to 15	90	128	0.703	10:59	30	12:25:22–13:29:54
15.12.	06:03:54–07:46:15	30	0 to 120	120	192	0.625	6:38, 7:01	26	10:13:54–11:56:15
15.12.	09:08:17–09:27:26	30	0 to 120	120	192	0.625	None	6	13:18:17–13:37:26
15.12.	09:28:30–10:59:54	150 (30)	0 to 120 (180–300)	120	192	0.625	None	29	11:18:30–12:49:54
16.12.	06:05:01–06:30:05	30	−60 to 60	120	192	0.625	None	8	07:55:01–08:20:05
16.12.	06:30:43–08:19:28	30	0 to 120	120	192	0.625	None	34	10:40:43–12:29:28
16.12.	08:20:06–09:30:24	30	−60 to 60	120	192	0.625	None	22	11:20:06–12:30:24
16.12.	09:31:28–10:59:54	150 (30)	0 to 120 (180–300)	120	192	0.625	None	28	11:21:28–12:49:54
17.12.	06:05:30–06:58:27	30	0 to 120	120	192	0.625	6:30, 6:52, 6:56	9	10:15:30–11:08:27
17.12.	10:01:01–10:59:44	150 (30)	0 to 120 (180–300)	120	192	0.625	10:58	19	11:51:01–12:49:44
18.12.	06:31:02–08:06:59	30	0 to 120	120	192	0.625	8:03	29	10:41:02–12:16:59
18.12.	09:22:59–10:31:47	150 (30)	0 to 120 (180–300)	120	192	0.625	10:30	21	11:12:59–12:21:47
18.12.	10:45:10–10:59:54	30	−225 to 135	360	512	0.703	None	2	13:45:10–13:59:54
19.12.	06:00:51–08:20:26	30	0 to 120	120	192	0.625	8.08, 8:17	41	10:10:51–12:30:26
19.12.	08:22:11–08:47:38	150 (30)	0 to 120 (180–300)	120	192	0.625	None	8	10:12:11–10:37:38
20.12.	06:00:01–07:58:22	30	0 to 120	120	192	0.625	7:37	33	10:10:01–12:08:22
20.12.	10:06:47–10:57:56	150 (30)	0 to 120 (180–300)	120	192	0.625	None	16	11:56:47–12:47:56
21.12.	06:00:38–10:59:15	30	−180 to 180	360	256	1.406	None	70	09:00:38–13:59:15

around Longyearbyen, resulting from the fact that the SP-NO-FASM does not receive data from below 200 km altitude or overhead the radar site.

2.2. SuperDARN Global Convection Maps

[14] SuperDARN consists of a network of HF radars with overlapping fields of view in the northern and southern hemispheres. HF radars are sensitive to backscatter from field-aligned ionospheric irregularities in the order of decameters. The main purpose of SuperDARN is to provide global and continuous observations of the large-scale ionospheric convection pattern. These convection maps are produced by combining the line-of-sight velocity data from the entire SuperDARN network in one hemisphere and information from a statistical model parameterized by IMF conditions where no velocity measurement is available. The technique was first developed by *Ruohoniemi and Baker* [1998] and has later been refined by *Shepherd and Ruohoniemi* [2000].

[15] In order to put the plasma convection and mesoscale features monitored by the ESR into a global polar cap convection context, SuperDARN convection maps were used. These convection maps were retrieved from the Johns Hopkins University Applied Physics Laboratory (JHU/APL) Web site and are averaged over 2 min. A new map is available every 10 min.

2.3. ACE IMF Data

[16] In order to put an event in the ionosphere in the context of IMF, it is necessary to determine the time lag between the ACE satellite orbiting the first Lagrange point and the ionospheric response.

[17] This propagation delay from ACE to the magnetopause was estimated by averaging the solar wind bulk speed and the geocentric solar magnetospheric (GSM) X coordinate for the satellite position over a time period of 1 hour around an event (30 min before and after event onset/stop). The position of the magnetopause was calculated by the formula used by *Rodger* [1998] and a 6 min delay was added to the total time lag to account for the propagation time from the magnetopause to the *F* region ionosphere [*Moen et al.*, 2004].

3. Presentation of the Database and Analysis

[18] This section starts by presenting the database (section 3.1), followed by a description of the criteria that have been used to analyze the data (section 3.2), and it concludes by giving an example of an RFE (section 3.3).

3.1. Database

[19] The data set examined in this study consists of all ESR line-of-sight data from daytime SP-NO-FASM scans at constant 30° elevation during 12 days between 16–20 January 2001 and 15–21 December 2001. All data have been checked carefully for quality, and intervals of transmitter problems affecting the reliability of the ion velocity measurements have been removed. This was the case for three scans from 17 January 2001 (0601–0602, 0611–0613, and 0613–0615 UT), seven scans from 20 January 2001 (0619–0634 UT), and all data on 18 January 2001. Furthermore, 18 incomplete scans were also excluded. The remaining data set consists of 35 hours and 49 min of observations in a total of 767 scans. Table 1 lists the dates (first column) and time intervals (second column) of avail-

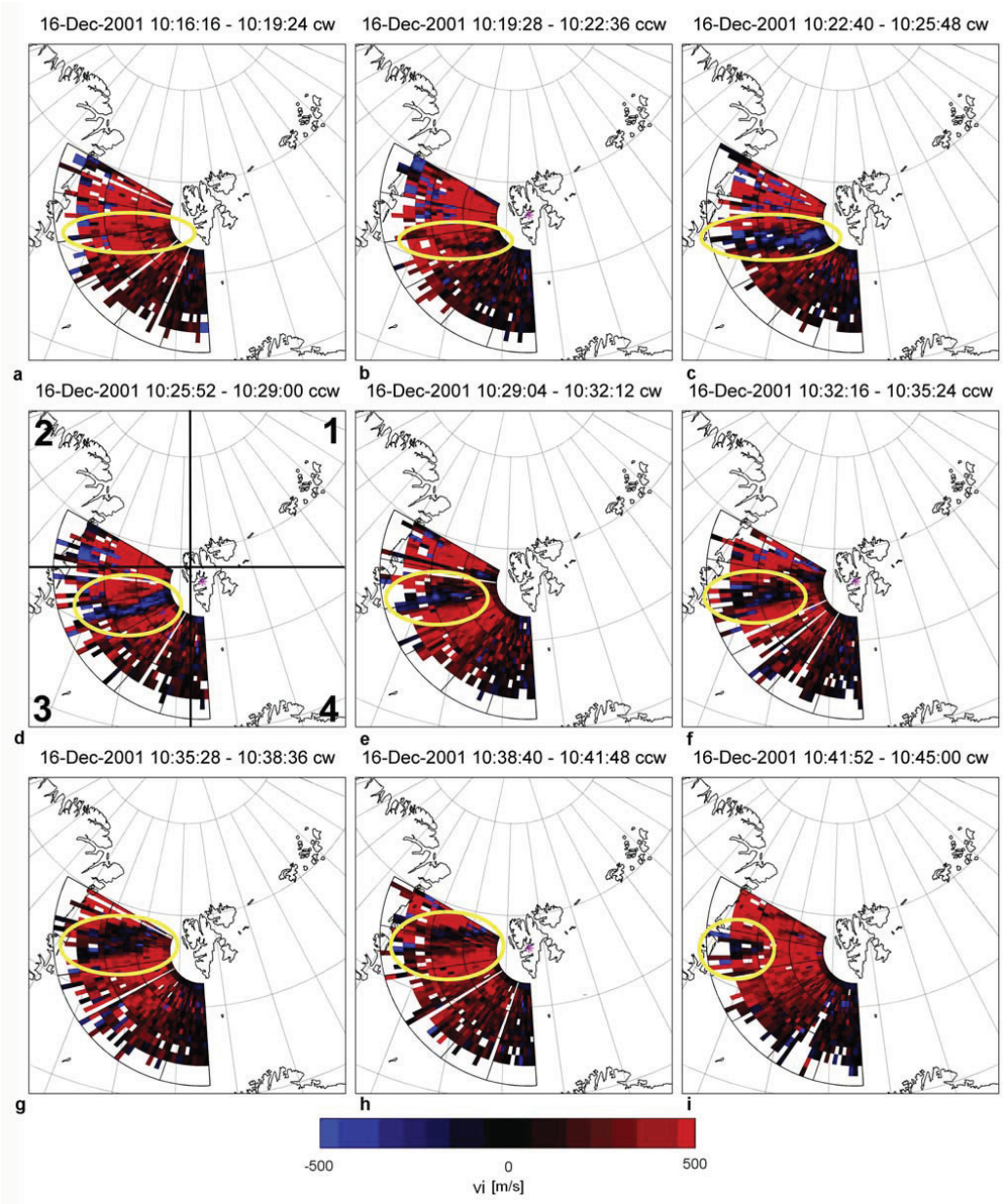

Figure 1. (a–i) A sequence of ion velocity fan plots from the European Incoherent Scatter (EISCAT) Fast Azimuth Scan Mode (FASM), in geographic coordinates. Data were projected along the magnetic field to a common reference altitude of 250 km. Positive velocities indicates line-of-sight ion flow directed away from the radar. The date and time as well as the radar sweep direction (clockwise "cw" and counterclockwise "ccw") are indicated on the top of each figure. The reversed flow event (RFE) is marked by a yellow ellipse. The quadrant definition in Figure 1d is used to sort the occurrence of RFEs in geographic regions relative to the EISCAT Svalbard radar (ESR) site. According to the definition, the RFE, seen as a blue stripe inside the yellow ellipse, is located in the third quadrant.

able data. Details about the scan pattern are specified in columns 3–7. Columns 3–5 list the constant elevation angle, the azimuth range and the azimuth width covered by a single sweep, and columns 6 and 7 contain the time it takes to complete a single sweep and the azimuthal speed of the ESR dish. The scans that are not used in the analysis are listed in column 8, and column 9 specifies the total number of scans that went into the analysis for each time period.

[20] Depending on the azimuth range, the ESR field of view extends 2–4 hours in MLT. The MLT listed in column 10 refers to the centre position in longitude of the ESR field of view.

[21] Since the ESR scans are at 30° elevation, the data is obtained from increasing altitude for increasing distance from the ESR site. In order to ease the comparison with data from other sources there is a need to project the data to a common reference altitude. At altitudes where collisions between charged particles and neutrals can be ignored, the frozen-in concept is valid and both electron and ions drift with same velocity perpendicular to the electric field. This is typically the case in the *F* region ionosphere above 200 km. As shown in Figure 1 (ion velocity plot), we have therefore projected the primary plasma parameter v_i along the magnetic field to a common reference altitude of 250 km, an altitude conventionally assumed for 630.0 nm optical emissions. Positive ion velocities (red) are directed away from the radar along the line of sight, whereas negative velocities toward the radar along the line of sight are colored blue. Missing data values are plotted as white.

3.2. Analysis Criteria

[22] Since the ion drift velocity data contained much fine structure, clear and strict selection criteria had to be defined:

3.2.1. Reversed Flow Event (RFE) Definition

[23] An RFE, or flow channel, is an elongated segment of enhanced ion flow in the opposite direction to the background flow. The background flow is the large-scale plasma convection in the polar cap. SuperDARN convection maps were retrieved from JHU/APL and used to verify the large-scale flow context of the ESR observations. In order for an event to qualify as RFE the following criteria have to be fulfilled:

[24] 1. The RFE has to be evident in more than one radar beam direction (azimuth position). This criterion eliminates questionable measurements.

[25] 2. The line-of-sight ion drift velocity inside the RFE must be >|250| m/s for at least one scan during the lifetime of the event.

[26] 3. The longitudinal extent of an RFE has to exceed 400 km in the radar field of view.

[27] 4. The RFE has to stay in clear contrast to the background flow, i.e., the background flow must exhibit uniform and opposite velocities >|250| m/s in the area surrounding the RFE for at least one scan.

[28] 5. The RFE has to be embedded within the background flow for at least one scan (this criterion avoids large-scale convection reversals being detected as RFE).

3.2.2. Flow Structure Definition

[29] Flow signatures which do not satisfy all criteria but resemble the beginning of an RFE (like in Figures 1a and 1b (1016 and 1019 UT)) have been classified as "flow structures."

[30] In addition to the fact that the ESR field of view is only capable of seeing parts of the active cusp and that there are uncertainties with regard to the exact location of the cusp, the direction of plasma flow inside an RFE as well as the orientation of the background convection is important for whether or not the ESR is sensitive to flow events. The ESR is only sensitive to plasma motion along its line-of sight, and insensitive to plasma flow perpendicular to the pointing direction. According to point 4 of the RFE definition, the background flow must exhibit uniform velocity higher than ±|250| m/s along the line-of-sight in the region of the RFE and the RFE itself must be higher than ±|250| m/s in the opposite direction. Hence RFEs cannot be detected when either the large-scale background convection and/or the RFE flow channel is oriented perpendicular to the radar line of sight. Assuming an ion flow velocity of ~1000 m/s, the ±|250| m/s criterion means a maximum angle between the flow vector and ESR line of sight of 75°. Any larger offset will result in an ion flow component along the ESR line of sight less than |250| m/s and hence not qualify for RFE detection.

3.3. An Example RFE

[31] Figure 1 shows a typical example of an ESR scan sequence. The nine scans on the 16 December 2001 from 1016 UT to 1045 UT indicate the development of an RFE in the ESR field of view. The RFE is highlighted by a yellow ellipse in each figure. As can be read from Table 1 column 4, the ESR scanned 120° azimuth from 180° to 300°. The background plasma convection monitored by the ESR is uniform and predominantly directed westward except from the southern part of the scan where the ESR line of sight velocity is not sensitive to zonal flow.

[32] Before we consider the high-resolution flow data in more detail, we will present the large-scale context provided by SuperDARN. Figure 2 shows a sequence of SuperDARN convection maps covering the whole time period of the RFE, with the ESR field of view indicated. SuperDARN had good coverage in the ESR field of view. Svalbard was located slightly postnoon in a region of high plasma convection directed mostly northwestward. This convection pattern is consistent with the background flow seen by the ESR.

[33] The IMF conditions for this time period are shown in Figure 3. As can be seen, IMF B_Y was strongly positive during the whole time interval. IMF B_Z was positive as well, except for a brief negative excursion around 1035 UT. The SuperDARN polar cap convection pattern exhibited a twin cell nature, indicative of reconnection driven flows, and the well-developed dusk convection cell is consistent with positive IMF B_Y.

[34] Having in mind that the ESR field of view was situated under westward large-scale convection in the post-noon sector, we return to Figure 1. The RFE started out as a reduction of the background flow (1016–1019 UT) before it rapidly developed to a pronounced channel of strongly reversed ion flow with respect to the background convection (seen from 1022–1025 UT). From 1029 to 1045 UT, the RFE moved northward and weakened before fading. Such narrow, well-defined, transient small-scale flow channels have been found frequently throughout the data set. Some, but not all, broaden and/or move north/south before they

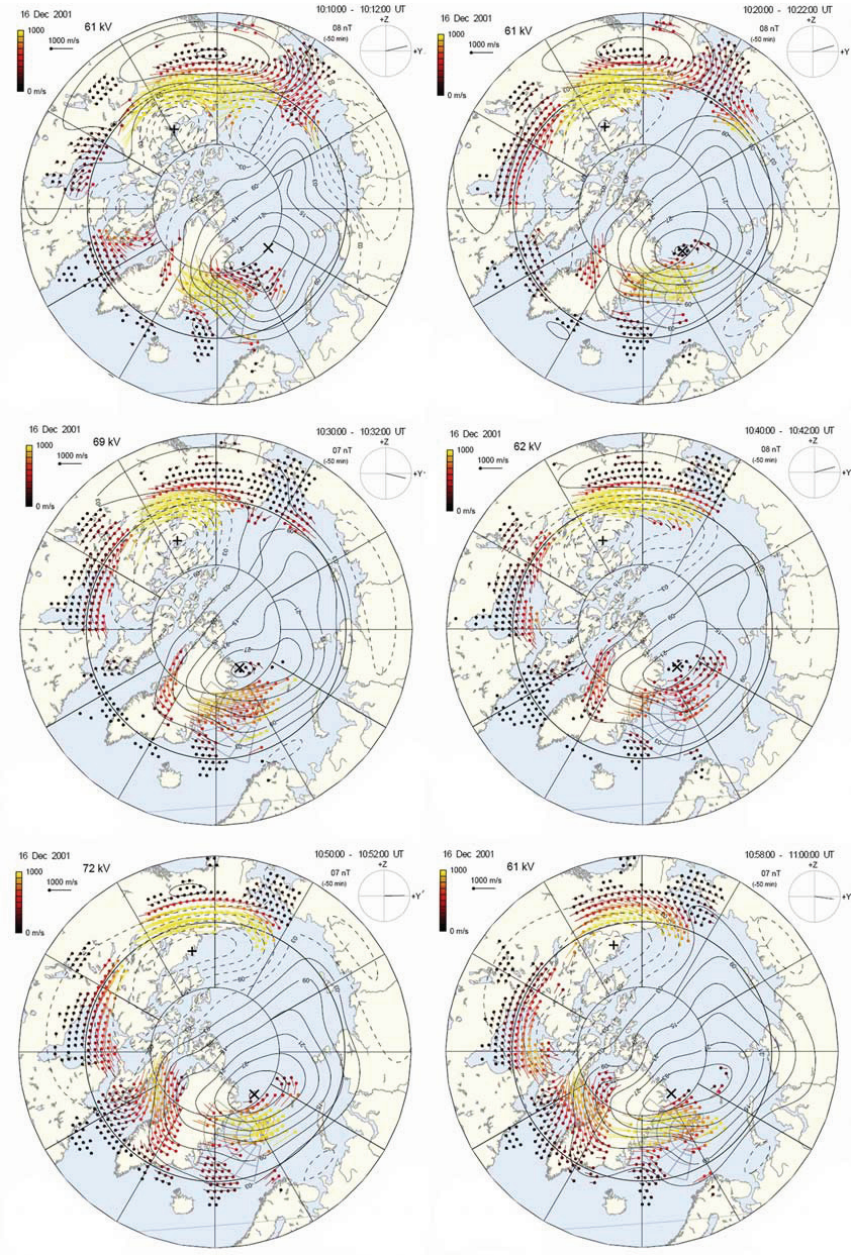

Figure 2. A sequence of SuperDARN global convection patterns, in magnetic coordinates. Indicated are polar cap potential contours and flow vectors based on SuperDARN measurements of the convection. Noon (1200 MLT) is at the bottom of each figure. In addition, the ESR field of view has been superimposed. The global convection maps were retrieved from the Johns Hopkins University Applied Physics Laboratory (JHU/APL). They are averaged over 2 min and a new map is available every 2 min. A propagation time from ACE to the ionospheric response of 50 min was assumed, which is consistent with the 47 min calculated for the actual time period (see section 2.3).

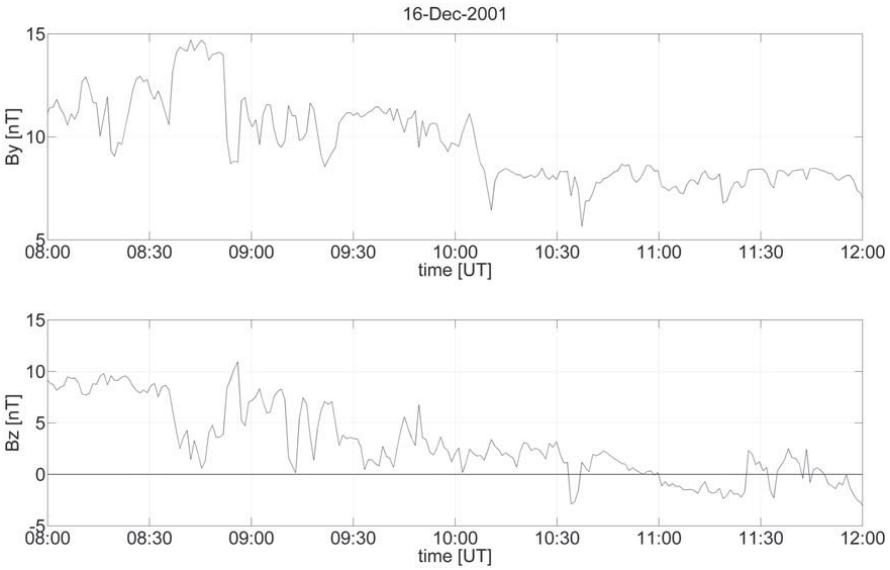

Figure 3. ACE measurements of the IMF B_Y and B_Z components between 0800 and 1200 UT on 16 December 2001. The time axis accounts for a time delay of 47 min from the spacecraft to the ionosphere. The time axis shown is thus time_{ACE} + 47 min.

fade. A number of flow structures have been found where a region of the background convection has reversed or diminished, as in Figures 1a and 1b from 1016–1022 UT. Unlike the case presented in Figure 1, however, these flow structures did not develop into RFEs.

4. Results

[35] This result section is divided into two main parts. The first part (section 4.1) explains the columns in Table 2 which lists the RFEs and flow structures identified in the dataset together with some attributes for further analysis. The second part (section 4.2) states the results of the analysis and is divided into three subsections (4.2.1–4.2.3) that elaborate on different aspects of the RFE occurrence.

4.1. Explanation of the Columns in Table 2

[36] Number indicates the serial number of a given RFE or flow structure. RFEs and Flow Structures are numbered separately. Class describes whether a given signature meets the criteria of a RFE (marked RFE) or a flow structure (marked FS). RFEs and their attributes are written in bold and flow structures in italic for easier distinction. Date lists the date when a given event or structure occurred. Start/End lists the start/stop times in UT of the first/last scan when an event was visible. The very first and last signs which could be associated with an RFE or flow structure have been taken as beginning and end times. Number of scans states the number of consecutive scans a given signature was visible. Dur. [s] (duration) gives the lifetime of one single RFE/flow structure. Q (quadrant) indicates in which of the four azimuthal quadrants of the ESR field of view an RFE or flow structure was located, as defined in Figure 1d. The particular RFE shown in Figure 1d, visible as a blue stripe inside the yellow ellipse, was located in the third quadrant. abs(v_i) is the absolute value of the ion velocity of the RFE or flow structure along the ESR line of sight, given within ranges of 0–250, >250 m/s. M (motion) indicates whether or not the RFE or flow signature moved north (N) poleward or south (S) equatorward. W (widening) indicates whether the RFE or flow signature widened throughout its lifetime, indicated by an "X." FOV (field of view) has an "X" set in this column whenever an event was cut short or its onset could not be observed as the radar field of view was altered to look in a different azimuth sector. "PD" (poor data) indicates that an RFE or structure was followed by questionable data. IMF B_Z states the polarity of IMF B_Z averaged over the lifetime of an event (cf section 2.3). The notation used is a plus symbol and a minus symbol for values larger or smaller than zero. IMF B_Y has the same notation as for IMF B_Z. θ (°) (clock angle) states the clock angle for RFEs and flow structures calculated from average IMF B_Y and B_Z values (see above). The clock angle is defined with respect to IMF B_Z north, increasing clockwise from 0 to 360° in the IMF B_Y/B_Z plane. SD Cov (SuperDARN coverage) indicates whether SuperDARN had data coverage at the location of the ESR field of view at any time. "N" means that there are no SuperDARN flow vectors at the location of the ESR fan, and convection is derived entirely based on the SuperDARN model [*Ruohoniemi and Baker*, 1998]. SD Match indicates if the large-scale convection observed by SuperDARN agreed with the line-of-sight measurements of the ESR, as determined qualitatively by eye inspection. F_t indicates whether or not the flow of an RFE was directed

Table 2. Occurrence of All Reversed Flow Events and Flow Structures Which Have Been Identified Throughout the Data Set With Columns Explained in Detail in Section 4.1

Number	Class	Date	Start	End	Number of Scans	Dur., s	Q	abs(v_i)	M	W	FOV	IMF B_Z	IMF B_Y	θ, deg	SD Cov	SD Match	F_t
1	FS	16.01.2001	0855	0859	2	256	3	> 250				–	+	154	Y	Y	
2	FS	16.01.2001	0859	0903	2	256	3	> 250				–	+	162	Y	Y	
3	FS	16.01.2001	0908	0910	1	128	3	> 250			PD	–	+	161	Y	Y	
4	FS	16.01.2001	0931	0933	1	128	3	0–250				–	–	212	Y	Poor	
1	**RFE**	**16.01.2001**	**1007**	**1016**	**4**	**512**	**3**	**> 250**				–	–	**237**	**Y**	**N**	**A**
5	FS	16.01.2001	1029	1033	2	256	3	> 250				–	+	174	Y	Y	
6	FS	16.01.2001	1050	1052	1	128	3	> 250				–	–	191	Y	Y	
7	FS	17.01.2001	0933	0935	1	128	2	> 250				+	+	39	N		
8	FS	19.01.2001	0611	0628	8	1024	1	> 250				+	+	44	Y	Y	
9	FS	19.01.2001	1027	1029	1	128	2	0–250				+	+	78	Y	Y	
10	FS	19.01.2001	1031	1033	1	128	2	0–250				+	+	71	Y	Y	
11	FS	19.01.2001	1035	1039	2	256	2	0–250				+	+	87	Y	Y	
12	FS	19.01.2001	1118	1122	2	256	2	0–250				–	+	152	Y	Y	
13	FS	19.01.2001	1135	1141	3	384	2	> 250				–	+	173	Y	Y	
14	FS	19.01.2001	1143	1146	1	128	2	> 250				–	+	175	Y	Y	
15	FS	19.01.2001	1154	1156	1	128	2	0–250				–	+	180	Y	Y	
2	**RFE**	**20.01.2001**	**0645**	**0649**	**2**	**256**	**1**	**> 250**	**N**			–	–	**189**	**Y**	**Y**	**O**
16	FS	20.01.2001	1001	1005	2	256	2	> 250				+	+	89	N		
17	FS	20.01.2001	1022	1027	2	256	2	> 250				+	+	73	N		
18	FS	20.01.2001	1022	1027	2	256	2	0–250	S			+	+	73	N		
19	FS	20.01.2001	1029	1031	1	128	2	0–250				+	+	67	N		
20	FS	20.01.2001	1031	1037	3	384	2	0–250				+	+	61	N		
21	FS	20.01.2001	1044	1048	2	256	2	0–250				+	+	53	N		
3	**RFE**	**15.12.2001**	**0736**	**0743**	**2**	**384**	**1**	**> 250**		**X**		–	**+**	**97**	**Poor**	**Y**	**O**
22	FS	15.12.2001	0914	0921	2	384	4	> 250				–	+	97	Y	Y	
4	**RFE**	**15.12.2001**	**0924**	**0927**	**1**	**192**	**1**	**> 250**				–	**+**	**90**	**Y**	**Y**	**O**
23	FS	15.12.2001	0941	0947	2	384	2	> 250				+	+	72	Y	Y	
5	**RFE**	**15.12.2001**	**1003**	**1058**	**17**	**3264**	**2**	**> 250**		**X**	**X**	**+**	**+**	**73**	**Y**	**Y**	**O**
6	**RFE**	**16.12.2001**	**0731**	**0737**	**2**	**384**	**4**	**> 250**				**+**	**+**	**44**	**Y**	**Y**	**O**
7	**RFE**	**16.12.2001**	**0803**	**0852**	**15**	**2880**	**1**	**> 250**				**+**	**+**	**60**	**Y**	**Y**	**O**
8	**RFE**	**16.12.2001**	**0839**	**0848**	**3**	**576**	**1**	**> 250**				**+**	**+**	**80**	**Y**	**Y**	**O**
9	**RFE**	**16.12.2001**	**0852**	**0930**	**12**	**2304**	**1**	**> 250**		**X**	**X**	**+**	**+**	**61**	**Y**	**N**	**O**
24	FS	16.12.2001	0944	0950	2	384	3	> 250				+	+	67	Y	Y	
10	**RFE**	**16.12.2001**	**1016**	**1045**	**9**	**1728**	**3**	**> 250**	**N**	**X**		**+**	**+**	**79**	**Y**	**Y**	**O**
25	FS	16.12.2001	1029	1035	2	384	2	> 250				–	+	94	Y	Y	
11	**RFE**	**16.12.2001**	**1051**	**1059**	**3**	**576**	**3**	**> 250**			**X**	**+**	**+**	**89**	**Y**	**Y**	**O**
26	FS	17.12.2001	1010	1013	1	192	3	0–250				+	+	86	Y	Y	
27	FS	17.12.2001	1017	1020	1	192	3	0–250				+	+	76	Y	Y	
12	**RFE**	**18.12.2001**	**0643**	**0650**	**2**	**384**	**1**	**> 250**				–	**+**	**118**	**N**		**O**
13	**RFE**	**18.12.2001**	**0754**	**0803**	**3**	**576**	**1**	**> 250**			**X**	–	**+**	**160**	**Y**	**Poor**	**O**
14	**RFE**	**18.12.2001**	**0938**	**1007**	**9**	**1728**	**3**	**> 250**	**N**	**X**		–	**+**	**140**	**Y**	**Y**	**O**
15	**RFE**	**18.12.2001**	**0951**	**1020**	**9**	**1728**	**3**	**> 250**	**N**	**X**		–	**+**	**157**	**Y**	**Y**	**O**
16	**RFE**	**18.12.2001**	**1007**	**1030**	**7**	**1344**	**3**	**> 250**	**N**	**X**		–	**+**	**170**	**Y**	**Y**	**O**
28	FS	19.12.2001	0841	0847	2	384	3	0–250				–	–	180	N		
17	**RFE**	**20.12.2001**	**0619**	**0622**	**1**	**192**	**1**	**> 250**				–	**+**	**102**	**Y**	**Poor**	**O**
29	FS	20.12.2001	0651	0657	2	384	1	> 250				+	+	83	Y	Y	
30	FS	20.12.2001	1016	1025	3	576	3	> 250				–	+	128	Y	Y	
18	**RFE**	**20.12.2001**	**1025**	**1051**	**8**	**1536**	**3**	**> 250**	**N**	**X**		–	**+**	**150**	**Y**	**Y**	**O**
19	**RFE**	**20.12.2001**	**1041**	**1057**	**5**	**960**	**3**	**> 250**			**X**	–	**+**	**105**	**Y**	**Y**	**O**
20	**RFE**	**21.12.2001**	**0738**	**0755**	**5**	**1280**	**3**	**> 250**		**X**		–	**+**	**113**	**N**		**A**
21	**RFE**	**21.12.2001**	**0855**	**0912**	**4**	**1024**	**3**	**> 250**				–	**+**	**156**	**N**		**A**
31	FS	21.12.2001	0929	0938	2	384	3	0–250				–	+	157	N		

along with (A) or opposite to (O) the direction of the IMF B_Y controlled magnetic tension force. For a positive (negative) IMF B_Y newly opened field lines are dragged by the magnetic tension force to the west (east) in the Northern Hemisphere before they convect tailward across the polar cap driven by the solar wind flow [*Heppner and Maynard*, 1987].

4.2. Data Analysis Results

[37] Throughout the data set the ion velocity exhibited much fine structure. In total 21 RFEs were identified in 123 of the 767 scans, meaning that they occur in 16% of the scans. Flow structures that failed to satisfy one or more of these strict criteria were registered separately and occurred in 7.8% of the scans. There may be no principal difference between the two, despite the fact that flow structures do not fully develop into RFEs for still unknown reasons.

[38] The average lifetime of RFEs was ~19 min. This lifetime includes (if observed) the growth and decay of RFEs, during which the ion flow not necessarily has to be reversed but may only be a reduction of the background convection. Almost every fourth RFE was however cut short as the radar field of view was altered to observe in a different azimuth sector. This obviously influences the

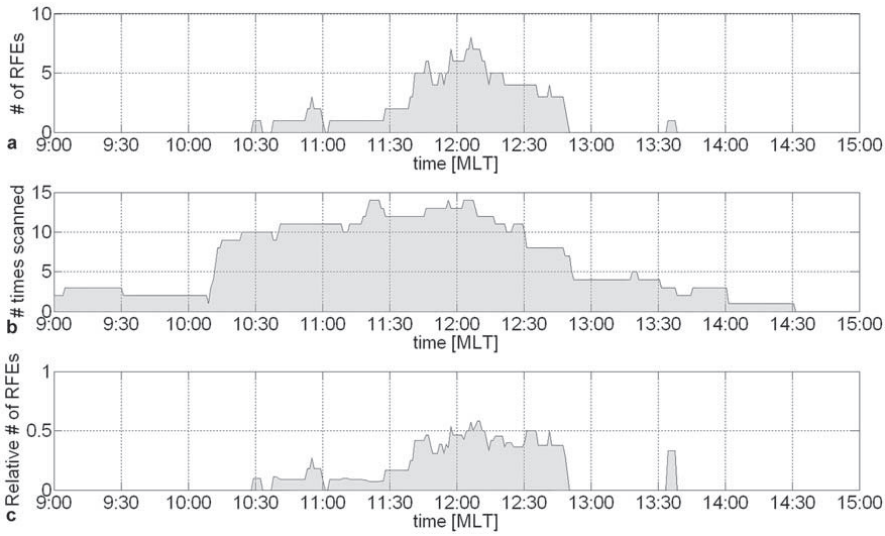

Figure 4. (a) The counted number of RFEs versus MLT corresponding to the radar fan midposition. The curve represents how many times an RFE was observed during a 1 min interval integrated over the entire data set. (b) Data coverage as a function of MLT corresponding to Figure 4a. For example if the radar scanned from 0900 until 1200 MLT, the number of times this region was scanned was augmented by one for every minute from 0900 until 1200 MLT. (c) Relative occurrence of RFEs with respect to the data coverage. This plot was inferred by dividing the RFE occurrence versus MLT (Figure 4a) by the number of times any given MLT minute had been scanned (Figure 4b).

calculated average lifetime. Four very long lived RFEs were found, each lasting for 28 min and hence ~10 min longer than the average lifetime of 19 min. They developed from a small-scale reduction of the background flow into a large RFE. One of these four RFEs is shown in Figure 1. The background flow in the ESR field of view was relatively uniform during these four RFEs. From a study like the one presented here, it is not possible to further parameterize the lifetime of RFEs. Around 30% of the RFEs exhibited latitudinal, poleward motion during their lifetime and all except one of these RFEs occurred during IMF B_Z negative. Around ~50% of the RFEs widened, but there was no correlation with IMF B_Z. However, no relationship between motion and widening has been found.

4.2.1. Quadrant Appearance of RFEs

[39] Of the time scanned in each of the four quadrants, the relative frequency of occurrence of RFEs was much higher in the first and third quadrant (Q1 and Q3) than in the second an fourth (Q2 and Q4), and RFEs occurred more than twice as often in Q3 than in Q1. In the context of the SuperDARN large-scale convection maps the RFEs were located in regions of enhanced plasma convection close to or within the cusp inflow region. Furthermore, it became clear that all events did have a nonzero IMF B_Y component with a large zonal flow component. During moderate activity the dayside auroral oval is centered on 75° MLAT, i.e., close to Longyearbyen. Owing to the dipole tilt, the auroral oval is oriented along the diagonal of Q1 and Q3 in Figure 1. Q4 will only be covered by aurora in case of an expanded polar cap. Similarly, the cusp may be situated in Q2 only when the polar cap is contracted. In cases where the zonal flow along the auroral oval dominates (large IMF B_Y) the ESR will, owing to geometry of the line-of-sight velocity measurements, be most sensitive to RFEs in Q1 and Q3 but not in Q2 and Q4 (cf. section 3.2).

[40] Examining the occurrence of flow structures, it is apparent that flow structures actually occurred most frequently in Q2. It seems as if the low appearance of RFEs in Q2 may be related to the fact that the ESR is less sensitive to Q2 for a nonzero IMF B_Y as discussed above.

4.2.2. MLT Occurrence of RFEs

[41] The ESR field of view spans over 2–4 hours in MLT depending on the azimuth range, and the RFEs often exceed the field of view. In order to derive the MLT occurrence of RFEs, the start and stop times of the RFEs inferred from Table 2 have been adjusted to account for the actual MLT of the measurements at the midposition in longitude of each ESR scan (listed in Table 1 column 10).

[42] The resulting MLT occurrence of RFEs was determined, and is shown in Figure 4. Figure 4a shows how many times an RFE was observed at a certain MLT throughout the data set, binned in minutes. The figure revealed that the maximum occurrence of RFEs was around 1200 MLT but skewed slightly over toward postnoon. The activity peaked with a total number of eight RFEs around 1215 MLT. No activity occurred before 1030 MLT and activity was low with on average one RFE occurring between 1030 and 1130 MLT, before it tripled from two

to six RFEs just after 1130 MLT. The RFE activity was high with four to eight RFEs between 1145 and 1245 MLT, before a steep decrease to zero just prior to 13 MLT. One event occurred around 1330 MLT.

[43] However, our database does not have uniform coverage between 0900 and 1500 MLT. Hence, Figure 4b indicates how many times the radar has scanned a certain MLT throughout the data set, binned in minutes. The figure reveals that the ESR scanned the region between 1015 and 1245 MLT more than five times (mostly around 10 times), whereas the regions between 0900 and 1015 MLT and 1245 and 1430 MLT were scanned less than five times. Hence a relative occurrence plot for RFEs has been generated and is shown in Figure 4c. In Figure 4b the number of RFEs at a certain MLT has been divided by the number of times the ESR has actually scanned that MLT. From Figure 4c it can be seen that the RFE activity onset occurred at 1030 MLT and was low between 1030 and ~1145 MLT. Please note that one single RFE occurred during an interval of low data coverage postnoon. Not much importance should be paid to the size of such a single-event peak. At 1145 MLT the activity increased steeply and remained high until a steep decrease at ~1245 MLT. During this time period RFEs were observed in 40% of the scans. Comparing Figures 4b and 4c, the increase of activity prenoon occurred in a region of high data coverage, but the steep decrease of event occurrence in the postnoon sector before 1300 MLT coincides with a steep decrease in data coverage. Hence the distribution on the postnoon side may be strongly affected by data coverage.

[44] Since IMF B_Y was predominantly positive in the available data set, the apparent postnoon shift of the RFE activity occurrence is consistent with RFEs being a cusp related phenomena, as the active cusp is expected to be shifted toward postnoon for positive B_Y [*Cowley et al.*, 1991].

[45] Placing the RFEs in the context of SuperDARN polar cap convection patterns showed that RFEs most often appeared in the cusp inflow region postnoon, near the equatorward border strong convection.

4.2.3. IMF Dependency and Ion Flow Direction With Respect to the Magnetic Tension Force

[46] The entire data set was biased toward IMF B_Y positive, and only 8.7% of the time, B_Y was negative. In total, 2 RFEs (9.5%) occurred during an interval of negative IMF B_Y. The IMF B_Z component was negative 57.2% of the time, and 14 RFEs (66.6%) occurred during an interval of negative B_Z. It seems thus as if the occurrence is independent of IMF B_Z. For IMF B_Y the number of scans and events involved is really too low to determine the B_Y polarity dependence. However, the occurrence of RFEs is not exclusively related to one IMF B_Y polarity. All RFEs and flow structures occurred in the clock angle range between 40° and 240°.

[47] The ion flow direction of RFEs was defined to be in the opposite direction of the background flow observed in the ESR field of view. Furthermore, 85.7% of the time (18 RFEs) the RFE flow direction was opposite to the direction of the magnetic tension force suggested by IMF conditions. This is illustrated with the RFE in Figure 1. The time shifted IMF for the actual time interval is shown in Figure 3. The RFE shown in Figure 1 takes place from 1016 to 1045 UT, thus in an interval of clearly positive IMF B_Y. Hence newly opened field lines would experience a pull dawnward. The ion flow direction of the RFE shown in Figure 1 however is clearly "blue" and hence duskward. Looking at the background flow in the ESR field of view, and comparing it to the SuperDARN plot for the actual time interval (Figure 2) shows that the background flow is uniform and directed dawnward, as expected for positive IMF B_Y. Moreover, the RFE is located in a region of enhanced dawnward plasma flow observed by SuperDARN.

[48] SuperDARN had good coverage for 17 of the 21 RFEs (81%), poor coverage for one RFE (5%), and no coverage for three RFEs (14%). The background flow seen by the ESR was confirmed by SuperDARN for 15 of the 17 RFEs (88%) with good coverage and for the one RFE with poor coverage. If the three RFEs without SuperDARN coverage are excluded, 17 of 18 RFEs (94.4%) had a flow opposite to the magnetic tension force. If only the 15 RFEs where SuperDARN had a sufficient coverage and was moreover confirming the background flow observed by the ESR are considered, 15 of 15 RFEs (100%) exhibit an ion flow opposite to the magnetic tension force.

5. Discussion: RFEs as Southwood FTE?

[49] The MLT occurrence and the location of RFEs with respect to the large-scale polar cap convection monitored by SuperDARN indicate that RFEs indeed are a regular phenomenon occurring near cusp inflow region. It is therefore reasonable to consider RFEs as a possible signature of reconnection events. The RFEs in this study were observed within the clock angle range between 40° and 240°, which is within the clock angle range for reconnection bursts at the magnetopause reported by *Neudegg et al.* [2000].

[50] However, since the ion flow direction of RFEs is per definition opposite to the large-scale convection and the IMF B_Y controlled magnetic tension force pulls on newly opened field lines, they can definitely not be interpreted in terms of the centre flux in an FTE twin-vortex flow pattern. If RFEs relate to the Southwood FTE model, they must correspond to the return flow, as suggested by *Oksavik et al.* [2004]. From the RFE definition in section 3.2, RFEs have to extend over at least 400–600 km in the ESR field of view. The longitudinal extent of almost all RFEs exceeded the ESR field of view and hence it seems as if RFEs usually exceed 600 km in length. Since the longitudinal dimension of the return flow would have to be approximately equal to the longitudinal extent of the centre flux according to the Southwood model, the spatial dimensions appear consistent with those suggested by *Lockwood et al.* [1990].

[51] The Southwood model predicts however two return flow channels; one on the equatorward edge and one on the poleward edge of the center flux. This means that the footprint of a single FTE in the ionosphere should consist of three flow channels, one in the newly open flux area with direction determined by the magnetic tension force and two flow channels of reduced or reversed return flow.

[52] Throughout the entire data set, only three occasions were identified in which two RFEs coexisted within the ESR field of view. Since these occasions were similar, only one of them, which was presented by *Oksavik et al.* [2004, 2005], is discussed in more detail and shown in Figure 5.

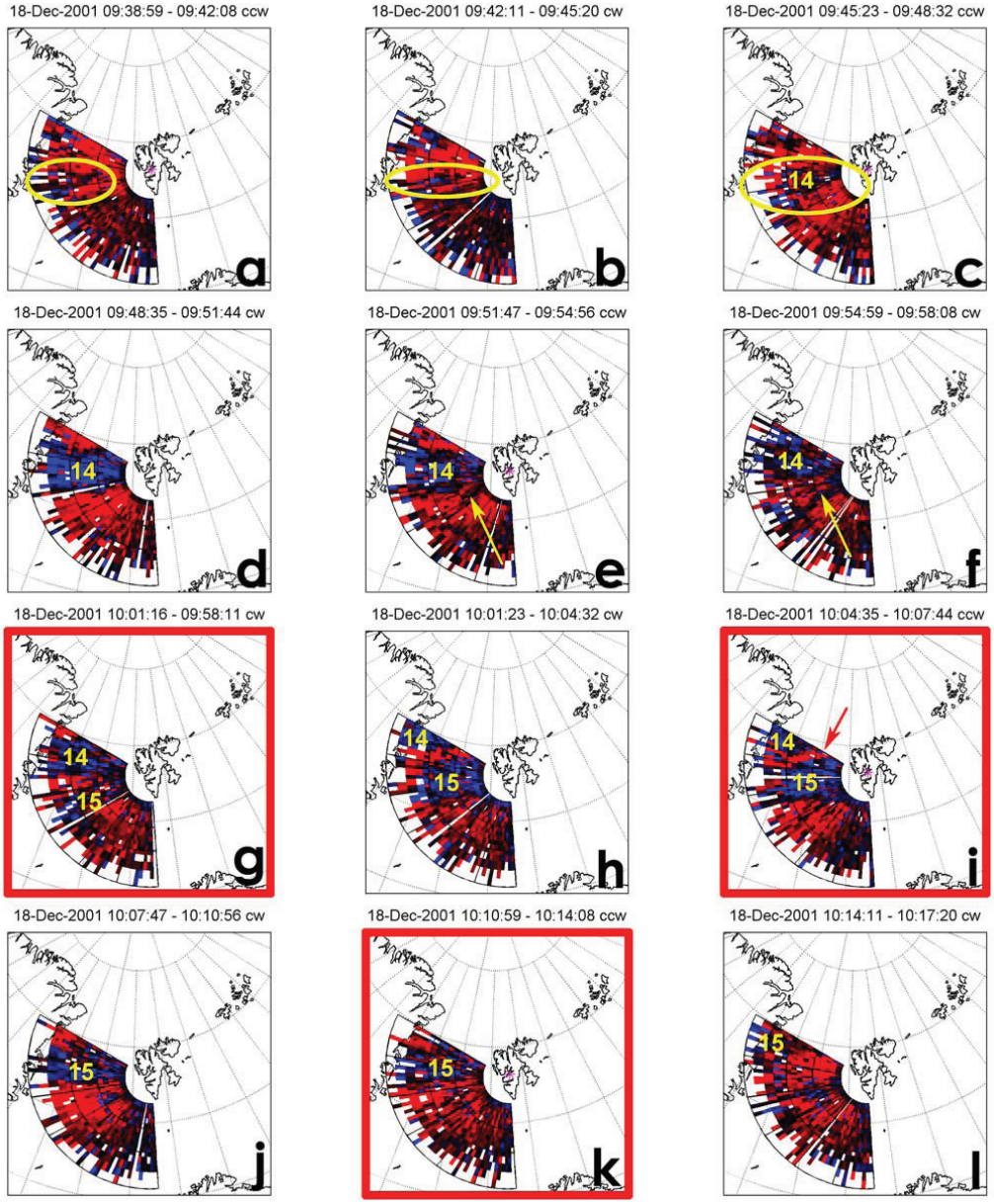

Figure 5. (a–l) A sequence of ion velocity fan plots from 18 December 2001 in geographic coordinates, covering the development of RFE 14 and RFE 15 (same format as Figure 1). The scans presented by *Oksavik et al.* [2004] are framed red. The first signs of RFE 14 are encircled by a yellow ellipse in Figures 5a–5c; the first signs of RFE 15 are indicated by a yellow arrow in Figures 5e and 5f. The red arrow in Figure 5i indicates the Southwood center flow as interpreted by *Oksavik et al.* [2004].

Oksavik et al. [2004] presented the scans which are framed, in Figures 5g, 5i, and 5k. They observed the signature of Southwood twin-vortex flow, where the narrow region of enhanced ion flow directed away from the radar indicated by the red arrow in Figure 5i, from 1004 to 1007 UT was classified as the signature of the center flux in the Southwood model, and the areas of flow directed toward the radar termed "RFE 14" and "RFE 15" as the return flow predicted by the Southwood model. The direction of the center flux as defined by *Oksavik et al.* [2004, 2005] is consistent with the background flow inferred from SuperDARN convection maps and the IMF B_Y controlled magnetic tension force on newly opened field lines for the given IMF conditions. However, as demonstrated in Figure 5, RFE 14 and RFE 15 did not develop simultaneously. The onset of RFE 14 occurred at 0938 UT, when reversed flow became visible; marked out by the yellow ellipse in Figure 5a. This flow signature grew in size and developed into a large and strong RFE at 0948 UT, Figure 5d. Some minutes later, at 0951 UT, a second region of reversed flow became visible and is indicated by the yellow arrow in Figure 5e. It rapidly developed into RFE 15. RFE 14 and RFE 15 coexisted from 0951 to 1007 UT (Figures 5e–5i). After 1007 UT, RFE 14 moved out of the field of view. Even though two RFEs coexisted inside the ESR field of view for some time, they did not develop simultaneously but with a ~13 min delay in onset.

[53] According to the Southwood FTE model, the return flow from a newly reconnected field line moving through the ionosphere is expected to occur simultaneously, and hence the two RFEs cannot be regarded as the return flow channels surrounding one single event of newly opened flux but have to be regarded as separate flow events. This is also the case for the other two occasions in which two RFEs were observed to coexist in the ESR field of view. They were both characterized by a time delay in onset of ~36 and ~17 min.

[54] If one were to attempt to fit the data to a Southwood model, there remains the question why the ESR does not observe two return flow channels with simultaneous onset as predicted by the Southwood FTE model within its field of view, and which of the two return channels would be represented by the RFE. From the ESR observations alone it cannot be determined for sure on which side of the RFE the flow enhancement associated with the motion of the newly reconnected flux tube would be located. For RFE 14, however, *Oksavik et al.* [2005] presented a comprehensive set of observations using the EISCAT Svalbard radar, the

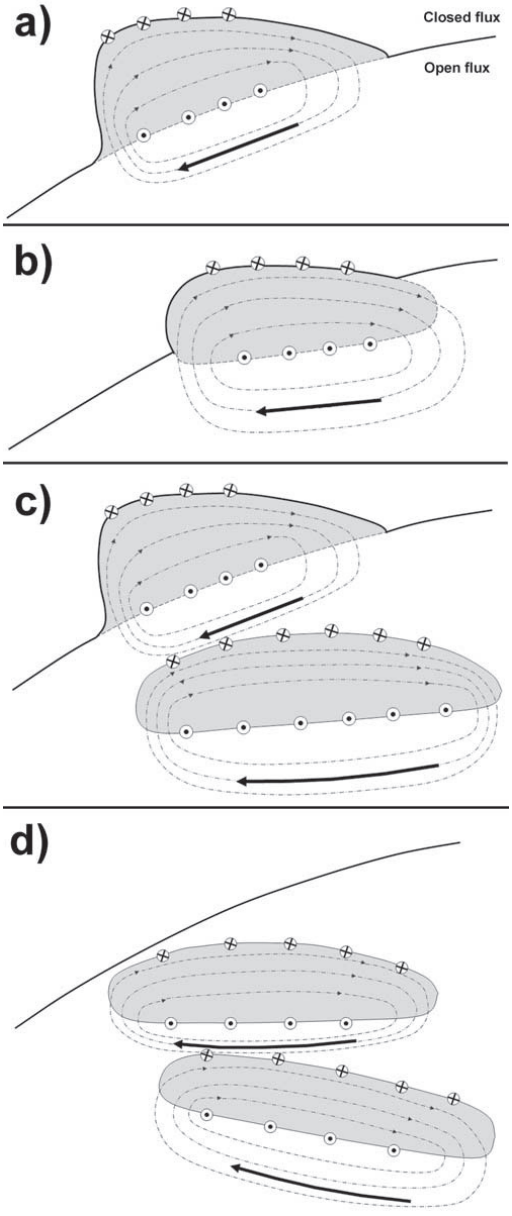

Figure 6. (a) Schematic illustration of the initial state of a suggested IMF B_Y asymmetry of the Southwood flux transfer event (FTE). The black line indicates the open-closed field line boundary, and the grey shaded region represents the region of newly opened flux due to an FTE for IMF $B_Y > 0$. Plasma streamlines are indicated by dashed-dotted arrows. Circled dots and crosses represent the location of the upward and downward field-aligned currents of the FTE current system, respectively. (b) The asymmetric Southwood model in a later state, after the magnetic tension force on the newly opened field line has pulled the field line dawnward and slightly into the polar cap. (c) A new pulse of reconnection takes place and pushes the previous reconnected flux tube further into the polar cap. (d) Both reconnected flux tubes have propagated into the polar cap and elongated due to the magnetic tension force and plasma convection.

SuperDARN HF radar network, ground-based optics, and three low-altitude polar orbiting spacecraft.

[55] At the same time as RFE 14 develops from a flow structure to an RFE in the ESR field of view over Figures 5a–5d, a region of strong, westward convection became visible at its equatorward side, consistent with the expected direction of motion of newly reconnected flux. *Oksavik et al.* [2005] found a PMAF coinciding with the equatorward edge of RFE 14, indicating an upward Birkeland current. Furthermore, a DMSP F13 satellite passage revealed the existence of a field-aligned current system with an upward Birkeland current flowing on the equatorward side of REF 14 confirming the location of the PMAF, and a downward Birkeland current on the equatorward side of the enhanced westward flow equatorward of RFE 14. These observations of FTE currents, a term inferred by *Oksavik et al.* [2005] to describe the Birkeland currents of individual flux transfer events, identify RFE 14 as the polewardmost of the two return flow channels. Hence RFE 14 and the region of enhanced westward flow equatorward of it are consistent with being the signature of the poleward clockwise cell of a Southwood FTE. RFE15 develops ~13 min after RFE14 and is as well associated with a belt of strong westward convection equatorward of it, best visible in Figures 5i and 5j. Moreover, *Oksavik et al.* [2005] found a second PMAF coinciding with the equatorward boundary of RFE 15, confirming that RFE 15 and the region of enhanced westward flow equatorward of it are consistent with being the poleward clockwise cell of a new FTE, pushing the previous FTE further into the polar cap.

[56] Since almost all RFEs observed in this study occurred during significant IMF B_Y conditions and the ESR never detected both return flow channels predicted by the Southwood model, we suggest that the Southwood model takes an asymmetric form in the case of strong IMF B_Y, in which only the poleward cell of the Southwood FTE model becomes observable. This conceptual idea of IMF B_Y asymmetry in the Southwood model is illustrated schematically in Figures 6a–6d.

[57] The grey shaded region in Figure 6a is the newly opened flux resulting from a pulse of magnetopause reconnection under large IMF B_Y positive. The open-closed field line boundary (OCB) leaps equatorward and eastward. On the flanks of the newly opened flux the FTE current system which consists of a pair of FACs is indicated by circled dots and crosses, which represent the upward and downward FACs, respectively. This current system marks off the poleward and equatorward boundary of the newly opened flux. The first force to act on the reconnected flux tube is the azimuthal magnetic stress due to IMF B_Y. The magnetic tension force initially pulls the newly reconnected flux tube westward along the adiaroic OCB. Hence the plasma pushed aside by this motion will move almost exclusively in the region of open field lines poleward of the FTE, since there cannot exist plasma flow across the OCB as indicated by the dashed-dotted plasma streamlines. A diffuse cell may, however, develop equatorward of the OCB due to induced Hall currents across the boundary. As a consequence, for significant IMF B_Y only the poleward cell of the Southwood model will develop, as observed in our data set where RFE 14 represents the poleward return flow of the first FTE. This differs from the FTE flow disturbance suggested by *Milan et al.* [2000] in their Figure 4a, which proposes a return flow channel on closed field lines, but no return flow channel on the poleward side of the upward FTE current sheet/PMAF. As the patch of newly opened flux evolves into the polar cap as indicated in Figure 6b, it elongates due to the magnetic tension and solar wind pull.

[58] A new pulse of reconnection creates a new region of open flux as indicated in Figure 6c. Its motion is initially as well determined by the magnetic tension force pull and pushes the previous FTE even further into polar cap. The first FTE is now entirely part of the older open flux in the polar cap. The grey shading is kept just to remind us about the area of flux that was added by the reconnection pulse. Owing to the current sheet on the equatorward side of the first FTE, no mixing of plasma occurs, and the two clockwise cells visible by their return flow channels RFE 14 and 15 coexist. Finally (Figure 6d), both FTEs have entirely propagated into the polar cap and form a train of cigar-shaped "recently opened flux." We think that the symmetric FTE twin cell flow pattern suggested by *Southwood* [1987] represents the situation when IMF is due south [*Cowley and Lockwood*, 1992], while the situation in Figure 6 represents the extreme of IMF B_Y dominance. The truth can be anything in between. Nevertheless, the schematic summarizes what we observe.

6. Summary and Concluding Remarks

[59] The phenomenon of transient small-scale flow channels in the cusp, observed by the ESR in a new fast scan mode, has been investigated systematically in order to reveal detailed characteristics and determine the occurrence of these features.

[60] From the discussion above it can be concluded that RFEs seem to be a regular feature of the cusp, occurring at least 16% of the time in the current data set. Since there are several constraints such as the cusp location and the limited ESR field of view, the line of sight viewing geometry with respect to the flow pattern, and a strict RFE definition, it is likely that the occurrence rate is higher. Flow structures that failed to satisfy one or more of these strict criteria were registered separately and occurred in 7.8% of the scans. Several constraints of detectability as well as the presence of less pronounced flow structures lead to the assumption that RFEs may occur even more frequently. There may be no fundamental difference between flow structures and RFEs, despite the fact that flow structures do not fully develop into an RFE for still unknown reasons.

[61] RFEs occurred near the cusp inflow region and were observed in 40% of the scans during the 60 min around 1200 MLT. They occurred in association with enhanced large-scale plasma flow observed by SuperDARN and seemed to be aligned with the auroral oval (L-shell aligned). RFEs thus seem to be a regular feature of the active cusp.

[62] The average lifetime of RFEs was 19 min. However, their lifetime can be even longer, since ~25% of the events were interrupted as the radar field of view was altered to look in a different azimuth sector. No general motion or widening could be found. Furthermore, RFEs seem to occur independently of the IMF B_Y and B_Z polarity, and for clock angles in the range of 40 to 240°. The data set is strongly biased toward IMF B_Z positive (IMF B_Y was positive for

~91% of the events). The fact that 9.5% of the RFEs occurred during IMF B_Y negative, however, indicates that the phenomenon is not exclusively related to one B_Y polarity.

[63] More than 85% of the RFEs were characterized by ion flow opposing the magnetic tension force. Since RFEs never occurred simultaneously in pairs, they cannot be interpreted as the return flow of a single Southwood twin cell FTE signature. However, an asymmetric version of the Southwood model for significant IMF B_Y conditions, where only the poleward cell located on open flux develops, has been suggested based on the observations made by *Oksavik et al.* [2005]. The asymmetry arises due to the fact that a flow vortex cannot develop across the OCB. However, owing to closure of Hall currents in the ionosphere, we believe that a diffuse cell might develop on closed flux.

[64] More observations are needed to better characterize the MLT-MLAT occurrence of RFEs and to quantify the eventual relationship to IMF orientation. The physical explanation for the RFE phenomenon will be further investigated. The discovery of RFEs by the ESR and the documentation presented here provide new and very important information about cusp dynamics that is relevant for studies of, e.g., cusp irregularities and patch formation.

[65] **Acknowledgments.** EISCAT is an international association supported by research organizations in China (CHIRP), Finland (SA), France (CNRS, until end 2006), Germany (DFG), Japan (NIPR and STEL), Norway (NFR), Sweden (VR), and the United Kingdom (PPARC). We thank the ACE Science Center and the ACE MAG and SWEPAM instrument teams for providing solar wind data from the ACE spacecraft. Financial support has been provided by the Norwegian Research Council and AFOSR task 2311AS. CUTLASS is supported the UK Particle Physics and Astronomy Research Council (PPARC), the Swedish Institute for Space Physics, and the Finnish Meteorological Institute in Helsinki. HCC wishes to acknowledge support from AFOSR under grant contract FA9550-06-1-0217, and KO is supported by NSF grant ATM-0418101.

[66] Wolfgang Baumjohann thanks Dave Neudegg and another reviewer for their assistance in evaluating this paper.

References

Carlson, H. C., K. Oksavik, J. Moen, A. P. van Eyken, and P. Guio (2002), ESR mapping of polar-cap patches in the dark cusp, *Geophys. Res. Lett.*, *29*(10), 1386, doi:10.1029/2001GL014087.

Cowley, S. W. H., and M. Lockwood (1992), Excitation and decay of solar wind-driven flows in the magnetosphere-ionosphere system, *Ann. Geophys.*, *10*, 103–115.

Cowley, S. W. H., J. P. Morelli, and M. Lockwood (1991), Dependence of convective flows and particle precipitation in the high-latitude dayside ionosphere on the X and Y components of the interplanetary magnetic field, *J. Geophys. Res.*, *96*, 5557–5564.

Denig, W. F., W. J. Burke, N. C. Maynard, F. J. Rich, B. Jacobsen, P. E. Sandholt, A. Egeland, S. Leontjev, and V. G. Vorobjev (1993), Ionospheric signatures of dayside magnetopause transients: A case study using satellite and ground measurements, *J. Geophys. Res.*, *98*, 5969–5980.

Dungey, J. W. (1961), Interplanetary magnetic field and the auroral zones, *Phys. Rev. Lett.*, *6*, 47–48.

Goertz, C. K., E. Nielsen, A. Korth, K. H. Glassmeier, C. Haldoupis, P. Hoeg, and D. Hayward (1985), Observations of a possible ground signature of flux transfer events, *J. Geophys. Res.*, *90*, 4069–4078.

Haerendel, G., G. Paschmann, N. Sckopke, H. Rosenbauer, and P. C. Hedgecock (1978), The frontside boundary layer of the magnetosphere and the problem of reconnection, *J. Geophys. Res.*, *83*, 3195–3216.

Heppner, J. P., and N. C. Maynard (1987), Empirical high-latitude electric field models, *J. Geophys. Res.*, *92*, 4467–4489.

Lockwood, M., P. E. Sandholt, S. W. H. Cowley, and T. Oguti (1989), Interplanetary magnetic field control of dayside auroral activity and the transfer of momentum across the dayside magnetopause, *Planet. Space Sci.*, *37*, 1347–1365.

Lockwood, M., S. W. H. Cowley, P. E. Sandholt, and R. P. Lepping (1990), The ionospheric signatures of flux transfer events and solar wind dynamic pressure changes, *J. Geophys. Res.*, *95*, 17,113–17,135.

Marchaudon, A., J.-C. Cerisier, R. A. Greenwald, and G. J. Sofko (2004), Electrodynamics of a flux transfer event: Experimental test of the Southwood model, *Geophys. Res. Lett.*, *31*, L09809, doi:10.1029/2004GL019922.

Maynard, N. C., E. J. Weber, D. R. Weimer, J. Moen, T. Onsager, R. A. Heelis, and A. Egeland (1997), How wide in magnetic local time in the cusp? An event study, *J. Geophys. Res.*, *102*, 4765–4776.

Milan, S. E., M. Lester, S. W. H. Cowley, and M. Brittnacher (2000), Convection and auroral response to a southward turning of the IMF: Polar UVI, CUTLASS, and IMAGE signatures of transient magnetic flux transfer at the magnetopause, *J. Geophys. Res.*, *105*, 15,741–15,755.

Moen, J., J. A. Holtet, A. Pedersen, B. Lybekk, K. Svenes, K. Oksavik, W. F. Denig, E. Lucek, and M. André (2001), Cluster boundary-layer measurements and optical observations at magnetic conjugate sites, *Ann. Geophys.*, *18*, 1655–1668.

Moen, J., M. Lockwood, K. Oksavik, H. C. Carlson, W. F. Denig, A. P. van Eyken, and I. W. McCrea (2004), The dynamics and relationships of precipitation, temperature and convection boundaries in the dayside auroral ionosphere, *Ann. Geophys.*, *22*, 1973–1987.

Neudegg, D. A., et al. (2000), A survey of magnetopause FTEs and associated flow bursts in the polar ionosphere, *Ann. Geophys.*, *18*, 416–435.

Newell, P. T., and C.-I. Meng (1992), Mapping the dayside ionosphere to the magnetosphere according to particle precipitation characteristics, *Geophys. Res. Lett.*, *19*, 609–612.

Newell, P. T., J. M. Ruohoniemi, and C.-I. Meng (2004), Maps of precipitation by source region, binned by IMF, with inertial convection streamlines, *J. Geophys. Res.*, *109*, A10206, doi:10.1029/2004JA010499.

Oksavik, K., J. Moen, and H. C. Carlson (2004), High-resolution observations of the small-scale flow pattern associated with a poleward moving auroral form in the cusp, *Geophys. Res. Lett.*, *31*, L11807, doi:10.1029/2004GL019838.

Oksavik, K., J. Moen, H. C. Carlson, R. A. Greenwald, S. E. Milan, M. Lester, W. F. Denig, and R. J. Barnes (2005), Multi-instrument mapping of the small-scale flow dynamics related to a cusp auroral transient, *Ann. Geophys.*, *23*, 2657–2670.

Pinnock, M., A. S. Rodger, J. R. Dudeney, K. B. Baker, P. T. Newell, R. A. Greenwald, and M. E. Greenspan (1993), Observations of an enhanced convection channel in the cusp ionosphere, *J. Geophys. Res.*, *98*, 3767–3776.

Rodger, A. S. (1998), Ionospheric signatures of magnetospheric processes, in *Polar Cap Boundary Phenomena,* edited by J. Moen, A. Egeland, and M. Lockwood, pp. 115–125, Kluwer Acad., Dordrecht, Netherlands.

Ruohoniemi, J. M., and K. B. Baker (1998), Large-scale imaging of high-latitude convection with Super Dual Auroral Radar Network HF radar observations, *J. Geophys. Res.*, *103*, 20,797–20,811.

Russell, C. T., and R. C. Elphic (1978), Initial ISEE magnetometer results: Magnetopause observations, *Space Sci. Rev.*, *22*, 681–715.

Russell, C. T., and R. C. Elphic (1979), ISEE observations of flux transfer events at the dayside magnetopause, *Geophys. Res. Lett.*, *6*, 33–36.

Sandholt, P. E., M. Lockwood, T. Oguti, S. W. H. Cowley, K. S. C. Freeman, B. Lybekk, A. Egeland, and D. M. Willis (1990), Midday auroral breakup events and related energy and momentum transfer from the magnetosheath, *J. Geophys. Res.*, *95*, 1039–1060.

Sandholt, P. E., C. J. Farrugia, J. Moen, Ø. Noraberg, B. Lybekk, T. Sten, and T. Hansen (1998), A classification of dayside auroral forms and activities as a function of interplanetary magnetic field orientation, *J. Geophys. Res.*, *103*, 23,325–23,345.

Shepherd, S. G., and J. M. Ruohoniemi (2000), Electrostatic potential patterns in the high-latitude ionosphere constrained by SuperDARN measurements, *J. Geophys. Res.*, *105*, 23,005–23,014.

Southwood, D. J. (1987), The ionospheric signature of flux transfer events, *J. Geophys. Res.*, *92*, 3207–3213.

van Eyken, A. P., H. Rishbeth, D. M. Willis, and S. W. H. Cowley (1984), Initial EISCAT observations of plasma convection at invariant latitudes 70°–77°, *Atmos. Terr. Phys.*, *46*, 635–641.

H. C. Carlson, J. Moen, and Y. Rinne, Department of Physics, University of Oslo, P. O. Box 1048, Blindern, N-0316 Oslo, Norway. (yvonner@fys.uio.no)

K. Oksavik, Johns Hopkins University Applied Physics Laboratory, 11100 Johns Hopkins Road, Laurel, MD 20723, USA.

II

JOURNAL OF GEOPHYSICAL RESEARCH, VOL. 113, A09220, doi:10.1029/2008JA013061, 2008

On the relationship between thin Birkeland current arcs and reversed flow channels in the winter cusp/cleft ionosphere

J. Moen,[1,2] Y. Rinne,[1] H. C. Carlson,[1,3] K. Oksavik,[4] R. Fujii,[5] and H. Opgenoorth[2]

Received 25 January 2008; revised 14 March 2008; accepted 1 May 2008; published 16 September 2008.

[1] In this paper we study reversed flow events (RFEs) that seem regulated by Birkeland current arcs in the winter cusp ionosphere above Svalbard. An RFE is a longitudinally elongated, 100–200 km wide channel, in which the flow direction is opposite to the background convection, persisting for 10–20 min. The RFE onset occurs with the brightening of a discrete arc near the open-closed boundary. The auroral arc is situated exactly at a sharp clockwise flow reversal, consistent with a converging electric field and an upward field-aligned current. One category of RFEs propagates into the polar cap in tandem with poleward moving auroral forms, while another category of RFEs moves with the cusp/cleft boundary. The RFE phenomenon is addressed to a region void of electron precipitation, and in lack of direct sunlight the E-region conductivity will be very low. We propose two possible explanations: (1) the RFE channel may be a region where two MI current loops, forced by independent voltage generators, couple through a poorly conducting ionosphere and (2) the reversed flow channel may be the ionospheric footprint of an inverted V-type coupling region. Electron beams of <1 keV will not give rise to significant conductivity gradients, and the form of a discontinuity in the magnetospheric electric field will be conserved when mapped down to the ionosphere, although reduced in amplitude. These two explanations may be related in the sense that the boundary discontinuity in the magnetospheric electric field in (1) may be the driver for the inverted V in (2).

Citation: Moen, J., Y. Rinne, H. C. Carlson, K. Oksavik, R. Fujii, and H. Opgenoorth (2008), On the relationship between thin Birkeland current arcs and reversed flow channels in the winter cusp/cleft ionosphere, *J. Geophys. Res.*, *113*, A09220, doi:10.1029/2008JA013061.

1. Introduction

[2] Since *Haerendel et al.* [1978] and *Russell and Elphic* [1979] discovered transient and spatially limited Flux Transfer Events (FTEs) at the magnetopause, there has been an ongoing search for FTE footprints in the ionosphere. *Goertz et al.* [1985] were the first to relate ionospheric flow bursts observed by the STARE radar to magnetopause reconnection. *Southwood* [1987] put forward a model for FTEs. According to the Southwood model, newly reconnected fast moving flux will set up a local twin vortex flow disturbance. Consistent with this flow picture there will be an upward field-aligned current (FAC) sheet at the clockwise flow shear and a downward FAC sheet at the counter clockwise cell of the flow disturbance, and these are closed via an ionospheric Pedersen current. *Lockwood et al.* [1989] discovered a correspondence between cusp auroral transients and flow enhancements, and this was interpreted by *Sandholt et al.* [1990] as Southwood FTEs. Afterwards there has been a systematic search for three observable elements of the Southwood twin cell model: (1) the newly open fast moving center flux, (2) the upward/dawnward pair of FACs on the flanks of newly open flux, and (3) the proposed return flows on either side.

[3] (1) *Pinnock et al.* [1993, 1995] identified a class of longitudinally extended Flow Channel Events (FCEs) by the PACE HF radar, consistent with the magnetic tension pull on newly open flux. The same category of events was further elaborated and termed pulsed ionospheric flows (PIFs) by *Provan et al.* [1998] and *Provan and Yoeman* [1999]. *Sandholt et al.* [2004] investigated spatial and temporal structures in the dayside aurora and flow channels for southeast IMF orientation. They identified three types of flow channels: (i) on sunward return flow on closed field lines, (ii) on newly open flux containing FTEs, and (iii) on old open field lines. Category (i) was found by *Lockwood et al.* [1993] and *Moen et al.* [1995, 2006] consistent with the *Cowley and Lockwood* [1992] model of flow generation by pulsed reconnection. Category (ii) contains the above mentioned FCEs and PIFs. Category (iii) flow channels were attributed by *Sandholt et al.* [2004], *Farrugia et al.* [2004], and *Sandholt and Farrugia* [2007]

[1]Department of Physics, University of Oslo, Oslo, Norway.
[2]European Space Agency, ESTEC, Noordwijk, Netherlands.
[3]Air Force Research Laboratory, EOARD, London, UK.
[4]Arctic Geophysics, The University Centre in Svalbard, Svalbard, Norway.
[5]Solar-Terrestrial Environmental Laboratory, Nagoya University, Nagoya, Japan.

0148-0227/08/2008JA013061$09.00

to the solar wind magnetosphere dynamo in the high-latitude boundary layer [*Stern*, 1984]. It should be noted that flow directions for all these categories are consistent with the large scale polar cap flow pattern. In this paper we will examine a fourth category of flow channels, the reversed flow events (RFEs) defined by *Rinne et al.* [2007]; reversed by means of flow opposing the background convection. We will come back to a more detailed description.

[4] (2) Candidate signatures of the FAC system of the Southwood FTE model have been reported in a series of papers. Sandholt and coworkers proposed that poleward moving auroral forms (PMAFs) are the optical footprint of the upward FTE current sheet [e.g., *Sandholt et al.*, 1990; *Sandholt and Farrugia*, 2007, and references therein]. Similarly, *Milan et al.* [2000], *McWilliams et al.* [2001], and *Lockwood et al.* [2001] located east–west elongated arcs observed by Polar UVI on one side of cusp flow channels consistent with an FTE current system. By direct measurements of FACs *Marchaudon et al.* [2004] placed a pair of upward and downward sheet currents on each side of a flow channel observed by SuperDARN consistent with the Southwood FTE model.

[5] (3) The final test of the Southwoood FTE model was to observe return flow channels. *Lockwood et al.* [1990] proposed that the return flow around Southwood FTEs may not be pronounced, but rather give rise to a reduction in the background flow. *Pinnock et al.* [1993] noticed a reduction in the background flow. *Thorolfsson et al.* [2000] carried out a detailed study of distorted flow around poleward moving auroral forms (PMAFs) combined with SuperDARN and optical data. They found clear evidence for return flow near the eastward and westward edges of east–west elongated PMAFs, consistent with their own simulation of Southwood FTEs, but no continuous return flow channels were to be expected.

[6] The Special Norwegian Fast Azimuth Scan Mode (SP-NO-FASM) on the EISCAT Svalbard Radar (ESR) provides a new important tool to map mesoscale flow structures in much greater detail. Applying this technique, *Oksavik et al.* [2004, 2005] were the first to observationally map out a clockwise flow shear around an east–west elongated PMAF that is consistent with an upward FAC sheet. They reported evidence for a twin-cell signature in support of the Southwood FTE model. *Rinne et al.* [2007] introduced the new term, reversed flow events, to characterize ~100–200 km wide east–west elongated channels that exceed the ESR field of view (~600 km) and have an average life time of ~18 minutes, i.e., quasi-static flow structures. In a systematic search through the SP-NO-FASM database of winter cusp observations, *Rinne et al.* [2007] did not find RFEs that developed in pairs, as the twin-cell FTE model predicts. Because the RFEs always occurred as east–west elongated channels, *Rinne et al.* [2007] proposed an asymmetric version of the Southwood FTE model, in which return flow develops predominantly on the poleward side of newly open flux since on the equatorward side it is inhibited by the open-closed boundary (OCB) boundary.

[7] The aim of this paper is to reveal more information about RFE flow channels and examine their relationship to discrete arcs/Birkeland currents sheets. Each RFE develops with the intensification of a discrete arc, consistent with converging electric fields and a sheet of upward FAC. The RFE phenomenon contains PMAFs as reported by *Oksavik et al.* [2004, 2005] but is not exclusively related to this category. They rather appear to be a specific feature of a Birkeland current arc system and we will propose two new explanations for the RFE phenomenon. In one explanation the RFE electric field, E_{RFE}, develops in the gap between two MI current loops. The other explanation links the flow perturbation to an auroral acceleration region.

[8] The paper is organized as follows. The instrumentation is briefly described in the following section. Section 3 presents combined radar and all-sky observations of RFEs observed on 16 and 20 December 2001. The observations are discussed in section 4, and section 5 provides a summary and concluding remarks.

2. Instrumentation

[9] The EISCAT data used in this study were obtained by the Special Norwegian Fast Azimuth Scan Mode (SP-NO-FASM [*Carlson et al.*, 2002]) that utilizes the 32 m steerable antenna at Longyearbyen (78.15°N, 16.03°E). The antenna beam was moved as a windshield wiper over the azimuth range from 180° to 300° at the lowest possible elevation of 30^0. The azimuth angle increases clockwise from geographic north. Geomagnetic north corresponds to 328° azimuth. At a slew speed of 0.625°/s it takes 192 seconds to complete one scan in each direction. During a scan data is stored every 3.2 s giving 60 adjacent beams each 2 degree wide in azimuth. The radial resolution is about 40 km and the azimuth resolution is varying from 10 km to 30 km with increasing distance from the radar. The altitude of the radar gates is increasing from 116 km at range 226 km to 585 km at range 1050 km.

[10] The all-sky imager located at Ny-Ålesund (78.92°N, 11.95°E) acquired 6 images per minute, one 630.0 nm image every 30 second followed by two 557.7 nm images. The exposure time was 1 sec for the 630.0 nm wavelength and 0.5 sec for the 557.7 nm wavelength. The aurora was red-dominated and we are only going to present 630.0 nm images projected on a geographic frame of reference assuming 250 km as the peak emission altitude.

[11] The Interplanetary magnetic field (IMF) and plasma parameters of the solar wind were obtained from the ACE spacecraft [*Chiu et al.*, 1998] located near the L1 point. In this paper we will present data from the magnetic field experiment [*Smith et al.*, 1998] and the Solar Wind Electron Proton Alpha Monitor (SWEPAM [*McComas et al.*, 1998]).

[12] SuperDARN convection maps [*Ruohoniemi and Baker*, 1998] are used to frame the large scale flow context of the mesoscale flow channels observed by ESR. These convection maps have been reanalyzed to yield IMF conditions for the estimated time lag.

3. Observations

3.1. 16 December 2001

[13] Figure 1a illustrates the fan swept by ESR in the framework of the SuperDARN convection map for 10:30–10:32 UT on 16 December 2001. The radar field of view spanned from ~12:00–13:30 MLT. The cusp inflow region was shifted several hours prenoon due to a strong IMF B_Y positive, and the ESR scan region was situated under north-

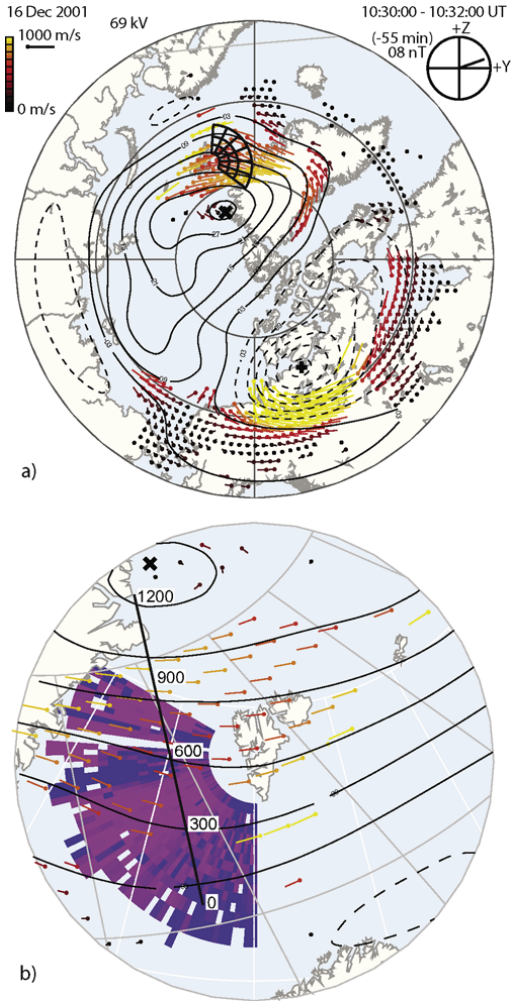

Figure 1. (a) SuperDARN convection map obtained for 10:30 UT on 16 December 2001. The fan-shaped grid located between Svalbard and Greenland indicates the ESR field of view. (b) Comparison of SuperDARN convection vectors and high-resolution velocity data measured by ESR west of Spitsbergen. Pink color in the ESR fan means line-of-sight velocity away from the radar, and blue color means flow toward the radar. The narrow blue channel elongated east–west between Svalbard and Greenland represents a reversed flow event, opposing the large scale background convection. The black measure bar from 0 to 1200 km indicates the orientation of the line used to stripe out keograms from all-sky data in Figures 4h and 5h.

westward flow of the afternoon cell. Figure 1b presents the line-of-sight velocity observed during the clockwise ESR scan from 10:29.04–10:32.12 UT together with SuperDARN convection vectors from Figure 1a. Pink color means away flow and blue means toward flow. The reversed flow event (RFE) is the blue channel elongated east–west between Svalbard and Greenland. The pink away flow is consistent with the north-westerly oriented large scale convection. However, it is the blue RFE channel of flow opposing the background that is of particular interest for this study. The black measure bar (0–1200 km) west of Spitsbergen marks the line from where we are going to present all-sky keograms (Figure 4h and Figure 5h). The ~100 km wide RFE channel was not resolved by the SuperDARN radars, probably due to a nonideal geometry.

[14] ESR scanned the area between Greenland and Svalbard from 09:30 UT to 11:00 UT. Rows 1–6 in Figure 2 display line-of-sight velocity data for six consecutive scans from 10:13–10:32 UT. Start and stop times (UT) for each ESR scan and the scan direction, clockwise (cw) or counter clockwise (ccw), are given on the top of each radar plot. Column 1 displays only the positive line-of-sight velocities radially away from the radar (negative values have been whitened out). This is complemented by column 2 that displays only the negative line-of-sight velocities (positive values have been whitened out). The first scan (10:13.04–10:16.12 UT) is entirely consistent with the large scale convection monitored by SuperDARN. Nearly homogenous strong westward flow (~1 km s^{-1}) is directed away from the radar (red color) in Sectors 4–6. Then there is a sharp transition to a blue region of weak flow further south. Comparing the first and the second row, the onset of a flow disturbance (Fs) occurred in the equator-most region of strong away flow, indicated by an arrow in Frame (2,1). In row 3 (10:19.28–10:22.36 UT) the reduced flow signature had developed in length to ~400 km, and the velocity at the centre was close to zero. In the subsequent scan ~3 minutes later (10:22.40–10:25.48 UT) the flow structure had developed in strength and size to accomplish the RFE definition introduced by *Rinne et al.* [2007]: the line-of-sight velocity inside the RFE must be larger than 250 m s^{-1} in at least 1 scan and a longitudinal extent of at least 400–600 km. The event presented in Figure 2 is RFE #10 in the statistical work by *Rinne et al.* [2007]. In the subsequent scan RFE10 exceeded the longitudinal extent of the ESR field of view (>600 km) and was ~150 km wide (Frame (4,1)). As annotated on the top row in Figure 2, the ESR field of view is subdivided in 6 wedge formed Sectors, 1 to 6 increasing clockwise, and 3 regions a–c with increasing distance in range. There are 10 beams in each sector. In order to quantify the flow disturbance of RFE10, we introduced a low-pass noise filter by averaging the velocity numbers for ~5 radar gates selected along iso-contours of the flow channel in Region b, Sectors 3–6. In the third column the averaged velocity numbers have been plotted referring to the ESR Beam number 21–60 from Sectors 3–6. From Frame (4,3) we see a flow minimum of −400 m s^{-1} within the RFE. RFE10 was located at nearly the same position in Row 5 (10:25.52–10:29.00 UT), the reversed flow had slightly reduced and the width had narrowed to ~100 km. It is also noticed that the flow equatorward of the channel had increased. 3 minutes later in Row 6, the equatorward boundary of RFE 10 had moved 100 km north, corresponding to an average drift speed of ~0.5 km s^{-1}. The westward flow equatorward of the RFE

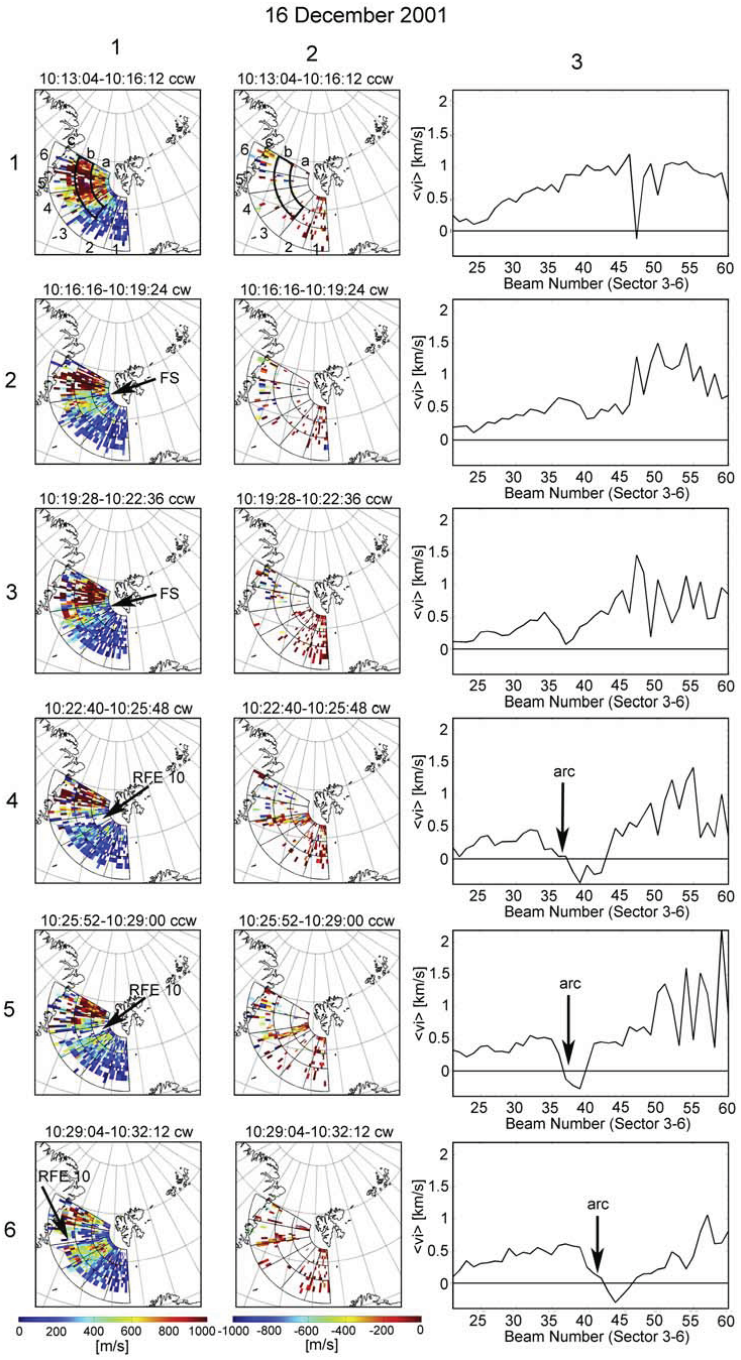
16 December 2001
1
2
3
10:13:04-10:16:12 ccw
10:16:16-10:19:24 cw
FS
10:19:28-10:22:36 ccw
10:22:40-10:25:48 cw
RFE 10
10:25:52-10:29:00 ccw
10:29:04-10:32:12 cw
<vi> [km/s]
Beam Number (Sector 3-6)
arc
0 200 400 600 800 1000
-1000 -800 -600 -400 -200 0
[m/s]

Figure 2

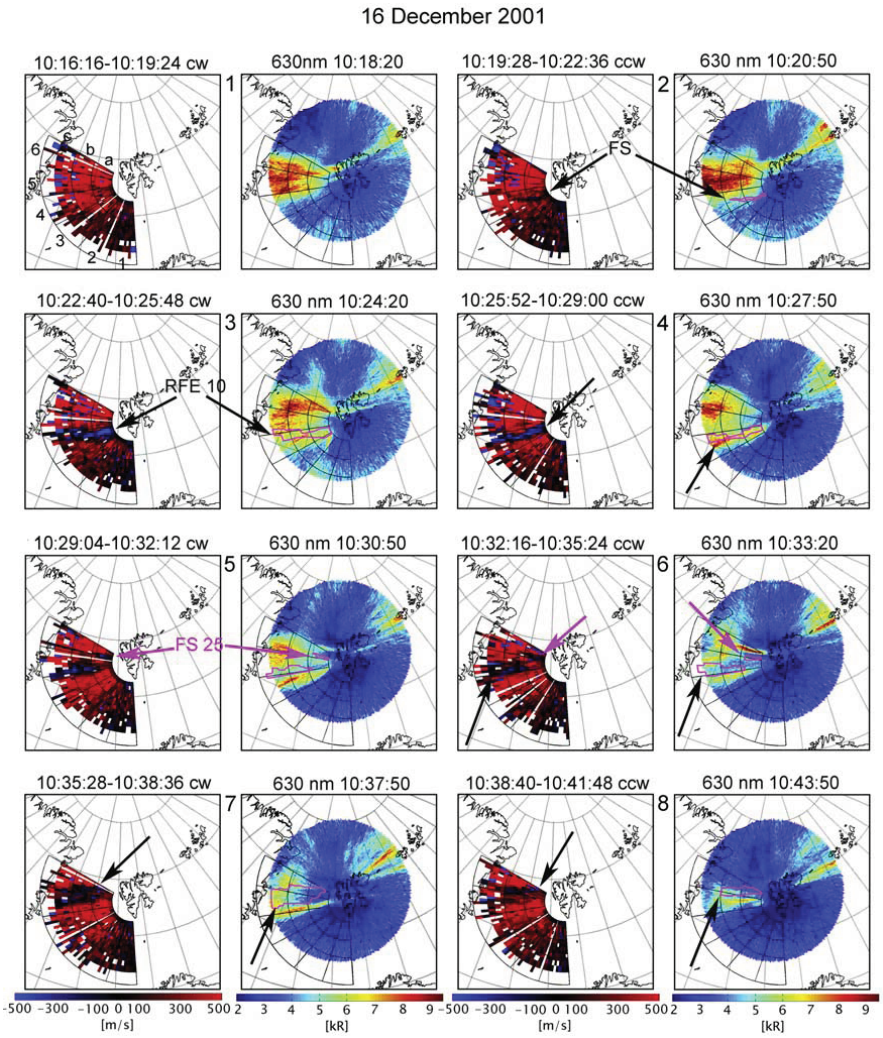

Figure 3. ESR velocity data side by side with 630.0 nm all-sky data. The ESR and the all-sky data have both been projected to 250-km altitude. The Fs (flow signature) and RFE10, indicated by arrows in the ESR scans, are ringed out with pink contours on the corresponding all-sky data. Please note that RFE10 is located on the poleward side of a discrete auroral form.

had increased further. The RFE had almost disappeared from Sector 5a, indicating it had moved westward, or, a gradual fade had started from the eastern end.

[15] In Figure 3, the evolution of RFE10 is placed in the context of the auroral morphology. A selection of 8 radar scans acquired during a half hour interval from 10:16.16–10:43.50 UT is presented side by side with the corresponding 630.0 nm all-sky image. As the 630.0 nm all-sky image was updated 6 times during each radar sweep, we have presented all-sky images from the middle of each

Figure 2. Column 1 displays positive line-of-sight velocities measured by ESR for six consecutive azimuth scans from 10:13 to 10:32 UT. Column 2 displays the corresponding negative line-of-sight velocities. Column 3 presents averaged velocity along RFE 10 in Region b, Sectors 3–6. This part of the ESR sweep is marked out with a black contour in Frame (1,1) and (1,2).

scan. The all-sky camera log book reports thick clouds around 08:00 UT, a slight weather improvement around 09:20 UT. At 10:15 UT it was reported clear sky with some clouds at the southern horizon, and entirely clear sky from 10:45 UT. In the image sequence, the cloud contamination is seen as turquoise glow in the southern part of the field of view that gradually faded. The aurora was dominated by the 630.0 nm line, and the 630.0 nm all-sky images have been projected to a common reference altitude of 250 km. The ESR reference grid has been overlaid on the all-sky images to ease the comparison. The all-sky data have been adjusted for zenith angle effects (loss of sensitivity toward the horizon), calibrated and plotted in kR with a color scale ranging from blue to red with increasing intensity. As pointed out by *Moen et al.* [1995] one has to execute care when dealing with projected data. Long auroral structures pointing at the observation site indicate the presence of tall rays projected to one altitude. The upper part of a tall ray filament will appear at a shorter radial distance from the observation site than the lower altitude part. For an auroral form that is located south of the observation site the part that is farthest away (i.e., at highest zenith angle) represents the bottom end of tall rays.

[16] Svalbard was situated near the transition between two different regimes of auroral activity. East of Svalbard in the direction of Franz Josef Land, the activity was less intense and we see examples of multiple arcs, which could be of boundary plasma sheet origin [*Sandholt et al.*, 1998]. In contrast, the cusp type auroras west of Svalbard were much more intense, a broad region with strong intensifications in the 630.0 nm aurora. A movie of the image sequence revealed episodes of eastward expansions of this cusp aurora followed by westward retreats. The first three images in Figure 3 (10:18.20–10:24.20 UT) demonstrate the end of such an eastward expansion, followed by a westward retreat out of the all-sky field of view (10:27.50–10:43.50 UT). The equatorward expansion arises through the appearance of a new auroral form equatorward of the preexisting activity at 10:24.20 UT. This new auroral form represents the new activity boundary that subsequently retreats poleward. In frame pair 3, the pink contour located adjacent to the new auroral form on the poleward side, represents the contour of RFE10 observed by ESR. In the following sequence, the auroral form and RFE10 moved together; that is, the auroral form stayed fixed to the equatorward border of RFE10 during the rest of its lifetime. Notably, the auroral form is situated near the clockwise flow reversal. A flow signature, Fs25, is annotated in ESR scans 5 and 6. It is sandwiched between two auroral brightenings. In frame pair 7 (10:37.50 UT) these two auroral filaments and Fs25 had disappeared.

[17] Figures 4a–4e presents solar wind plasma and IMF conditions for the period of interest, Figure 4g presents time variations in the SuperDARN polar cap potential, and Figure 4h presents a 630.0 keogram derived from the all-sky imager along the black line drawn across the ESR field of view in Figure 1b. The ACE satellite was located around $[X, Y, Z]_{GSM} = [239, 29, 2]R_E$. The radial solar wind velocity was around 530 km s^{-1} which means an advection time of ~50 minutes from ACE to the magnetopause. Since ACE was off the sun–earth axis by 29 R_E we used the formula provided by *Lockwood et al.* [1989] and found the time lag to be varying between 50–60 minutes, and we introduced a time shift of −55 min for the ACE data. IMF B_Y was steadily positive (~10 nT) throughout the one hour time interval presented. IMF B_Z fluctuated but was predominantly positive. A brief negative excursion occurred at the end of the primary time interval but it is not considered to have any relationship to RFE10. However, it may be related to a narrowing of the auroral activity. IMF B_X underwent large fluctuations as well, but was predominantly negative.

[18] In Figure 4h, the poleward and the equatorward flow reversal boundaries of RFE 10 are drawn as the two pink lines for the duration of the event from 10:22 UT to 10:39 UT. It is clear that the onset of the RFE occurred in association with the brightening of a new discrete auroral form equatorward of the previous activity. The discrete auroral form stayed close to the equatorward edge of RFE 10 during the 17 minute lifetime of the event. The auroral form and the boundary moved poleward together. The location of the auroral form at the flow reversal is confirmed by ESR. It gave rise to discrete intensifications in the electron concentration below 200 km consistent with particle impact ionization exactly at the equatorward edge of the RFE (data not presented). A subsequent reversed flow event, RFE11, was detected by ESR at 10:56 UT, and was seen in only two scans before the radar experiment was stopped. From Figure 4h the onset of RFE11 was also associated with the occurrence of an auroral form equatorward of the previous activity.

[19] The broad cusp activity poleward of the RFE covered Sectors 5 and 6 of the radar fan, was associated with strong north-westward flow seen by SuperDARN. Figure 4g presents the SuperDARN Polar Cap Potential. The cross polar voltage was pulsed between 60–80 kV with 4 maxima in one hour. There is no apparent relationship between the pulsing in the local cusp luminosity and the global polar cap potential. The onset of RFE10 occurred 5 minutes prior to the onset of the enhanced polar cap potential. The duration of RFE10 and the enhanced polar cap potential was about the same. The polar cap potential was decaying during the onset of RFE11.

3.2. 20 December 2001

[20] Figure 5 presents observations from 20 December 2001 in the same format as Figure 4. The ACE data has been time shifted 70 minutes to account for the approximate signal delay between ACE and the ionospheric response. IMF Bz was steadily negative around −5 nT until 10:50 UT when it rapidly turned to +5 nT and then back negative 7 minutes later. The ESR scanned the same area as on 16 December, and monitored northwestward flow of the afternoon cell. It continuously swept this area from 10:06 UT to 10:58 UT. The auroral activity displayed in Figure 5h represents the classical sequence of PMAFs. The onset of RFE18 occurred in the middle of a sequence of poleward moving forms (PMAFs). The RFE developed in association with a new auroral form, on the poleward side. This RFE event moved poleward in tandem with the PMAF. By definition of reversed flow, the RFE faded around 10:42 UT, but a reduction in the background flow

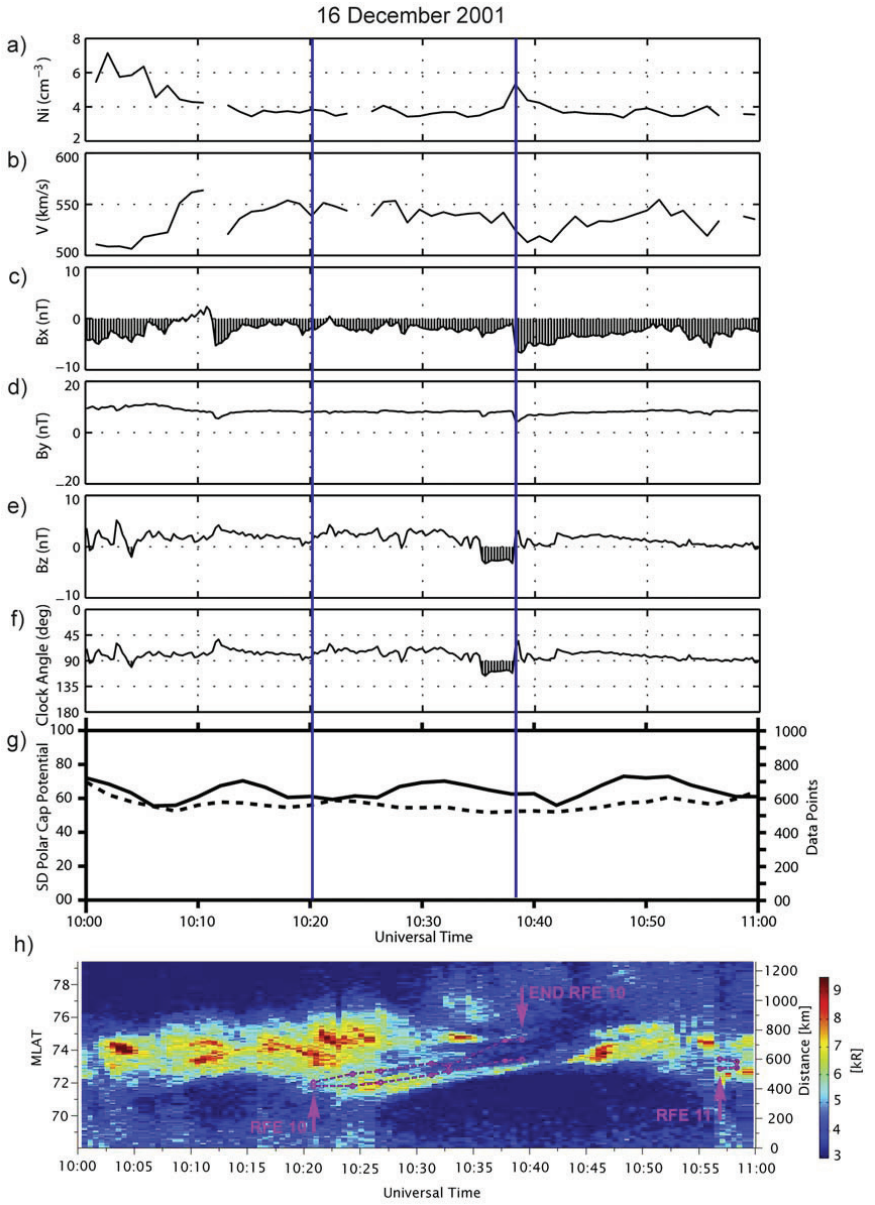

Figure 4. (a–f) Solar wind parameters from the ACE satellite measured in GSM coordinates on 16 December 2001 and shifted in time to correspond with ground observations from 10 to 11 UT. The IMF clock angle increases from 0° due north to 180° due south. (g) The solid curve represents the northern hemisphere polar cap potential (kV, left axis) derived from SuperDARN convection maps. The dashed curve represents the number of data points (right axis) from which the convection maps were calculated. (h) Color-coded 630.0 nm emission intensity (kR) versus time and MLAT along the black measure bar in Figure 1b (also given on the right axis). The pink lines mark the RFE boundaries. The vertical blue guidelines in panels a–g mark the duration of RFE10.

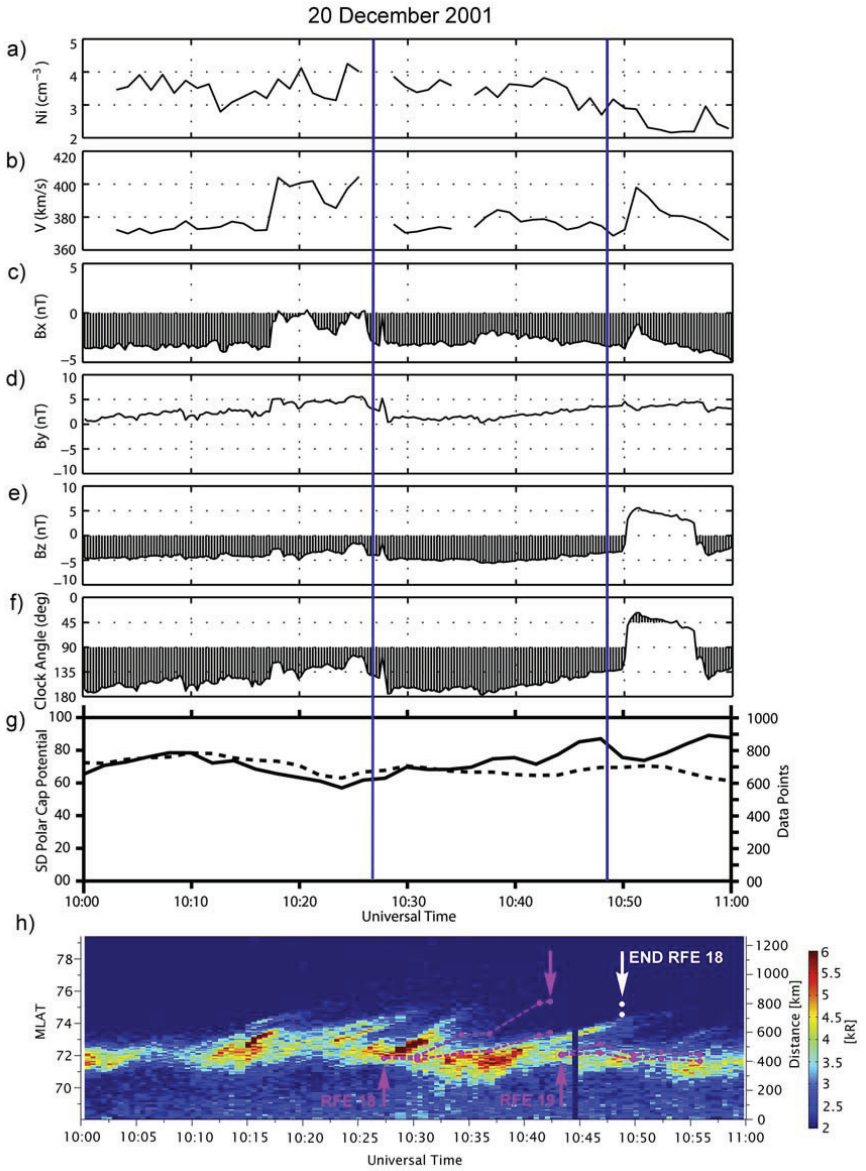

Figure 5. Solar wind, SuperDARN, and optical data for 10 to 11 UT on 20 December 2001, presented in the same format as Figure 4. The vertical blue guidelines in panels a–g mark the duration of RFE18.

was observed until 10:48 UT, marked by the two white dots, that is, as long as the PMAF was observed. The subsequent event (RFE19) also occurred in association with a brightening auroral form. However, instead of moving poleward with the faint PMAF that broke loose from the background arc around 10:53 UT, it stayed with the bright background arc. Traces of particle impact ionization were observed at the equatorward edge of both RFE 18 and 19; that is, the discrete auroral forms were located on the clockwise flow reversal.

[21] Although the RFE onsets occurred in association with increased polar cap potential, over their life time there is no clear trend between RFEs and the modulation of the polar cap potential. The RFE-FAC system is likely to be part of a localized current–voltage system.

4. Discussion

4.1. Observation Summary

[22] Up to now we only have three days of combined radar and optical observations of reversed flow events (RFEs). One of these days was reported by *Oksavik et al.* [2004, 2005] and the other two days were presented in section 3 above. *Oksavik et al.* [2005] analyzed a sequence of RFE channels located on the poleward side of discrete PMAFs, in the sense consistent with a clockwise flow shear and an upward FAC. Their RFEs occurred under conditions of IMF B_Y positive and IMF B_Z negative. With regard to the auroral morphology, the situation is more complex on 16 December 2001 presented here when IMF B_Z and B_Y are both positive (Figure 4). RFE 10 occurred in association with a brightening arc filament equatorward of a broad region of preexisting cusp type auroral activity. Also, in this case, the RFE clockwise flow shear is collocated with a discrete auroral form consistent with an upward Birkeland current sheet. The RFE and the Birkeland current arc moved poleward in tandem, and the RFE disappeared when the arc fainted. On 20 December 2001, IMF B_Z was south and IMF B_Y was positive, and the classical sequence of PMAFs was observed (Figure 5h). On this day, RFE18 moved in tandem with a PMAF, but RFE19 did not; it stayed with the background instead of breaking loose to follow a weak PMAF. It should however be noted that no RFE occurrence does not necessarily mean lack of flow disturbance. *Rinne et al.* [2007] reported a flow structure (Fs30) lasting from 10:16–10:25 UT, and from Figure 4h we see that a weak but discrete PMAF actually separated from the background aurora during that time interval. Fs25 in Figure 3 occurred between two arc filaments (frame 5 and 6). Hence the RFEs may represent the "top of the iceberg" of flow disturbances, strong enough to reverse the flow, while the less prominent flow structures may be related to a flow reduction only.

[23] Most of the RFEs documented so far developed post noon, near the equatorward boundary of the cusp inflow region for IMF B_Y positive. However, the current SP-NO-FASM database is strongly biased toward IMF B_Y positive [*Rinne et al.*, 2007].

[24] In contrast, to the three categories of flow channels reported by *Sandholt et al.* [2004], all speeding up the large scale convection pattern, the RFE category reverts the background flow (cf. Introduction). The RFEs reported here occurred in the afternoon cell, as 100–200 km wide channels of eastward flow, i.e., flow opposing the magnetic tension pull for IMF B_Y positive. *Farrugia et al.* [2004] reported antisunward (eastward) flow bursts in the same time sector, but for IMF B_Z negative. Their flow events occurred in a broad region of antisunward flow, poleward of a well-defined flow reversal consistent with a crescent shaped dusk cell. Their flow bursts were in same direction as the background flow and attributed to the solar wind magnetosphere dynamo in the high-latitude boundary layer [*Stern*, 1984], i.e., fundamentally different from RFEs.

4.2. Comments on the FTE Twin-Cell Explanation for RFEs

[25] The connection between PMAFs and RFEs was readily documented by *Oksavik et al.* [2004, 2005]. In a statistical work *Rinne et al.* [2007] found that all their flow events (31 flow structures and 21 RFEs) were scattered within the IMF clock angle range from 40–240°, i.e., within the wide range of clock angles (30–330°) for which bursty reconnection at the magnetopause may occur [*Neudegg et al.*, 2000]. *Oksavik et al.* [2004, 2005] interpreted the reversed flow channels in terms of the return flows of the twin-cell FTE model by *Southwood* [1987]. However, there are problems with this FTE explanation:

[26] (1) *Rinne et al.* [2007] did not find evidence for RFEs developing in pairs as the twin-cell FTE model predicts. In cases when two RFEs coexisted within the radar field of view there was ~10–30 minutes delay in the onset time between the first and the second event.

[27] (2) The RFE channels remain extremely narrow during their life time. The RFE channels are usually around 100 km wide but up to 250 km on occasion. In the rest frame of a Southwood FTE event there will be return flow on either side of the newly opened centre flux moving fast under the action of the magnetic tension force, pushing its way through the ambient plasma moving more slowly. In the case of no background flow, one would also see the return flow in the rest frame of the radar. Due to incompressibility the return flow pattern will broaden very quickly. However, in the normal case when one event after the other superimposes on decent background convection, the "return" flow around each event should rather appear as reductions in the background flow, as suggested by *Lockwood et al.* [1990] and *Pinnock et al.* [1993], and simulated by *Thorolfsson et al.* [2000].

[28] (3) The category of PMAF events in the cusp have been attributed to transient magnetopause reconnection [e.g., *Sandholt et al.*, 1990, 1993; *Denig et al.*, 1993; *Milan et al.*, 1999, 2000; *Thorolfsson et al.*, 2000; *Moen et al.*, 2001]. From Figure 5 we noted that the RFE phenomenon does not uniquely relate to the category of PMAFs; RFE 19 stayed with the background arc.

[29] Let us now consider an FTE approach on RFE10 on 16 December (Figures 2, 3, and 4). RFE10 and the associated Birkeland current arc developed equatorward of a broad region of cusp precipitation (cf. Figure 3 and Figure 4h). From the image sequence in Figure 3 the broad region of intense cusp auroral activity at the beginning subsequently faded and/or moved westward out of the all-sky field of view. RFE10 moved with the trailing edge of the cusp activity. Assume that the arc brightening was part of an FTE event. In this case when IMF B_Y was large and positive, the initial magnetic tension on newly open flux is expected to have a strong westward component [*Cowley et al.*, 1991]. This excludes the RFE channel itself from being the newly opened flux, but potentially it could represent the return flow on the poleward side of the newly opened flux region [*Oksavik et al.*, 2004, 2005; *Rinne et al.*, 2007]. For IMF B_Y large positive, a longitudinally elongated channel of newly opened flux pulled westward, will be bounded by an upward FAC sheet on the poleward edge and a downward FAC sheet on the equatorward edge [*Taguchi et al.*, 1993]. However, if the Birkeland current arc actually

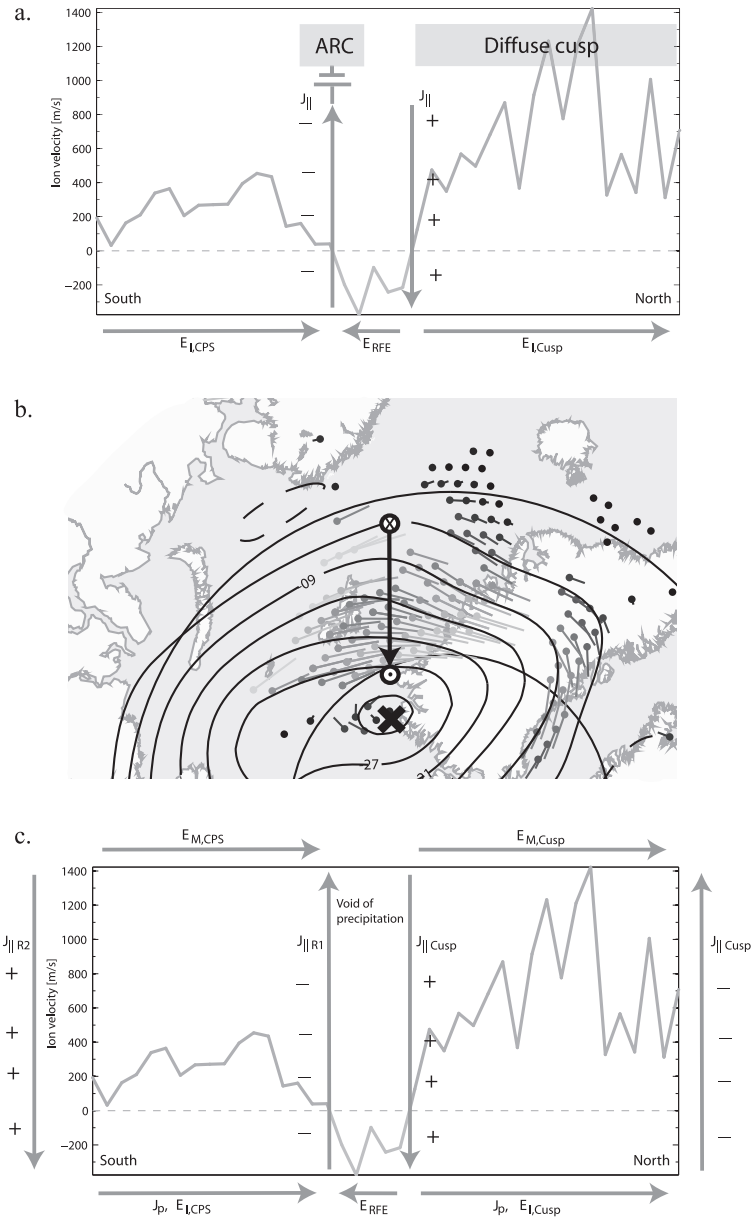

Figure 6. (a) A schematics to summarize the observations of RFE10 on 16 December 2001. The ⟨vi⟩ curve is from Figure 2. ⟨vi⟩ negative east corresponds to a southward electric field within the RFE flow channel. ⟨vi⟩ positive west corresponds to a northward electric field addressed to the closed magnetosphere equatorward of this channel, and open cusp field lines correspond to poleward of this channel. The discrete arc represents an upward FAC at the clockwise flow reversal boundary. (b) The large scale north electric field vector associated with the dusk cell overlaid the SuperDARN flow pattern as shown in Figure 1 for 10:30 UT on 16 December 2001. (c) A schematic illustration of the RFE phenomenon that occurs between two current loops, forced by two separate voltage generators. The E_{RFE} is located in a region void of precipitation.

marked the poleward border of newly opened flux, the region of newly opened flux equatorward of it was invisible to our all-sky imager. Newly opened flux is supposed to be associated with bulk injection of magnetosheath plasma, and magnetosheath electron precipitation efficiently heats F2 region electron plasma [*Lockwood et al.*, 1993; *Waterman et al.*, 1994; *Nilsson et al.*, 1996; *Pryse et al.*, 2000; *Doe et al.*, 2001; *Moen et al.*, 2004b]. With certain constraints the elevated electron temperature (T_e) can be used to identify the cusp open-closed boundary [*Doe et al.*, 2001; *Moen et al.*, 2004b]. ESR did observe elevated T_e with the discrete auroral form, but not equatorward of it. This makes us conclude that the RFE10 Birkeland current arc was either located on closed field lines, or it was a signature of the OCB. That is, we discard the possibility of newly open flux equatorward of the RFE10 channel and the RFE10-Birkeland current arc system does not fit into the FTE picture anticipated.

[30] On December 20 in Figure 5 on the other hand, a broad 630 nm flash, ~2 degrees in latitude, was observed equatorward of RFE18 at the beginning, before it narrowed to a thin arc at ~10:42. This region was associated with elevated T_e observed by ESR (data not presented). The flash region may indeed signalize the expected bulk injection of magnetosheath electrons on newly opened field lines, bounded with an upward FAC sheet on the poleward side and a downward FAC sheet on the equatorward side. That is, RFE18 is consistent with a PMAF-FTE signature for IMF B_Y positive and B_Z negative.

4.3. Relationship Between RFEs and Birkeland Current Arcs

[31] For all the RFEs observed with complementary optics, the clockwise shear does always develop together with a discrete auroral form consistent with an upward Birkeland current sheet. Discrete auroral forms represent a footprint of accelerated electron precipitation. There are two acceleration mechanisms frequently observed above the ionospheric cusp: Kinetic Alfvén waves (KA waves [*Chaston et al.*, 2007]) and inverted Vs [*Lin and Hoffman*, 1982]. Inverted V-type electron precipitation gives rise to monoenergetic beams while dispersive KA waves give rise to a broader energy range within the beam [*Chaston et al.*, 2007]. The maximum energy of KA waves is very similar to that reported for dayside inverted Vs [*Lin and Hoffman*, 1982], both around 1 keV. Inverted Vs and KA waves can easily be distinguished from each other in satellite and rocket data, while more difficult from ground.

[32] The schematics in Figure 6a is based on the averaged $\langle v_{los} \rangle$ curve in Frame (4,3) of Figure 2. Superimposed on this plot is the location of the Birkeland current arc, and the diffuse 630.0 nm auroral cusp region that straddled the northern part of the radar field of view. It is noted from Figure 3.1, that intense cusp auroral activity covered Sectors 5 and 6 of the ESR fan, while the region of strong flows covered Sectors 4–6. That is, the background of strong westward flow was extended well equatorward of the cusp auroral boundary, taken as a proxy of the open-closed boundary [*Moen et al.*, 1996, 1998]. The electric field $E_{I\ CPS}$, south of the discrete arc structure is located at subauroral latitudes. $E_{I,CUSP}$ is the electric field associated with the strong westward flow in the auroral cusp region. E_{RFE} is situated in a region void of auroral precipitation. The most poleward flow reversal (counter-clockwise) is consistent with a downward current.

[33] Let us now put these observations in the context of expected large scale current systems. Figure 6b illustrates the convection electric field vector consistent with sunward flow in the dusk cell. As indicated this E-field vector requires a downward FAC near the equatorward boundary of the dusk cell and an upward FAC at the dusk cell flow reversal. The poleward part of this vector was straddled with cusp auroral activity on open field lines.

[34] The portion of this vector at subauroral latitudes; that is, equatorward of the discrete auroral form was likely mapping to the central plasma sheet (CPS). On the top of Figure 6c, we have therefore indicated two different electric fields forcing a westward movement of ionospheric plasma; $\mathbf{E}_{M,CUSP}$ and $\mathbf{E}_{M,CPS,}$ representing open and closed flux, respectively. The RFE channel itself could be on open or it could be on closed field lines. Anyway, this idealized picture suggests two different MI-current loops. One is the Region 2–Region 1 current system on closed field lines, and the other is the large scale cusp current system forced by the solar wind. The polarity of the cusp current system is consistent with reconnection for IMF B_Y positive [*Taguchi et al.*, 1993]. In this large scale perspective, the RFE convection channel was located at the boundary between two different current systems mapping to widely different flow generators in the magnetosphere. In this perspective, it appears that the E-field discontinuity associated with RFE10 developed locally at a boundary transition region. According to the auroral arc classification made by *Marklund* [1984], the RFE flow signature bear resemblance to his category II_b of Birkeland current arcs, with a double flow reversal.

[35] We can think about two possible explanations for the RFE phenomenon:

[36] (1) In Figure 6c, the E_{RFE} is located in between two MI-current loops, each forced by a separate voltage generator. For this particular case one loop was on open field lines and the other loop appears to be on closed field lines. However, in a sequence of RFEs/PMAFs as presented by *Oksavik et al.* [2005], it could be that successive current loops map to distinct reconnection sites. The major point here is that each current loop is forced by an independent voltage generator, and that there is a small gap or E-field discontinuity between them. RFE10 was located between the discrete auroral form and the cusp auroral activity, i.e., in a region void of precipitation. In absence of solar EUV ionization in the E and lower F region, this means very low height-integrated Pedersen conductivity there. A large E_{RFE} arises if the two current loops at different potential couple through the low conducting ionosphere. Low Pedersen conductivity and poor cross coupling provides an explanation for the long life time.

[37] (2) The bipolar form of RFE10 may possibly be the ground signature of an inverted V acceleration region. As was noted in Figure 2 the background flow was gradually suppressed in the development phase of RFE10. This may indicate a partial decoupling from the magnetosphere due to a field-aligned potential drop. A dayside inverted V is

typically of the order of 1 keV and it will have a very different effect on the ionosphere than a nighttime inverted V of the order of 10 keV.

[38] Due to the relatively long life time RFEs can be treated as a quasi-stationary phenomenon. Assuming that the E and F region neutral winds are negligible compared to the $E_\perp \times B$ drift, the current density perpendicular to the electric field can be written as

$$j_\perp = \sigma E_\perp + \sigma_H B^{-1} B \times E_\perp \quad (1)$$

where σ_H and σ_P are the Hall and Pedersen conductivities, respectively, and B is the magnitude of Earth magnetic field. [e.g., *Boström*, 1964; *Burch et al.*, 1976]. Assuming divergence free currents, $\nabla \times j = 0$ or $\nabla \times j_\perp + \nabla \times j_{||} = 0$ (i.e., no accumulation of space charges), and quasi-stationary electric field structures, $\nabla \times \mathrm{E} = \nabla \times \mathrm{E}_\perp + \nabla \times \mathrm{E}_{||}$, we have the following expression for the FAC:

$$-\nabla \cdot j_{||} = \sigma_P \nabla \cdot E_\perp + (\nabla \sigma_P) \cdot E_\perp + (\nabla \sigma_H) B^{-1} (B \times E_\perp) + \sigma_H B^{-1} B \cdot (\nabla \times E_{||}) \quad (2)$$

Escoubet et al. [1995] found narrow 0.2–1 keV electron precipitation structures on the boundaries of the cusp in 80% of the DE2 cusp/cleft crossings, typically 1 or 2 structures per cusp/cleft crossing, possibly related to shears in plasma convection [*Escoubet et al.*, 1992]. Such low energy electron beams will not give rise to significant enhancements in E-region Hall and Pedersen conductivities. For the events presented here on 16 and 20 December 2001, traces of particle impact ionization were observed down to 140–200 km, i.e., gradients in the electron concentration occurred well above the peak in the Pedersen and Hall mobility coefficients [*Moen and Brekke*, 1990]. Hence the conductivity gradient terms in the second and the third term in equation (2) can be neglected. Furthermore, if we assume no field-aligned acceleration underneath the ESR flow measurements, the fourth term on the right hand side can also be neglected as well and the field-aligned distribution of current density is directly proportional to $\nabla \times E_\perp$ and will hence peak at the flow shear, as actually observed for all the RFE events presented here.

[39] The 10 keV electron beams at night will give rise to strong gradients in the Pedersen conductivity and subsequently a short circuiting effect due to the second term on the right-hand side in equation (2) [*Burch et al.*, 1976]. Auroral potential structures at night are therefore observed as spikes in the E-field [e.g., *Burch et al.*, 1976; *Marklund*, 1984, and references therein]. However, in the cusp ionosphere, an auroral potential structure of a few hundred eV will not give rise to significant modulation in the Pedersen conductivity and is therefore not subject to a significant E-region short cutting effect. A flow shear that develops near a magnetospheric discontinuity will therefore be preserved when mapped down to the ionosphere.

[40] From ground-based data alone we are not in the position to describe the auroral potential region. Features driven by KA waves will generally be highly variable (on second timescales) and have forms/structures generally less than 10 km in width [e.g., *Kletzing*, 1994; *Chaston et al.*, 2007]. The 10–20 min long RFE life time means a quasi-static nature. The half-width of the RFE disturbance is of the order 100–200 km as for inverted Vs [*Lyons*, 1980]. The flow potential across the RFE in Figure 6a is 0.8 kV, i.e., of the same order as the field-aligned potential drop.

[41] All the RFEs covered by optics developed near the OCB, which is an observed feature also for inverted Vs. *Burch et al.* [1990] found that the dayside inverted Vs typically occur on the immediate equatorward side of the cusp/cleft region which contains trapped electrons. *Menietti and Smith* [1993] presented examples of dayside inverted Vs for IMF B_Z negative which they attributed to the low-latitude boundary layer (LLBL), on closed or freshly open flux. As pointed out in a recent work by *Menietti et al.* [2007] it is still not clear if dayside inverted Vs are magnetically connected to reconnection sites or not. *Moen et al.* [2004a] observed the connection between PMAFs and ion up-flow events observed by ESR. The ion up-flow events broadened in a characteristic V-shape consistent with an inverted V-potential structure moving over the radar. However, future work is needed to eventually establish a connection between RFEs and inverted Vs.

5. Summary and Concluding Remarks

[42] Reversed Flow Events (RFEs) are characterized by longitudinally elongated 100–200 km wide channels of 10–20 min life time, i.e., a mesoscale quasi-stationary phenomenon. The direction of zonal motion within the channel opposes the background convection governed by magnetic tension [*Rinne et al.*, 2007]. The RFEs stay in stark contrast to the 3 categories of flow channels reported by *Sandholt et al.* [2004], which all added drive to the large-scale convection. (cf. section 1). In this paper we have performed a detailed examination of this event category by comparing EISCAT Svalbard Radar and all-sky camera observations near winter solstice.

[43] For every RFE there was a thin auroral form aligned with the clockwise convection reversal, consistent with a converging electric field and an upward Birkeland current sheet. The RFE phenomenon appears to be an intimate part of a Birkeland current arc system with a double flow shear, similar to category $\mathrm{II_b}$ in *Marklund* [1984]. As discussed in section 4.2 there are problems with the Southwood FTE interpretation of the RFE phenomenon. The *Southwood* [1987] FTE model is lacking a current sheet to put a latitudinal constraint on the return flow. Instead, the return flows are supposed to broaden very quickly due to incompressibility [*Thorolfsson et al.*, 2000]. In section 4.3 we proposed two alternative explanations for the RFE phenomenon:

[44] (1) The RFE electric field arises in between two large-scale current loops as schematically illustrated in Figure 6c; each mapping to a different boundary layer/reconnection site. Notably the RFE channel is a region void of precipitation and particle impact ionization will not contribute to the Pedersen conductance. This interpretation works only for low Pedersen conductance across RFE channel, which means a summer–winter asymmetry in the occurrence rate.

[45] (2) The quasi-stationary nature and the bipolar form of the RFE flow disturbance seem consistent with an inverted V type potential structure. Inverted Vs is a com-

monly observed phenomenon near the dayside OCB [*Burch et al.*, 1990; *Menietti and Smith*, 1993; *Menietti et al.*, 2007]. Electron beams of <1 keV on the dayside will not give rise to significant conductivity gradients and the shape of the magnetospheric E-field discontinuity will be conserved when mapped down onto the ionosphere. As was noted in Figure 2 the background flow was gradually suppressed (Fs) in the development phase of RFE10. This may indicate a partial decoupling from the magnetosphere due to a field-aligned potential drop.

[46] The two explanations above may be closely related to each other. For example, the discontinuity in the magnetospheric electric field proposed in (1) may be the precondition for the inverted V proposed in (2). Combined ground and in situ observations will be needed to establish the electrodynamic context of the RFE phenomenon, including Alfvén waves and field-aligned acceleration, small and large scale FACs, and how these flow channels map relative to active reconnection sites/FTEs.

[47] We plan to continue SP-FASM experiments at EISCAT Svalbard Radar to search for summer–winter asymmetry in the occurrence rate of reversed flow channels. Although the RFE phenomenon has not yet been reported based on SuperDARN observations, given their spatial dimension and long lifetime they should be observable. For the large scale convection picture the RFEs are negligible. The flow potential of a typical event is ~1 kV. However, this phenomenon may in fact be very important for the production of HF backscatter irregularities in the cusp region. KHI will grow very rapidly at the RFE flow reversals [*Carlson et al.*, 2007].

[48] **Acknowledgments.** EISCAT is an international association supported by research organizations in China (CRIRP), Finland (SA), France (CNRS, till end 2006), Germany (DFG), Japan (NIPR and STEL), Norway (NFR), Sweden (VR), and the United Kingdom (STFC). We thank the ACE Science Center and the ACE MAG and SWEPAM instrument teams for providing data from the ACE space craft. We acknowledge the Johns Hopkins University Applied Physics Laboratory for providing web access to SuperDARN convection maps. Financial support has been provided by the Norwegian Research Council, AFOSR task 2311AS, and Nagoya University.

[49] Wolfgang Baumjohann thanks Eric Lund and Stephan Buchert for their assistance in evaluating this paper.

References

Boström, C. (1964), A model of the auroral electrojets, *J. Geophys. Res.*, *69*, 4983.

Burch, J. L., W. Lennartsson, W. B. Hanson, R. A. Heelis, J. H. Hoffman, and R. A. Hoffman (1976), Properties of Spikeline shear flow reversals observed in the auroral plasma by atmospheric explorer C, *J. Geophys. Res.*, *22*, 3886–3896.

Burch, J. L., J. D. Menietti, and J. A. Slavin (1990), Dayside auroral particle acceleration mechanisms derived from dynamics explorer data, *J. Geomag. Geoelectr.*, *42*, 1365–1378.

Carlson, H. C., K. Oksavik, J. Moen, A. P. van Eyken, and P. Guio (2002), ESR mapping of polar cap patches in the dark cusp, *Geophys. Res. Lett.*, *29*(10), 1386, doi:10.1029/2001GL014087.

Carlson, H. C., T. Pedersen, S. Basu, M. Keskinen, and J. Moen (2007), Case for a new process, not mechanism, for cusp irregularity production, *J. Geophys. Res.*, *112*, A11304, doi:10.1029/2007JA012384.

Chaston, C. C., C. W. Carlson, J. P. McFadden, R. E. Ergun, and R. J. Strangeway (2007), How important are dispersive Alfvèn waves for auroral particle acceleration?, *Geophys. Res. Lett.*, *34*, L07101, doi:10.1029/2006GL029144.

Chiu, M. C., et al. (1998), ACE spacecraft, *Space Sci. Rev.*, *86*, 257–284.

Cowley, S. W. H., J. P. Morelli, and M. Lockwood (1991), Dependence of convective flows and particle precipitation in the high-latitude dayside ionosphere on the X and Y components of the interplanetary magnetic field, *J. Geophys. Res.*, *96*, 5557–5564.

Cowley, S. W. H., and M. Lockwood (1992), Excitation and decay of solar wind-driven flows in the magnetosphere-ionosphere system, *Ann. Geophys.*, *10*, 103–115.

Denig, W. F., W. J. Burke, N. C. Maynard, F. J. Rich, B. Jacobsen, P. E. Sandholt, A. Egeland, S. Leontjev, and V. G. Vorobjev (1993), Ionospheric signatures of dayside magnetopause transients: A case study using satellite and ground measurements, *J. Geophys. Res.*, *98*, 5969–5980.

Doe, R. A., J. D. Kelly, and E. R. Sánchez (2001), Observations of persistent dayside F region electron temperature enhancements associated with soft magnetosheath-like precipitation, *J. Geophys. Res.*, *106*, 3615–3630.

Escoubet, C. P., M. F. Smith, S. F. Fung, P. C. Anderson, R. A. Hoffman, E. M. Basinska, and J. M. Bosqued (1992), Staircase ion signature in the polar cusp: A case study, *Geophys. Res. Lett.*, *19*, 1735–1738.

Escoubet, C. P., M. F. Smith, S. F. Fung, and R. A. Hoffman (1995), Electron structures in the cusp/cleft region observed by DE 2 satellite, *J. Geophys. Res.*, *100*, 1597–1610.

Farrugia, C. J., et al. (2004), Pulsed flows at the high-altitude cusp poleward boundary, and associated ionospheric convection and particle signatures, during Cluster-FAST-SuperDARN-Søndrestrøm conjunction during southwest IMF, *Ann. Geophys.*, *22*, 2891–2905.

Goertz, C. K., E. Nilsen, A. Korth, K. H. Glassmeier, C. Haldoupis, P. Hoeg, and D. Hayward (1985), Observations of possible ground signatures of flux transfer events, *J. Geophys. Res.*, *90*, 4069–4078.

Haerendel, G., G. Pashmann, N. Sckopke, H. Rosenbauer, and P. C. Hedgecock (1978), The frontside boundary layer of the magnetosphere and the problem of reconnection, *J. Geophys. Res.*, *83*, 3195–3216.

Kletzing, C. A. (1994), Electron acceleration by kinetic Alfvèn waves, *J. Geophys. Res.*, *99*, 11,095–11,103.

Lin, C. S., and R. A. Hoffman (1982), Observations of inverted-V electron precipitation, *Space Sci. Rev.*, *33*, 415–457.

Lockwood, M., and M. F. Smith (1992), The variation of reconnection rate at the dayside magnetopause and cusp ion precipitation, *J. Geophys. Res.*, *97*, 14,841–14,847.

Lockwood, M., P. E. Sandholt, S. W. H. Cowley, and T. Oguti (1989), Interplanetary magnetic field control of dayside auroral activity and the transfer of momentum across the dayside magnetopause, *Planet. Space Sci.*, *37*, 1347–1365.

Lockwood, M., S. W. H. Cowley, P. E. Sandholt, and R. P. Lepping (1990), The ionospheric signatures of flux transfer events and solar wind dynamic pressure changes, *J. Geophys. Res.*, *95*, 17,113–17,135.

Lockwood, M., J. Moen, S. W. H. Cowley, A. D. Farmer, U. P. Løvhaug, H. Lühr, and V. N. Davda (1993), Variability of dayside convection and motions of the cusp/cleft aurora, *Geophys. Res. Lett.*, *20*, 1011–1014.

Lockwood, M., S. E. Milan, T. Onsager, C. H. Perry, J. A. Scudder, C. T. Russell, and M. Brittnacher (2001), Cusp ion steps, field aligned currents and poleward moving auroral forms, *J. Geophys. Res.*, *106*, 29,555–29,569.

Lyons, L. (1980), Generation of large-scale regions of auroral currents, electric potentials, and precipitation by the divergence of the convection electric field, *J. Geophys. Res.*, *85*, 17–24.

Marklund, G. (1984), Auroral arc classification scheme on the observed arc-associated electric field pattern, *Planet. Space Sci.*, *32*, 193–211.

Marchaudon, A., J.-C. Cerisier, R. A. Greenwald, and G. J. Sofko (2004), Electrodynamics of a flux transfer event; Experimental test of the Southwood model, *Geophys. Res. Lett.*, *31*, L09809, doi:10.1029/2004GL019922.

McComas, D. J., S. J. Bame, P. Barker, W. C. Feldman, J. L. Phillips, P. Riley, and J. W. Griffee (1998), Solar wind electron proton alpha monitor (SWEPAM) for the advanced composition explorer, *Space Sci. Rev.*, *86*, 563–612.

McWilliams, K. A., T. K. Yoeman, and S. W. H. Cowley (2001), Two-dimensional electric field measurements in the ionospheric footprint of a flux transfer event, *Ann. Geophys.*, *19*, 1584–1598.

Menietti, J. D., and M. F. Smith (1993), Inverted Vs spanning the cusp boundary layer, *J. Geophys. Res.*, *98*, 11,391–11,400.

Menietti, J. D., R. A. Frahm, A. Korth, F. S. Mozer, and Y. Khotyaintsev (2007), Polar and cluster observations of a dayside inverted-V during conjunction, *Ann. Geophys.*, *25*, 543–555.

Milan, S. E., M. Lester, S. W. H. Cowley, J. Moen, P. E. Sandholt, and C. J. Owen (1999), Meridian-scanning photometer, coherent HF radar, and magnetometer observations of the cusp: A case study, *Ann. Geophys.*, *17*, 159–172.

Milan, S. E., M. Lester, S. W. H. Cowley, and M. Brittnacher (2000), Convection and auroral response to a southward turning of the IMF: Polar UVI, CUTLASS, and IMAGE signatures of transient magnetic flux transfer at the magnetopause, *J. Geophys. Res.*, *105*, 15,741–15,755.

Moen, J., and A. Brekke (1990), On the importance of ion composition to conductivities in the auroral ionosphere, *J. Geophys. Res.*, *95*, 10,687–10,693.

Moen, J., P. E. Sandholt, M. Lockwood, W. F. Denig, U. P. Løvhaug, B. Lybekk, A. Egeland, D. Opsvik, and E. Friis-Christensen (1995), Events of enhanced convection and related dayside auroral activity, *J. Geophys. Res.*, *100*, 23,917–23,934.

Moen, J., D. Evans, H. C. Carlson, and M. Lockwood (1996), Dayside moving auroral transients related to LLBL dynamics, *Geophys. Res. Lett.*, *23*, 3247–3250.

Moen, J., D. A. Lorentzen, and F. Sigernes (1998), Dayside moving auroral forms and bursty proton auroral events in relation to particle boundaries observed by NOAA-12, *J. Geophys. Res.*, *103*, 14,855–14,863.

Moen, J., A. P. van Eyken, and H. C. Carlson (2001), EISCAT Svalbard Radar observations of ionospheric plasma dynamics in relation to dayside auroral transients, *J. Geophys. Res.*, *106*, 21,453–21,461.

Moen, J., K. Oksavik, and H. C. Carlson (2004a), On the relationship between ion upflow events and cusp auroral transients, *Geophys. Res. Lett.*, *31*, L11808, doi:10.1029/2004GL020129.

Moen, J., M. Lockwood, K. Oksavik, H. C. Carlson, W. F. Denig, A. P. van Eyken, and I. W. McCrea (2004b), The dynamics and relationships of precipitation, temperature and convection boundaries in the dayside auroral ionosphere, *Ann. Geophys.*, *22*, 1973–1987.

Moen, J., H. C. Carlson, K. Oksavik, C. P. Nielsen, S. E. Pryse, H. R. Middleton, I. W. McCrea, and P. Gallop (2006), EISCAT observations of plasma patches at sub-auroral cusp latitudes, *Ann. Geophys.*, *24*, 2363–2374.

Neudegg, D. A., et al. (2000), A survey of magnetospause FTEs and associated flow bursts in the polar ionosphere, *Ann. Geophys.*, *18*, 416–435.

Nilsson, H., M. Yamauchi, L. Eliasson, O. Norberg, and J. Clemmons (1996), Ionospheric signature of the cusp as seen by incoherent scatter radar, *J. Geophys. Res.*, *101*, 10,947–10,963.

Oksavik, K., J. Moen, and H. C. Carlson (2004), High-resolution observations of the small-scale flow pattern associated with a poleward moving auroral form in the cusp, *Geophys. Res. Lett.*, *31*(11), L11807, doi:10.1029/2004GL019838.

Oksavik, K., J. Moen, H. C. Carlson, R. A. Greenwald, S. E. Milan, M. Lester, W. F. Denig, and R. J. Barnes (2005), Multi-instrument mapping of the small-scale flow dynamics related to a cusp auroral transient, *Ann. Geophys.*, *23*, 2657–2670.

Pinnock, M., A. S. Rodger, J. R. Dudeney, K. B. Baker, P. T. Newell, R. A. Greenwald, and M. E. Greenspan (1993), Observations of an enhanced convection channel in the cusp ionosphere, *J. Geophys. Res.*, *98*, 3767–3776.

Pinnock, M., A. S. Rodger, J. R. Dudeney, F. Rich, and K. B. Baker (1995), High spatial and temporal resolution of the ionospheric cusp, *Ann. Geophys.*, *13*, 919–925.

Provan, G., and T. K. Yoeman (1999), Statistical observations of the MLT, latitude and size of pulsed ionospheric flows with the CUTLASS Finland radar, *Ann. Geophys.*, *17*, 855–867.

Provan, G., T. K. Yoeman, and S. E. Milan (1998), CUTLASS Finland radar observations of the ionospheric signatures of flux transfer events and the resulting plasma flows, *Ann. Geophys.*, *16*, 1411–1422.

Pryse, S. E., A. M. Smith, L. Kersley, I. K. Walker, C. N. Mitchell, J. Moen, and R. W. Smith (2000), Multi-instrument probing of the polar ionosphere under steady northward IMF, *Ann. Geophys.*, *18*, 90–98.

Rinne, Y., J. Moen, K. Oksavik, and H. C. Carlson (2007), On the occurrence of reversed flow events in the cusp ionosphere observed by european incoherent scatter (EISCAT) Svalbard radar, *J. Geophys. Res.*, *112*, A10313, doi:10.1029/2007JA012366.

Ruohoniemi, J. M., and K. B. Baker (1998), Large-scale imaging of high-latitude convection with super dual auroral radar network HF radar observations, *J. Geophys. Res.*, *103*, 20,797–20,811.

Russell, C. T., and R. C. Elphic (1979), ISEE observations of flux transfer events at the dayside magnetopause, *Geophys. Res. Lett.*, *6*, 33–36.

Sandholt, P. E., and C. J. Farrugia (2007), Role of poleward moving auroral forms in the dawn-dusk auroral precipitation asymmetries induced by IMF B_Y, *J. Geophys. Res.*, *112*, A04203, doi:10.1029/2006JA011952.

Sandholt, P. E., M. Lockwood, T. Oguti, S. W. H. Cowley, K. S. C. Freeman, B. Lybekk, A. Egeland, and D. M. Willis (1990), Midday auroral breakup events and related energy and momentum transfer from the magnetosheath, *J. Geophys. Res.*, *95*, 1039–1060.

Sandholt, P. E., J. Moen, A. Rudland, D. Opsvik, W. F. Denig, and T. Hansen (1993), Auroral event sequences at the dayside polar cap boundary for positive and negative IMF B_Y, *J. Geophys. Res.*, *98*, 7737–7755.

Sandholt, P. E., C. J. Farrugia, J. Moen, Ø. Noraberg, B. Lybekk, T. Sten, and T. L. Hansen (1998), A classification of dayside auroral forms and activities as a function of IMF orientation, *J. Geophys. Res.*, *103*, 23,325–23,345.

Sandholt, P. E., C. J. Farrugia, and W. F. Denig (2004), Detailed dayside auroral morphology as a function of local time for southeast IMF orientation: Implications for solar wind coupling, *Ann. Geophys.*, *22*, 3537–3560.

Smith, C. W., J. L'Heureux, N. F. Ness, M. H. Acuna, L. F. Burlaga, and J. Scheifele (1998), The ACE magnetic fields experiment, *Space Sci. Rev.*, *86*, 613–632.

Southwood, D. J. (1987), The ionospheric signature of flux transfer events, *J. Geophys. Res.*, *92*, 3207–3213.

Stern, D. (1984), Magnetospheric dynamo processes, in *Magnetospheric Currents*, *Geophys. Monogr. Ser.*, vol. 28, edited by T. Potemra, pp. 200–207, AGU, Washington, D. C.

Taguchi, S., M. Sugiura, J. Winningham, and J. Slavin (1993), Characterization of the IMF B_Y-dependent filed-aligned currents in the cleft region based on DE 2 observations, *J. Geophys. Res.*, *98*, 1393–1407.

Thorolfsson, A., J.-C. Cerisier, M. Lockwood, P. E. Sandholt, C. Senior, and M. Lester (2000), Simultaneous optical and radar signatures of poleward moving auroral forms, *Ann. Geophys.*, *18*, 1054–1066.

Waterman, J., D. Lummerzheim, O. de la Beaujardiere, P. T. Newell, and F. J. Rich (1994), Ionospheric footprint of magnetosheathlike particle precipitation observed by an incoherent scatter radar, *J. Geophys. Res.*, *99*, 3855–3867.

H. C. Carlson, J. Moen, and Y. Rinne, Department of Physics, University of Oslo, Sem Saelandsvei 24, P.O. Box 1048, Blindern, N-0316, Oslo Norway. (jmoen@fys.uio.no)

R. Fujii, Solar-Terrestrial Environmental Laboratory, Nagoya University, Chikusa-ku, Nagoya 464-8602, Japan.

K. Oksavik, Arctic Geophysics, The University Centre in Svalbard, P.O. Box 156, Longyearbyen, N-9171 Svalbard, Norway.

H. Opgenoorth, European Space Agency, ESTEC (SCI/SM), P.O. Box 299, 2200 AG Noordwijk, Netherlands.

III

GEOPHYSICAL RESEARCH LETTERS, VOL. 37, L13102, doi:10.1029/2010GL043307, 2010

Stratification of east-west plasma flow channels observed in the ionospheric cusp in response to IMF B_Y polarity changes

Y. Rinne,[1,2] J. Moen,[1,2] H. C. Carlson,[1,3] and M. R. Hairston[4]

Received 5 May 2010; revised 5 June 2010; accepted 10 June 2010; published 14 July 2010.

[1] During a period of predominantly north-westward flow for IMF B_Z negative and IMF B_Y positive, a sequence of three distinct negative excursions of IMF B_Y resulted in a train of three eastward directed flow channels, interleaved by westward flow enhancements propagating into the polar cap. The high resolution of the EISCAT Svalbard radar data enables us to track formation and movement of the flow channels, which are interpreted as a sequence of intermittent reconnection alternating between different reconnection sites. Our observations are consistent with the view that a new region of reconnected flux manifests as development of a distinct flow channel near the polar cap boundary, and that successive events stay separated while pushing each other into the polar cap. Each flow channel will remain separated from neighboring channels mapping to different reconnection sites as long as the magnetic tension force with its associated field aligned current systems is maintained. **Citation:** Rinne, Y., J. Moen, H. C. Carlson, and M. R. Hairston (2010), Stratification of east-west plasma flow channels observed in the ionospheric cusp in response to IMF B_Y polarity changes, *Geophys. Res. Lett.*, *37*, L13102, doi:10.1029/2010GL043307.

1. Introduction

[2] The Interplanetary Magnetic Field (IMF) B_Y control of the zonal flow in the ionospheric cusp is a key characteristic of magnetopause reconnection. The east-west component of the IMF (B_Y) displaces the reconnection site out to the flanks towards dawn for negative values and towards dusk for positive values, and the magnetic tension associated with the kink in newly opened flux gives rise to an initial eastward drag for negative, and westward for positive IMF B_Y [e.g., *Heelis et al.*, 1982; *Heppner and Maynard*, 1987; *Cowley et al.*, 1991; *Moen et al.*, 1999]. Magnetic stress is transferred to the ionosphere via a pair of field aligned current sheets along the magnetic field [*Southwood and Hughes*, 1982; *Southwood*, 1985, 1987; *Glassmeier and Stellmacher*, 1996].

[3] *Pinnock et al.* [1993, 1995] reported a longitudinally elongated, latitudinal narrow channel of enhanced convection by the PACE HF radar, consistent with the magnetic tension pull on newly open flux. *Marchaudon et al.* [2004] documented a pair of field-aligned current (FAC) sheets on each side of such a cusp flow channel observed by SuperDARN, and found their observation consistent with the current sheets in *Southwood*'s [1985, 1987] Flux Transfer Event (FTE) model. The polarity of the FTE currents is consistent with the IMF B_Y dependent polarity of large scale cusp currents [*Taguchi et al.*, 1993]. In case of a westward flow channel for IMF B_Y positive, there is a sheet of downward current near the equatorward border of the flow channel and a sheet of upward current near the poleward border of the flow channel.

[4] *Lockwood et al.* [2001] suggested that channels of newly opened flux due to very short reconnection pulses would append immediately adjacent to each other. The field aligned current sheets associated with each channel would decrease in strength with increasing time elapsed since reconnection. *Lockwood et al.* [1990] estimated that newly opened flux tubes only excite plasma flows for ~10 minutes. According to *Saunders* [1989] it should take ~7 minutes to release curvature on newly opened field. Hence, one would expect ionospheric flow channels only to be actively driven for ~7–10 minutes after reconnection.

[5] We present high resolution incoherent scatter radar observations of the convection in the vicinity of the ionospheric projection of the magnetospheric cusp during a sequence of IMF B_Y polarity reversals. We observe the formation of a series of latitudinally localized shear reversals extending through the EISCAT Svalbard radar (ESR) field of view ~1.5 hours in local time in response to the sequence of IMF B_Y polarity reversals. The series of alternating east/westward flow channels forming inside the ESR field-of-view is interpreted as signature of reconnection events at the magnetopause, and they provide the opportunity to test the conceptual model for how a sequence of reconnection events stacks in the polar cap.

2. Data Presentation

[6] Figures 1a–1c show the three components of the IMF measured by the Advanced Composition Explorer (ACE) on September 6th, 2005 in GSM coordinates. In the fourth panel, the calculated IMF clock angle is shown. The time displayed in Figure 1 has been lagget by one hour which is the time lag for the solar wind from ACE to the ionospheric response, calculated following the approach used by *Moen et al.* [1999]. The IMF B_Y component undergoes a sequence of three negative excursions starting at 10:49, 11:05 and 11:17 UT (shaded grey in Figure 1), after having been steadily positive for more than two hours. Each excursion in B_Y, together with almost simultaneous positive excursion of IMF B_Z moved the clock angle θ in the GSM YZ-plane from 90–180° to 45–90°. The solar wind speed as well as the particle density remained nearly constant (~−440 km/s and ~5 #/cm^{-3}

[1]Department of Physics, University of Oslo, Oslo, Norway.
[2]Arctic Geophysics, University Centre in Svalbard, Svalbard, Norway.
[3]CASS, SWC, Utah State University, Logan, Utah, USA.
[4]Center for Space Sciences, University of Texas at Dallas, Richardson, Texas, USA.

0094-8276/10/2010GL043307

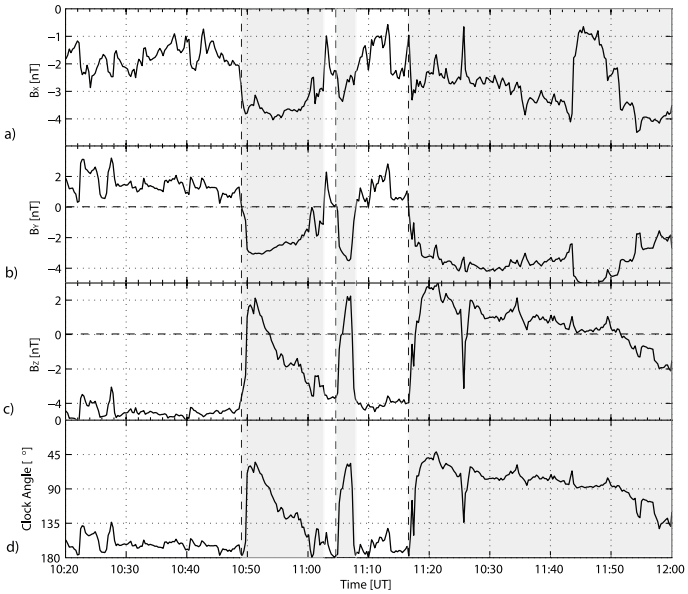

Figure 1. ACE data. Data from the Advanced Composition Explorer registered on 6 September 2005. Shown are the IMF (a) B_X, (b) B_Y and (c) B_Z component as well as (d) the IMF clock angle, $\theta = \arctan[\mathrm{abs}(B_Y)/B_Z]$ for $B_Z > 0$ and $\theta = 180 - \arctan[\mathrm{abs}(B_Y/B_Z)]$ for $B_Z < 0$. Periods with negative IMF B_Y are shaded grey.

respectively) during an at least 2 hour interval comprising the time of interest.

[7] A sequence of six counterclockwise scans showing ion velocity data from the ESR are displayed in Figure 2a. Start and stop times of each scan are indicated at the respective beams by time tags. Located on Svalbard at 78.09°N, 16.03°E, the magnetic local time (MLT) at the ESR is approximately UT + 3h. During the time of interest, the ESR was scanning an area of 120° in azimuth at a constant 30° elevation [*Carlson et al.*, 2002]. Positive values (colored from grey through yellow and red to dark red) indicate the line-of-sight component of the ion flow directed away from the ESR, while negative velocities (colored from black through blue to light blue) indicate line-of-sight component of the ion motion towards the ESR. In order to give a complete picture of the development of the features seen inside the ESR field-of-view, a movie sequence (Movie 1) is added, displaying all available scans during the time period of interest.

[8] Between 10:42 and 11:43 UT, the ESR observed a sequence of alternating eastward/westward flow channels in response to the IMF B_Y polarity changes. The selection of scans in Figure 2a shows snapshots of their development.

[9] The background flow measured inside the ESR field-of-view before 10:42 UT was directed westwards. This is consistent with the large scale convection expected in the early post-noon sector for steady IMF B_Z negative and B_Y positive conditions.

[10] The first eastward flow channel (marked E1), developed from 10:42 UT in the ESR field of view (Figure 2a, scans 1 + 2) in response to the first negative excursion of the IMF B_Y at 10:49 UT, which yields the expected eastward tension drag on newly opened field lines. The channels orientation can be determined unambiguously as it is oriented along several beams in the lower part of the field of view. In addition, its narrow flow reversal boundary, delimiting the eastward flow inside the channel from the surrounding westward convection, is also aligned along the ESR beams. E1 widens polewards as reconnection for the given IMF conditions proceeds and more flux is opened, and velocities increase up to 1300m/s before the entire channel starts to move polewards (scan 3 + 4) and leaves the field of view (scan 5 + 6). Velocity measurements in the upper part of the field of view are distorted by the unfavorable channel beam geometry as the ESR is only sensitive to plasma motion along its line of sight.

[11] An enhancement in westward convection (W1) appears at 11:01 UT in response to the IMF B_Y polarity reversal at 11:03 UT at the equatorward boundary of E1 (Figure 2a, scan 3). A DMSP F16 pass through the ESR field-of-view at 11:04 UT (Figure 2b, scan 1) confirms the E1 and W1 flow channels by drift meter measurements. The ion data show a clear transition between two particle regimes coinciding with the velocity reversal at 11:04:15 UT, and confirm W1 as a footprint of ongoing low latitude magnetopause reconnection. The opening of new flux by W1 immediately equatorwards of E1 pushes E1 polewards. The second eastward flow channel, E2, appears sometime between 11:02 and 11:07 UT in response to the brief negative excursion of IMF B_Y at 11:05 UT. E2 does not widen to more than around 50 km due to the short duration of the IMF B_Y excursion, and is immediately pushed polewards by the opening of new flux associated with the second westward flow enhancement (W2) on its equator side (scans 4 − 5). W2 appears around

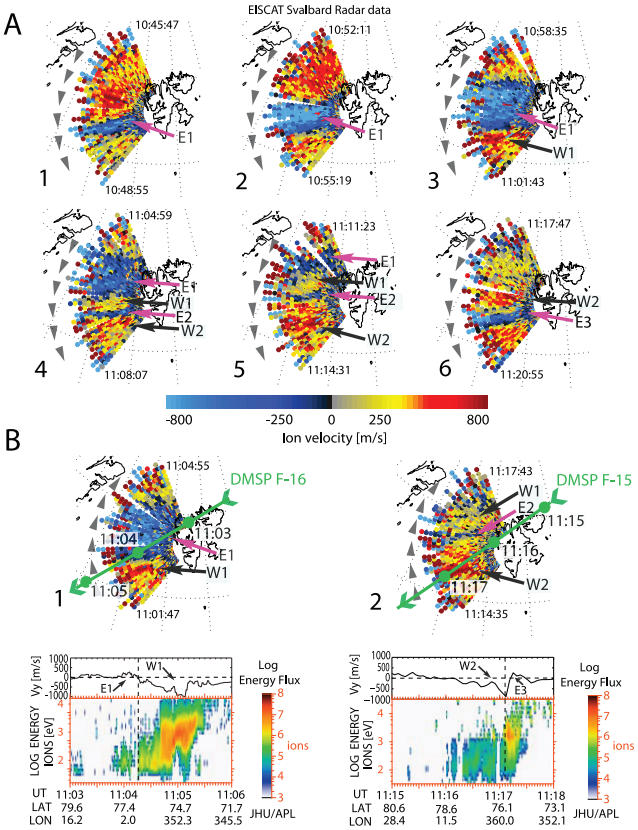

Figure 2. EISCAT Svalbard Radar data. (a) Six ion velocity scans from the ESR. The spatial resolution is ~15 km in azimuthal direction and 30 km in radial direction. Data retrieved from increasing altitude were projected along the magnetic field to a common reference altitude of 250 km and plotted in geographic coordinates. The eastward (E1-3) and westward (W1+W2) flow channels are marked by arrows. (b) Two counter-clockwise ESR scans intersected by a DMSP F16 (left) and DMSP F15 (right) pass as well as the respective driftmeter and precipitating ion data. Positive flow measured by DMSP indicate sunward velocities.

11:07 UT (Figure 2a, scan 4) as response to the second positive IMF B_Y period from 11:08 UT onwards. The third eastward channel, E3, appears at 11:14 UT (Figure 2a, scan 5) in response to the third IMF B_Y polarity reversal at 11:16 UT. A pass by DMSP F15 at 11:16 UT (Figure 2b, scan 2) confirms the velocity reversals seen inside the ESR field-of view for W2 and E3. The velocity decrease marking the beginning of E3 at 11:17 UT coincides with the transition between two particle regimes. A clear step to higher ion energy and flux marks the transition to cusp like precipitation and confirms E3 as a footprint of reconnection. E3 evolves similar to E1, and is seen inside the ESR field-of-view for 30 minutes until the experiment at the ESR was stopped at 11:43 UT.

3. Discussion

[12] The flow channel events presented here appear to be of the same class as those mapped out by *Pinnock et al.* [1993, 1995], and further elaborated by *Provan et al.* [1998, 2002]. The sequence of IMF B_Y polarity changes enables us to bring evidence that patches of reconnection keep separated as they are being pushed into the polar cap [*Lockwood et al.*, 2001]. It should be noted that the flow channels in this study are fundamentally different from the reversed flow events presented by *Rinne et al.* [2007] and *Moen et al.* [2008], as the direction of plasma flow inside the channels observed by these authors was in opposite direction of magnetic tension pull on newly opened field lines.

[13] The ESR field-of-view extends ~600 km to the west in the middle of each scan, and previous studies have reported cusp convection channels of up to 2500 km in length [*Pinnock et al.*, 1993, 1995; *Milan et al.*, 1999; *Nishitani et al.*, 1999; *Lockwood et al.*, 2001]. Hence, we most likely only see part of the channels and cannot observe east- or westward motion of the channels as a whole. An essential feature of the eastward channels, which stay in stark contrast to the background flow, is the uniform latitudinal thickening. E2, attributed to the brief 2 min negative excursion in IMF B_Y, was fully

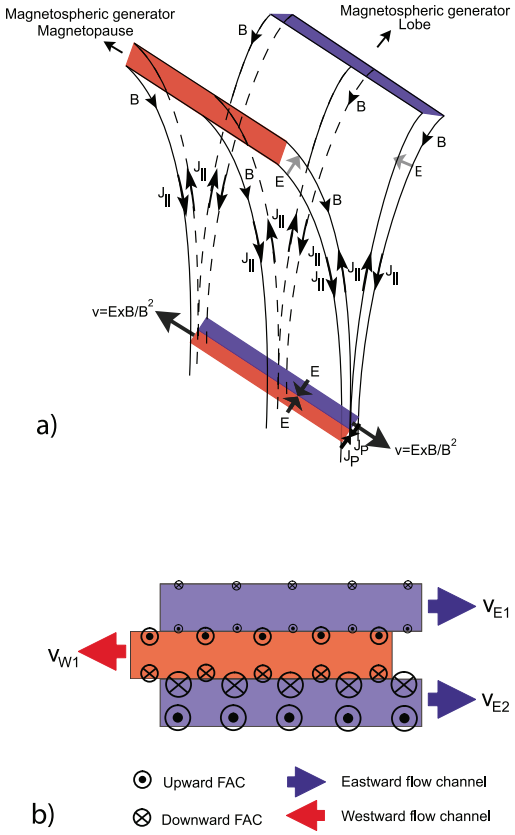

Figure 3. Schematic illustrations. (a) Schematic illustration of how idealized ionospheric flow channels, here a blue eastward and a red westward channel, couple via FAC sheets along the flanks of the channels to different generator regions in the magnetopause. (b) Schematic illustration showing two eastward channels (E1 and E2) as well as the first westward flow enhancement (W1) appended immediately adjacent to each other. Since the channels coupled to different magnetospheric generators they do not share FAC sheets but remain separated until magnetic tension and their FAC system is exhausted. For the eastward channels, the flow reversal on the poleward edge is consistent with a downward FAC sheet, and the flow reversal on the equatorward edge with an upward FAC sheet. The tension force and the FAC sheet required for each channel decays with increasing time elapsed since reconnection, and hence E1 has a weaker FAC sheet than W1.

developed as ~50 km wide channel around ~11:07 UT and faded into the background around 9 min later, which is consistent with the expected time it takes to release magnetic tension [*Saunders*, 1989; *Lockwood et al.*, 1990]. E1, which was due to a ~13 min negative excursion in IMF B_Y, was first detected at ~10:43 UT and started to fade around 10:57 UT, which is consistent with a 13 minute growth time. The sharp well-defined boundaries of E1, and strong flow across the entire width of the channel during the growth phase, lead us to conclude that E1 is consistent with continuous reconnection [*Lockwood et al.*, 2001] during the ~13 min interval of negative IMF B_Y. E3 developed in a similar manner to E1. From its first appearance in the ESR data at 11:20 UT until 11:29 UT (Movie 1) there was strong flow across the entire channel and sharp boundaries consistent with quasi-continuous reconnection. Since B_Y stayed negative, the poleward edge blurred as it expanded out of the field of view. We cannot tell how long quasi continuous reconnection continued for E3 since the radar stopped operating when E3 still was active. However, we conclude that the flow channels developing inside the field of view are footprints of ongoing reconnection in contrast to a flux tube convecting across our field of view.

[14] The reconnection site on the dayside is controlled by the IMF orientation. Reconnection is favored at the low latitude magnetopause for clock angles θ = 90–180° [*Sandholt et al.*, 1998], and the westward background enhancements are most likely the footprint of low latitude reconnection. For clock angles θ = 45–90°, reconnection has been reported to occur either polewards of the dayside cusp at the high latitude magnetopause, at the low-latitude magnetopause, or even at both locations simultaneously [*Sandholt et al.*, 1998; *Chisham et al.*, 2004]. DMSP F16 intersected both E1 and W1. The ion signature of W1 is prominent cusp ion injection telling us that W1 was actively driven at the time of pass, and the sharp drop in energy and flux density near the E1/W1 flow reversal is consistent with E1 not being actively driven at the same time. Similarly for the DMSP F15 passage, it is the equatormost channel E3 that is actively driven (Figure 2). For the eastward channels E1–E3 the location of reconnection on the magnetopause cannot be determined unambiguously. Independent of flow direction, the equatorward boundary of the equator most flow channel represents the OCB. Lobe reconnection which is yields stirring of already open flux will develop poleward of the OCB and the poleward widening of the blue eastward channels give an indicative of lobe reconnection. However, the important point for the main objective of this paper is that the near simultaneous polarity changes in the IMF B_Y and B_Z component altering the IMF clock angle between θ = 90–180° and θ = 45–90° leads to the activation of two spatially different reconnection sites on the magnetopause as indicated in Figure 3a, and only one of these two sites are active at a time.

[15] In reconnection perspective each flow channel represents a patch of newly opened flux, which is constrained by a pair of field aligned currents, constituting adiaroic boundaries across which there is no plasma flow [*Lockwood et al.*, 2001]. The sharp flow reversal boundary on each side of the flow channel implies the existence of a FAC sheet. The clock wise flow reversal at equatorward boundary is consistent with an upward current and the counter clock wise reversal at the poleward side is consistent with a downward FAC sheet, consistent with the polarities of FAC systems observed by *Taguchi et al.* [1993]. Hence, all three eastward channels (E1–E3) are longitudinally delimited by a system of FACs delimiting them from the surrounding flux, and connected to one magnetospheric region or generator, driven by the release of magnetic tension. This interpretation is further substantiated by the ion

data boundaries evident in Figure 2b (scan 1). The westward flow enhancements (W1 and W2) coupled to their respective generator and are sandwiched in between the self contained eastward channels E1–E3, as indicated in Figure 3b. The flow channel systems remain hence separated from each other and the surrounding plasma since no flux can cross the FAC sheet boundaries. This is visible in scan 4–6; the channels remain well-defined and do not intermix. They stack as individual flow channels, event by event and drift into the polar cap when more open flux is created during the episodes of magnetopause reconnection. The very first observational evidence for stratification of newly reconnected flux; that is stratification of the E1, W1, E2, W2 channels is visible in the fourth scan in Figure 2a. With increasing time elapsed since reconnection, however, the magnetic tension force and the FAC system transferring stress to the ionosphere decay, and once magnetic tension has been released the FAC system fades. With no FAC system exerting electromagnetic forcing and thereby locally accelerating plasma, the new flux is assimilated into the large scale background flow, on a timescale of about 10 minutes after reconnection stops [*Lockwood et al.*, 1990].

4. Summary

[16] The ESR data presented here give new detailed insight into the complex mesoscale cusp dynamics which have not yet been resolved satisfactory. They uncover the formation and development of ionospheric meso-scale flow channels in response to a sequence of IMF B_Y polarity changes in more detail than previously seen, and show how a series of reconnection events arranges and coexists in the ionosphere, separated from each other by FAC sheets. The systematic change in the direction of magnetic tension enabled us to tag and track alternately eastward and westward directed flow channels, the ionospheric footprint of newly reconnected flux. Our observations provide a clear conceptual picture for how newly reconnected flux stacks as separate flow channels, event by event, pushing each other into the polar cap. They do not intermix with each other across the FAC/flow reversal boundary but are kept separated. The strong flow shears associated with the flow channels should create plasma instabilities and turbulence with severe impact for communication and navigation systems in the Polar Regions, applying the same physics for shears associated with patch formation [*Carlson et al.*, 2007].

[17] **Acknowledgments.** EISCAT is an international association supported by research organizations in China (CRIRP), Finland (SA), France (CNRS, until the end of 2006), Germany (DFG), Japan (NIPR and STEL), Norway (NFR), Sweden (VR), and the United Kingdom (STFC). We thank the ACE Science Center and the ACE MAG and SWEPAM instrument teams for providing data from the ACE space craft. The DMSP particle detectors were designed by Dave Hardy of AFRL, and data obtained from JHU/APL. We gratefully acknowledge the Center for Space Sciences at the University of Texas at Dallas and the US Air Force for providing the DMSP thermal plasma data. This research was supported, in part, by the Utah Science, Technology And Research (USTAR) initiative via the Space Weather Center at Utah State University. Financial support has been provided by the Norwegian Research Council, and Air Force Office of Scientific Research, Air Force Material Command, USAF, under grant FA8655-10-1-3003, COST action ES0803.

References

Carlson, H. C., K. Oksavik, J. Moen, A. P. van Eyken, and P. Guio (2002), ESR mapping of polar-cap patches in the dark cusp, *Geophys. Res. Lett.*, *29*(10), 1386, doi:10.1029/2001GL014087.

Carlson, H. C., T. Pedersen, S. Basu, M. Keskinen, and J. Moen (2007), Case for a new process, not mechanism, for cusp irregularity production, *J. Geophys. Res.*, *112*, A11304, doi:10.1029/2007JA012384.

Chisham, G., M. P. Freeman, I. J. Coleman, M. Pinnock, M. R. Hairston, M. Lester, and G. Sofko (2004), Measuring the dayside reconnection rate during an interval of due northward interplanetary magnetic field, *Ann. Geophys.*, *22*, 4243–4258, doi:10.5194/angeo-22-4243-2004.

Cowley, S. W. H., J. P. Morelli, and M. Lockwood (1991), Dependence of convective flows and particle precipitation in the high-latitude dayside ionosphere on the X and Y component of the interplanetary magnetic field, *J. Geophys. Res.*, *96*(A4), 5557–5564, doi:10.1029/90JA02063.

Glassmeier, K.-H., and M. Stellmacher (1996), Mapping flux transfer events to the ionosphere, *Adv. Space Res.*, *18*(8), 151–160, doi:10.1016/0273-1177(95)00983-3.

Heelis, R. A., J. K. Lowell, and R. W. Spiro (1982), A model of the high-latitude ionospheric convection pattern, *J. Geophys. Res.*, *87*(A8), 6339–6345, doi:10.1029/JA087iA08p06339.

Heppner, J. P., and N. C. Maynard (1987), Empirical high-latitude electric field models, *J. Geophys. Res.*, *92*(A5), 4467–4489, doi:10.1029/JA092iA05p04467.

Lockwood, M., S. W. H. Cowley, and M. P. Freeman (1990), The excitation of plasma convection in the high-latitude ionosphere, *J. Geophys. Res.*, *95*(A6), 7961–7972, doi:10.1029/JA095iA06p07961.

Lockwood, M., S. E. Milan, T. Onsager, C. H. Perry, J. A. Scudder, C. T. Russell, and M. Brittnacher (2001), Cusp ion steps, field-aligned currents and poleward moving auroral forms, *J. Geophys. Res.*, *106*, 29,555–29,569, doi:10.1029/2000JA900175.

Marchaudon, A., J.-C. Cerisier, R. A. Greenwald, and G. J. Sofko (2004), Electrodynamics of a flux transfer event: Experimental test of the Southwood model, *Geophys. Res. Lett.*, *31*, L09809, doi:10.1029/2004GL019922.

Milan, S. E., M. Lester, R. A. Greenwald, and G. Sofko (1999), The ionospheric signature of transient dayside reconnection and the associated pulsed convection return flow, *Ann. Geophys.*, *17*, 1166–1171, doi:10.1007/s00585-999-1166-2.

Moen, J., H. C. Carlson, and P. E. Sandholt (1999), Continuous observation of cusp auroral dynamics in response to an IMF by polarity change, *Geophys. Res. Lett.*, *26*(9), 1243–1246, doi:10.1029/1999GL900224.

Moen, J., Y. Rinne, H. C. Carlson, K. Oksavik, R. Fujii, and H. Opgenoorth (2008), On the relationship between Birkeland current arcs and reversed flow channels in the winter cusp/cleft ionosphere, *J. Geophys. Res.*, *113*, A09220, doi:10.1029/2008JA013061.

Nishitani, N., T. Ogawa, M. Pinnock, M. P. Freeman, J. R. Dudeney, J.-P. Villain, K. B. Baker, N. Sato, H. Yamagishi, and H. Matsumoto (1999), A very large scale flow burst observed by the SuperDARN radars, *J. Geophys. Res.*, *104*(A10), 22,469–22,486, doi:10.1029/1999JA900241.

Pinnock, M., A. S. Rodger, J. R. Dudeney, K. B. Baker, P. T. Newell, R. A. Greenwald, and M. E. Greenspan (1993), Observations of an enhanced convection channel in the cusp ionosphere, *J. Geophys. Res.*, *98*(A3), 3767–3776, doi:10.1029/92JA01382.

Pinnock, M., A. S. Rodger, J. R. Dudeney, F. J. Rich, and K. B. Baker (1995), High spatial and temporal resolution observations of the ionospheric cusp, *Ann. Geophys.*, *13*, 919–925, doi:10.1007/s00585-995-0919-9.

Provan, G., T. K. Yeoman, and S. E. Milan (1998), CUTLASS Finland radar observations of the ionospheric signature of flux transfer events and the resulting plasma flow, *Ann. Geophys.*, *16*, 1411–1422, doi:10.1007/s00585-998-1411-0.

Provan, G., S. E. Milan, M. Lester, T. K. Yeoman, and H. Khan (2002), Simultaneous observations of the ionospheric footprint of flux transfer events and dispersed ion signatures, *Ann. Geophys.*, *20*, 281–287, doi:10.5194/angeo-20-281-2002.

Rinne, Y., J. Moen, K. Oksavik, and H. C. Carlson (2007), Reversed flow events in the winter cusp ionosphere observed by the European Incoherent Scatter (EISCAT) Svalbard radar, *J. Geophys. Res.*, *112*, A10313, doi:10.1029/2007JA012366.

Sandholt, P. E., C. J. Farrugia, J. Moen, Ø. Noraberg, B. Lybekk, T. Sten, and T. Hansen (1998), A classification of dayside auroral forms and activities as a function of interplanetary magnetic field orientation, *J. Geophys. Res.*, *103*(A10), 23,325–23,345, doi:10.1029/98JA02156.

Saunders, M. A. (1989), Origin of the cusp Birkeland currents, *Geophys. Res. Lett.*, *16*(2), 151–154, doi:10.1029/GL016i002p00151.

Southwood, D. J. (1985), Theoretical aspects of ionosphere-magnetosphere-solar wind coupling, *Adv. Space Res.*, *5*(4), 7–14, doi:10.1016/0273-1177(85)90110-3.

Southwood, D. J. (1987), The ionospheric signature of flux transfer events, *J. Geophys. Res.*, *92*(A4), 3207–3213, doi:10.1029/JA092iA04p03207.

Southwood, D. J., and W. J. Hughes (1982), Theory of hydromagnetic waves in the magnetosphere, *Space Sci. Rev.*, *35*, 301–366.

Taguchi, S., M. Sugirua, J. D. Winningham, and J. A. Slavin (1993), Characterization of the IMF BY–dependent field-aligned currents in the cleft region based on DE 2 observations, *J. Geophys. Res.*, *98*(A2), 1393–1407, doi:10.1029/92JA01014.

H. C. Carlson, CASS, SWC, Utah State University, 4405 Old Main Hill, Logan, UT 84322-4405, USA.

M. R. Hairston, Center for Space Sciences, University of Texas at Dallas, Richardson, Texas, USA.

J. Moen and Y. Rinne, Department of Physics, University of Oslo, Postboks 1048 Blindern, N-0316 Oslo, Norway. (yvonne.rinne@fys.uio.no)

IV